

Supporting Information

Multifaceted behavior of a doubly reduced arylborane in B–H-bond activation and hydroboration catalysis

Sven E. Prey, Christoph Herok, Felipe Fantuzzi, Michael Bolte, Hans-Wolfram Lerner,
Bernd Engels* and Matthias Wagner*

Table of contents:

1. Experimental details and characterization data	ESI1
1.1 General procedure for the reaction of reduced DBA-derivatives with HBpin	ESI2
1.2 Characterization data of the DBA/HBpin primary activation products	ESI4
1.3 Characterization data of crystallized Bpin-substituted DBAs	ESI6
2. Reactivity of the type-II compound Li[5] and considerations regarding a possible hydroboration catalysis	ESI10
3. Hydroboration reactions with DBA derivatives	ESI15
3.1 General procedures and characterization data	ESI15
3.2 Additional experimental data regarding the hydroboration reactions	ESI19
3.3 Control hydroboration experiments	ESI24
4. NMR spectra of the DBA derivatives	ESI25
5. NMR spectra of the hydroboration reactions	ESI41
6. X-ray crystal structure analyses	ESI49
7. Additional details on quantum chemical calculations	ESI59
8. References	ESI65

1. Experimental details and characterization data

General considerations. All reactions, manipulations, and analyses were carried out in an argon-filled glovebox or by applying standard Schlenk techniques under an argon atmosphere. Toluene, Et₂O, and THF were dried over Na/benzophenone; C₆D₆, DME, and THF-*d*₈ were dried over Na-K alloy without benzophenone. Prior to use, the solvents were distilled from the drying agent; C₆D₆, DME, THF, and THF-*d*₈ were degassed by applying four freeze-pump-thaw cycles.

NMR spectra were recorded at 298 K using the following spectrometers: Bruker DPX-250, Avance-300, Avance-400, or Avance-500.

Chemical shifts are referenced to (residual) solvent signals (¹H/¹³C{¹H}): C₆D₆: δ = 7.16/128.06 ppm, CDCl₃: δ = 7.26/77.16, THF-*d*₈: δ = 3.58/67.21 ppm)¹ or external BF₃·OEt₂ (¹¹B; ¹¹B{¹H}). Abbreviations: s = singlet, d = doublet, t = triplet, vt = virtual triplet, q = quartet, sept = septet, m = multiplet, br = broad, n.o. = not observed, n.r. = not resolved.

The compounds 9,10-dibromo-DBA,² **1**,³ **2**,⁴ and their respective dilithio-, disodio-, and dipotassio salts⁵ were synthesized according to literature procedures.

High-resolution mass spectra were measured in positive mode using a Thermo Fisher Scientific MALDI LTQ Orbitrap XL and α-cyano-4-hydroxycinnamic acid or 4-chloro-α-cyanocinnamic acid as the matrix. Exact masses were calculated based on the predominant combination of natural isotopes.

The 9,10-dihydro-9,10-diboraanthracene scaffolds will usually be abbreviated as “DBA”.

1.1 General procedure for the reaction of reduced DBA-derivatives with HBpin

The respective neutral DBA derivative (see Tables S1 and S2) was reduced in THF-*d*₈ (0.5 mL) following literature procedures.⁵ The resulting solution was separated from residual reducing agent and transferred to an NMR tube. Neat pinacol borane (HBpin) was added to the solution at room temperature and the tube was flame-sealed.

THF solutions of the DBA salts are intensely colored (Li: deep red; Na, K: deep green), whereas the products of HBpin activation are pale yellow. Naked-eye inspection of the sample colors indicated that all reactions had reached their maximum conversions already after 10 min. The individual conversions were quantified by ¹H NMR spectroscopy and found to depend both on the counteranion and the boron-bonded substituent of the DBA salt used.

Table S1. Overview of the reactions between reduced DBA derivatives and HBpin (1 equiv.) in THF-*d*₈. To our experience, upscaling does not have an impact on the reaction outcome.

DBA derivative			Reducing agent (exc.)	HBpin		Conversion %	primary product (by NMR)
	<i>m</i> / mg	<i>n</i> / mmol		<i>V</i> / μL	<i>n</i> / mmol		
1	11	0.063	Li	9.1	0.063	50 ^a	type-I
2	15	0.074	Li	10.4	0.074	19 ^a	type-II ^b
2	12	0.068	Na	9.9	0.068	quant.	type-I
2	14	0.069	Na	10.0	0.069	61 ^a	type-I
1	11	0.063	KC ₈	8.9	0.061	quant.	type-I
2	9	0.043	KC ₈	6.0	0.041	85 ^a	type-I

^a dynamic equilibrium between starting materials and product.

^b [BH₄]⁻ is detected as second product.

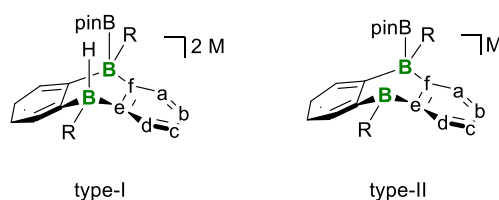


Figure S1. We postulate that all HBpin activation reactions performed here initially lead to type-I products (addition of the H–B bond across the two DBA-boron centers). Only in the case of Li₂[**2**] does rapid formal LiH elimination lead to a type-II species as the only DBA-containing product detectable by NMR. The letters a-f are the numbering scheme used for the assignment of NMR signals.

In cases where 1 equiv. of HBpin was insufficient to achieve quantitative conversion of the reduced DBA, the reactions were repeated with exc. HBpin (Table S2). The fact that increasing the amounts of added HBpin ultimately leads to quantitative conversions further supports our understanding of the reactions as equilibrium processes.

Table S2. Overview of the reactions between reduced DBA derivatives and HBpin (*n* equiv.) in THF-*d*₈. The numbers *n* given are the smallest excesses required to achieve full conversion of the reduced DBA.

DBA derivative			Reducing agent (exc.)	exc. HBpin	
	<i>m</i> / mg	<i>n</i> / mmol		<i>V</i> / μ L	<i>n</i> / mmol
1	9	0.049	Li	14	0.097 (2 equiv.)
2	10	0.049	Li	50	0.340 (7 equiv.)
2	10	0.049	Na	28.5	0.196 (4 equiv.)
2	10	0.049	KC ₈	14	0.097 (2 equiv.)

1.2 Characterization data of the DBA/HBpin primary activation products

Note: The assignments of NMR signals are based on ^1H - ^{11}B -HMBC experiments (as well as ^1H - ^{13}C -HSQC, -H2BC, and -HMBC spectra) and the assumption that $^3J_{\text{HB}} \gg ^4J_{\text{HB}}$.

Li₂[3] (type-I structure)

$^1\text{H}\{^{11}\text{B}\}$ NMR (500.2 MHz, THF-*d*₈): $\delta = 7.39 - 7.34$ (m, 2H, H-d), $7.27 - 7.23$ (m, 2H, H-a), $6.71 - 6.65$ (m, 4H, H-b and H-c), 2.49 (d, $^2J_{\text{HH}} = 16.7$ Hz, 1H, HBH), 2.29 (d, $^2J_{\text{HH}} = 16.7$ Hz, 1H, HBH), 2.10 (s, 1H, pinBBH), 1.10 (s, 12H, OC(CH₃)₂).

^{11}B NMR (160.5 MHz, THF-*d*₈): $\delta = 41.6$ ($h_{1/2} = 890$ Hz, Bpin), -17.5 (vt, av, $^1J_{\text{BH}} = 78$ Hz, BH₂), -22.4 (d, $^1J_{\text{BH}} = 68.6$ Hz, pinBBH).

$^{13}\text{C}\{^1\text{H}\}$ NMR (125.8 MHz, THF-*d*₈): $\delta = 162.8 - 161.2$ (m, C-e), $159.7 - 158.4$ (m, C-f), 135.0 (C-d), 133.1 (C-a), 122.6 (C-b), 122.5 (C-c), 81.4 (OC(CH₃)₂), 25.0 (OC(CH₃)₂).

Li[5] (type-II structure)

The reaction between Li₂[2] and HBpin generates substantial amounts of the side product LiBH₄ (from eliminated LiH and HBpin). An additional purification step is therefore required to isolate pure Li[5]: LiBH₄ was quenched with neat Et₃SiCl (8.3 μL , 0.049 mmol, 1 equiv.) to form BH₃·thf, Et₃SiH, and LiCl. *n*-Hexane was added to the reaction solution until a colorless precipitate formed. The mother liquor was removed *via* syringe, and the solid residue washed with *n*-hexane (2 \times 1 mL), dried, and dissolved in THF-*d*₈ (0.5 mL). **Note:** The NMR sample likely contained some LiCl that coprecipitated with the DBA product. [Li(thf)₂][5] free of LiCl can be obtained through recrystallization (see below).

^1H NMR (500.2 MHz, THF-*d*₈): $\delta = 8.00$ (br d, $^3J_{\text{HH}} = 7.5$ Hz, 2H, H-d), 7.78 (br d, $^3J_{\text{HH}} = 6.3$ Hz, 2H, H-a), 7.08 (vtd, av, $^3J_{\text{HH}} = 7$ Hz, $^4J_{\text{HH}} = 1.5$ Hz, 2H, H-b), 6.86 (vtd, av, $^3J_{\text{HH}} = 7$ Hz, $^4J_{\text{HH}} = 1.4$ Hz, 2H, H-c), 1.30 (s, 3H, BCH₃), 0.94 (s, 12H, OC(CH₃)₂), $0.16 - 0.12$ (m, 3H, pinBBCH₃).

^{11}B NMR (160.5 MHz, THF-*d*₈): $\delta = 61.8$ ($h_{1/2} = 590$ Hz, BCH₃), 41.9 ($h_{1/2} = 250$ Hz, Bpin), -19.7 (pinBBCH₃).

$^{13}\text{C}\{^1\text{H}\}$ NMR (125.8 MHz, THF-*d*₈): $\delta = 181.7$ (q, $^1J_{\text{CB}} = 45.8$ Hz, C-f), 144.2 (br, C-e), 134.9 (C-d), 134.4 (C-a), 128.4 (C-b), 120.4 (C-c), 80.6 (OC(CH₃)₂), 25.0 (OC(CH₃)₂), 11.9 (q, $^1J_{\text{CB}} = 37.9$ Hz, pinBBCH₃), 4.7 (br, BCH₃).

Na₂[3] (type-I structure)

$^1\text{H}\{^{11}\text{B}\}$ NMR (500.2 MHz, THF-*d*₈): $\delta = 7.34 - 7.28$ (m, 2H, H-d), $7.22 - 7.17$ (m, 2H, H-a), $6.66 - 6.61$ (m, 4H, H-b and H-c), 2.84 (d, $^2J_{\text{HH}} = 20.4$ Hz, 1H, HBH), 2.65 (d, $^2J_{\text{HH}} = 20.4$ Hz, 1H, HBH), 2.46 (br s, 1H, pinBBH), 1.08 (s, 12H, OC(CH₃)₂).

^{11}B NMR (160.5 MHz, THF-*d*₈): $\delta = 42.2$ ($h_{1/2} = 1110$ Hz Bpin), -19.3 (vt, av, $^1J_{\text{BH}} = 78$ Hz, BH₂), -23.4 (d, $^1J_{\text{BH}} = 74.5$ Hz, BH).

$^{13}\text{C}\{^1\text{H}\}$ NMR (125.8 MHz, THF- d_8): $\delta = 159.7$ (q, $^1J_{\text{CB}} = 42.0$ Hz, C-f), 157.6 (q, $^1J_{\text{CB}} = 47.0$ Hz, C-e), 136.3 (C-d), 135.6 (C-a), 122.5 (C-c), 122.0 (C-b), 80.6 (OC(CH $_3$) $_2$), 25.1 (OC(CH $_3$) $_2$).

Na $_2$ [4] (type-I structure)

$^1\text{H}\{^{11}\text{B}\}$ NMR (500.2 MHz, THF- d_8): $\delta = 7.48 - 7.27$ (n.r., 4H, H-a and H-d), 6.74 (n.r., 4H, H-b and H-c), 2.14 (s, 1H, BH), 1.02 (s, 12H, OC(CH $_3$) $_2$), -0.18 (br s, 6H, HBCH $_3$ and pinBBCH $_3$).

^{11}B NMR (160.5 MHz, THF- d_8): $\delta = 42.6$ ($h_{1/2} = 990$ Hz, Bpin), -17.4 (d, $^1J_{\text{BH}} = 68.2$ Hz, BH), -22.0 (BBpin).

$^{13}\text{C}\{^1\text{H}\}$ NMR (125.8 MHz, THF- d_8): $\delta = 168.3$ (C-e or C-f), 164.5 (C-e or C-f), 130.3 (C-a or C-d), 129.8 (C-a or C-d), 122.2 (C-b or C-c), 121.3 (C-b or C-c), 80.8 (OC(CH $_3$) $_2$), 25.0 (OC(CH $_3$) $_2$), 7.3 (HBCH $_3$ or pinBBCH $_3$), 5.6 (HBCH $_3$ or pinBBCH $_3$).

Note: A full assignment of the resonances by 2D NMR experiments was not possible due to signal broadening (for a rationale of this phenomenon see the corresponding discussion in the X-ray-crystallography section).

K $_2$ [3] (type-I structure)

$^1\text{H}\{^{11}\text{B}\}$ NMR (500.2 MHz, THF- d_8): $\delta = 7.26 - 7.20$ (m, 2H, H-d), 7.17 - 7.12 (m, 2H, H-a), 6.61 - 6.55 (m, 4H, H-c and H-d), 2.57 (br s, 2H, HBH), 2.28 (s, 1H, pinBBH), 1.06 (s, 12H, OC(CH $_3$) $_2$).

^{11}B -NMR (96.3 MHz, THF- d_8): $\delta = 41.7$ ($h_{1/2} = 1390$ Hz, Bpin), -17.6 (vt, av. $^1J_{\text{BH}} = 75$ Hz, BH $_2$), -22.1 (d, $^1J_{\text{BH}} = 71.7$ Hz, BH).

$^{13}\text{C}\{^1\text{H}\}$ NMR (125.8 MHz, THF- d_8): $\delta = 162.8$ (br, C-f), 161.1 (br, C-e), 135.1 (C-d), 134.8 (C-a), 122.1 (C-b), 121.7 (C-c), 80.5 (OC(CH $_3$) $_2$), 25.3 (OC(CH $_3$) $_2$).

K $_2$ [4] (type-I structure)

Since this reaction is less selective than in the case of Na $_2$ [4], an additional workup step is advisable: *n*-Hexane (2 mL) was added to the reaction mixture until a colorless precipitate formed. The mother liquor was removed *via* syringe, and the solid residue washed with *n*-hexane (2 \times 0.5 mL), dried, and dissolved in THF- d_8 (0.5 mL).

^1H NMR (500.2 MHz, THF- d_8): $\delta = 7.39 - 7.32$ (m, 2H, H-d), 7.26 - 7.19 (m, 2H, H-a), 6.86 - 6.78 (m, 4H, H-b and H-c), 0.99 (s, 12H, OC(CH $_3$) $_2$), 0.28 - 0.19 (n.r., 3H, HBCH $_3$), 0.07 (s, 3H, pinBBCH $_3$), n.o. (BH).

^{11}B NMR (160.5 MHz, THF- d_8): $\delta = 24.6$ (br, Bpin) -17.7 (br, HBCH $_3$), -21.7 (pinBBCH $_3$).

^{13}C NMR (125.8 MHz, THF- d_8): $\delta = 171.8$ (br, C-f), 168.7 (br, C-e), 128.3 (C-d), 127.7 (C-a), 122.6 (C-b), 121.8 (C-c), 80.3 (OC(CH $_3$) $_2$), 25.4 (OC(CH $_3$) $_2$), 5.4 (br, BBCH $_3$), 3.4 (br, HBCH $_3$).

Note: In the absence of HBpin, K $_2$ [4] tends to undergo the reverse reaction to regenerate small amounts of HBpin and K $_2$ [2]. Likely due to this dynamic equilibrium between K $_2$ [4] and K $_2$ [2]/HBpin, the NMR signal of the BH-fragment (^1H NMR) of K $_2$ [4] is broadened beyond detection.

1.3 Characterization data of crystallized Bpin-substituted DBAs

[Li(thf)₂][5]:

X-ray quality crystals of [Li(thf)₂][5] were grown by gas-phase diffusion of *n*-hexane into a C₆H₆ solution of Li[5].

[Na(thf)₂][5]:

In contrast to the case of Li[5] (type-II structure), the primary product of the reaction between HBpin and Na₂[2] is the type-I species Na₂[4]. However, over the course of several hours, also this compound is slowly converted to a secondary product in solution (note that the related Na₂[3] remains stable for at least 10 h even at 50 °C according to NMR spectroscopy in THF-*d*₈). The mixture of the primary product Na₂[4] and the secondary product gives rise to broad ¹H NMR signals of limited diagnostic value. Single crystals of [Na(thf)₂][5] (type-II structure) suitable for X-ray diffraction were obtained from a dimethoxyethane (DME) solution of Na₂[4] containing small amounts of THF. To confirm that Na[5] is identical to the above-mentioned secondary product in solution, two further experiments were performed:

- 1) An ¹H NMR spectrum recorded on re-dissolved crystals of [Na(thf)₂][5] in THF-*d*₈ showed perfectly resolved resonances, confirming the molecular structure determined by X-ray crystallography. All chemical shift values were identical to those of the broad signals belonging to the ‘secondary product’.
- 2) Addition of the hydride-scavenger Et₃SiCl to a THF-*d*₈ solution of the freshly prepared addition product of HBpin and Na₂[2] led to the quantitative formation of Na[5] (NMR-spectroscopic control; see below).

We conclude that compound Na₂[4] tends to formally eliminate NaH to give Na[5]. As long as both species are present in the same NMR sample, H⁻-exchange between them leads to motional broadening.

Synthesis of Na[5] (type-II structure)

Neat Et₃SiCl (6.3 μL, 0.037 mmol) was added to a freshly prepared solution of Na₂[4] (0.039 mmol) in THF (0.5 mL), whereupon a colorless precipitate formed (NaCl). The solid was removed by centrifugation and all volatiles were removed from the yellow supernatant *in vacuo*. The residue was extracted with C₆H₆ (3 × 0.5 mL), dried *in vacuo*, and dissolved in THF-*d*₈ (0.5 mL). The solution was transferred to an NMR tube and the tube was flame-sealed.

¹H NMR (500.2 MHz, THF-*d*₈): δ = 8.11 (br d, ³J_{HH} = 7.6 Hz, 2H, H-d), 7.82 (n.r., 2H, H-a), 7.21 (vtd, av. ³J_{HH} = 7 Hz, ⁴J_{HH} = 1.4 Hz, 2H, H-b), 7.01 (vtd, av. ³J_{HH} = 7 Hz, ⁴J_{HH} = 1.4 Hz, 2H, H-c), 1.35 (s, 3H, BCH₃), 1.01 (s, 12H, OC(CH₃)₂), 0.17 – 0.14 (m, 3H, pinBBCH₃).

¹¹B NMR (160.5 MHz, THF-*d*₈): δ = 62.4 (BCH₃), 41.8 (Bpin), –19.6 (pinBBCH₃).

¹³C{¹H} NMR (125.8 MHz, THF-*d*₈): δ = 181.2 (q, ¹J_{CB} = 41.4 Hz, C-f), 143.4 (br, C-e), 135.5 (C-d), 135.1 (C-a), 129.4 (C-b), 121.6 (C-c), 81.1 (OC(CH₃)₂), 25.0 (OC(CH₃)₂), 12.5 (q, ¹J_{BC} = 38.8 Hz, pinBBCH₃), 4.9 (br, BCH₃).

[Na(dme)]₂[7]:

X-ray quality crystals of [Na(dme)]₂[7] were grown by partial evaporation of a dimethoxyethane/diethyl ether solution of Na₂[3] at room temperature. NMR analysis (THF-*d*₈) of the residue obtained after full evaporation of the mother liquor *in vacuo* revealed the formation of Na₂[8].⁵ Apparently, a redistribution reaction takes place upon crystallization.

NMR data of re-dissolved crystals of Na₂[7]

¹H NMR (500.2 MHz, THF-*d*₈): $\delta = 7.18 - 7.12$ (m, 4H, H-a), 6.62 – 6.57 (m, 4H, H-b), 2.42 (q, ¹J_{BH} = 73.1 Hz, 2H, BH), 1.06 (s, 24H, OC(CH₃)₂).

¹¹B NMR (160.5 MHz, THF-*d*₈): $\delta = 40.4$ (Bpin), -23.3 (d, ¹J_{HB} = 73.1 Hz, BH).

¹³C{¹H} NMR (125.8 MHz, THF-*d*₈): $\delta = 158.6 - 156.8$ (m, C-f), 136.3 (C-a), 122.3 (C-b), 80.6 (OC(CH₃)₂), 25.1 (OC(CH₃)₂).

Additional information regarding the equilibrium between $M_2[R_2\text{-DBA}]$ and their HBpin-addition products

As mentioned above (Tables S1 and S2), the HBpin-activation products $M_2[X]$ ($X = 3, 4$) exist in a dynamic equilibrium with the starting materials $M_2[R_2\text{-DBA}]/\text{HBpin}$ ($M = \text{Li} - \text{K}$; $R = \text{H}, \text{Me}$). Furthermore, some of the products $M_2[4]$ tend to formally eliminate MH, leading to type-II structures $M[5]$ ($M = \text{Li}, \text{Na}$; $R = \text{Me}$). Since MH ($M = \text{Li}, \text{Na}$) is still soluble to some extent in THF, the question arises, whether addition of MH to the type-II structures can force the reaction back to the starting materials $M_2[R_2\text{-DBA}]$ and HBpin. To answer this question, we performed an exemplary reaction between $\text{Li}[5]$ and LiH :

In a glovebox, LiH (1 mg, 0.126 mmol) was added to a freshly prepared solution of $\text{Li}[5]$ (0.049 mmol) in $\text{THF-}d_8$ (0.5 mL). The color of the suspension turned from pale yellow to deep red within a few minutes. The NMR tube was flame-sealed. Already after 2 h, ^1H NMR spectroscopy revealed 50% conversion of $\text{Li}[5]$ to $\text{Li}_2[2]$ (see Figure S2); some of the released HBpin reacted further with the excess LiH to give $\text{Li}[\text{BH}_4]$ (not shown in Figure S2).

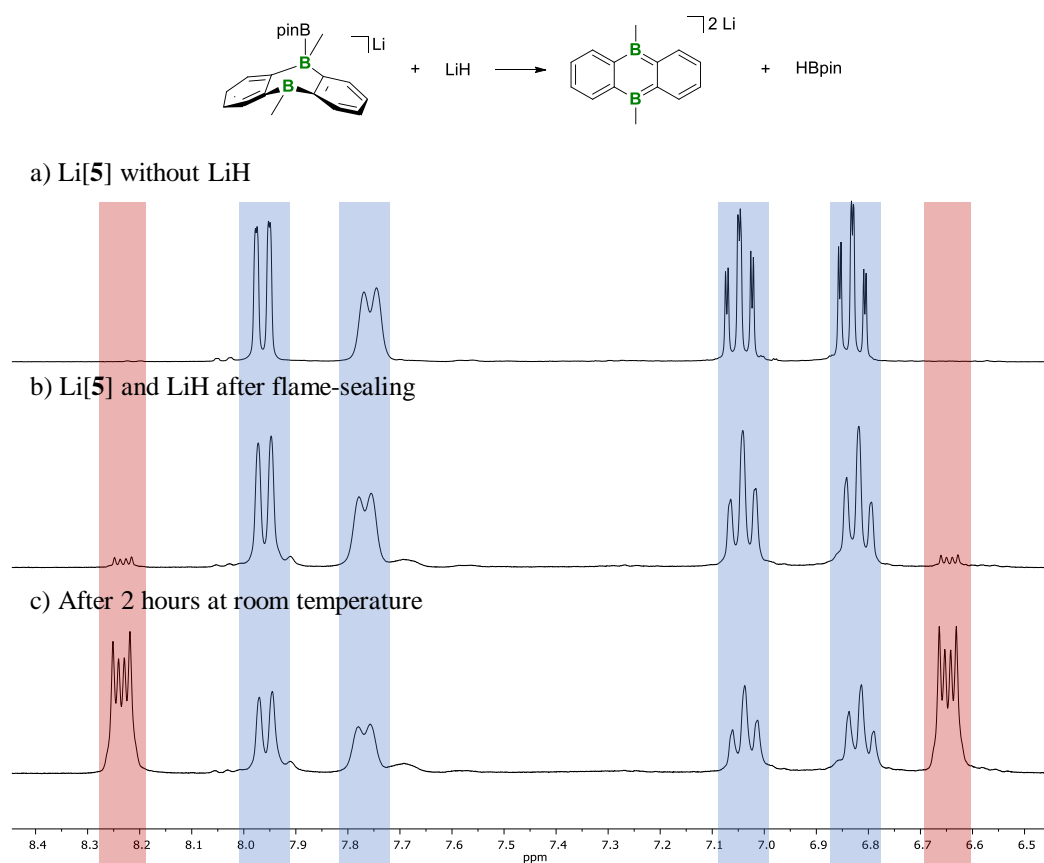


Figure S2. ^1H NMR spectra (300.0 MHz, $\text{THF-}d_8$) recorded on a) a sample of $\text{Li}[5]$ prior to the addition of LiH , b) the same sample after the addition of LiH and after flame-sealing of the NMR tube, and c) after further storage of the sample for 2 h at room temperature.

The tendency to eliminate HBpin from type-I structures depends on the counter cation ($\text{Li} \gg \text{Na} > \text{K}$) and the boron bonded substituent ($\text{Me} \gg \text{H}$). Therefore, 1 equiv. of HBpin is sufficient for quantitative conversion of $\text{Na}_2[\mathbf{1}]$ and $\text{K}_2[\mathbf{1}]$, while more than 1 equiv. of HBpin is required to achieve full conversion of $\text{Li}_2[\text{R}_2\text{-DBA}]$ ($\text{R} = \text{H}, \text{Me}$), $\text{Na}_2[\mathbf{2}]$, and $\text{K}_2[\mathbf{2}]$.

This finding may be explained as follows: The Li^+ cations form contact-ion pairs with $[\text{DBA}]^{2-}$ even in THF, whereas Na^+/K^+ form solvent-separated ion pairs.^{5,6} This leads to an increased stability of $\text{Li}_2[\text{DBA-R}_2]$, promoting HBpin elimination from $\text{Li}_2[\mathbf{X}]$ ($\mathbf{X} = \mathbf{3}, \mathbf{4}$; a similar trend was observed for the rates of H_2 transfer from H_2 -activation products of $\text{M}_2[\text{R}_2\text{-DBA}]$).⁵ In addition, bulkier substituents lead to higher steric congestion of type-I addition products, so that reductive elimination of HBpin is energetically favored for $\text{R} = \text{Me}$ relative to $\text{R} = \text{H}$.

2. Reactivity of the type-II compound Li[5] and considerations regarding a possible hydroboration catalysis

The reaction between Li[5] and LiH shown above can be seen either as a reductive elimination of HBpin from the type-I intermediate Li₂[4] or as a transfer of [Bpin]⁺ to a hydride anion. Transfer of a [Bpin]⁺ moiety also to other suitable nucleophiles would regenerate Li₂[2] and thus could ultimately lead to hydroboration catalysis. We therefore performed further experiments to gain more insight into the reactivity of Li[5].

Reaction of Li[5] with Ph₃SiLi

Ph₃SiLi was prepared by stirring Ph₃SiCl (15 mg, 0.051 mmol) with an exc. of Li granules (8 mg, 1.15 mmol) in THF-*d*₈ (0.5 mL) for 3 h at room temperature.⁷ The dark brown solution was separated from unconsumed Li metal and added to an NMR tube charged with solid Li[5]·0.25 THF (18 mg, 0.051 mmol). The reaction mixture turned deep red within 10 min. The NMR tube was flame-sealed. ¹H and ¹¹B NMR analysis revealed the signals of Li₂[2]⁴ and Ph₃SiBpin⁸ along with the resonances of the starting materials and other species. After storage overnight at room temperature, the sample contained almost exclusively Li₂[2] and Ph₃SiBpin (Figure S3).

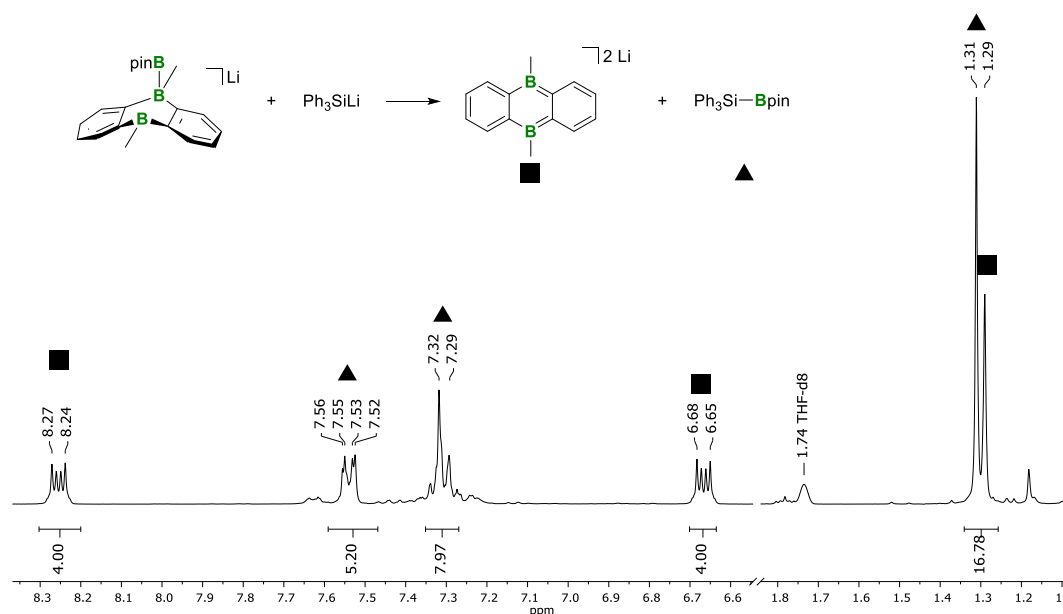


Figure S3. ¹H NMR spectrum (300.0 MHz, THF-*d*₈) recorded on the reaction mixture of Li[5] and Ph₃SiLi after storage for one night at room temperature.

This reaction shows that Li[5] can be considered as a [Bpin]⁺ source. This unusual “inverse” reactivity of an sp²-sp³ diborane is unprecedented. To further substantiate the polarity-inverted nature of the Bpin substituent, we prepared the corresponding hydridoborate Li[6] and tested whether it can be deprotonated.

Synthesis of Li[6]

In a glovebox, **2** (10 mg, 0.049 mmol) and exc. LiH (7 mg, 0.9 mmol) were placed in a screw-capped vial, suspended in THF-*d*₈ (0.5 mL), and stirred overnight at room temperature. Unconsumed LiH was removed with the aid of a syringe filter, and the filtrate was used for follow-up reactions and NMR analysis without further treatment. For growth of single crystals, the NMR sample was evaporated to dryness in the glovebox and re-dissolved in C₆H₆/dimethoxyethane in the presence of 12-crown-4. X-ray quality crystals of [Li(12-c-4)₂][**6**]·C₆H₆ formed upon partial evaporation of the solution.

¹H NMR (500.2 MHz, THF-*d*₈): δ = 7.94 (d, ³J_{HH} = 7.3 Hz, 2H, H-d), 7.69 (n.r., 2H, H-a), 7.06 (vt, av. ³J_{HH} = 7 Hz, 2H, H-b), 6.86 (vt, av. ³J_{HH} = 7 Hz, 2H, H-c), 2.49 (q, ¹J_{HB} = 74.5 Hz, 1H, BH), 1.26 (s, 3H, BCH₃), -0.01 (n.r., 3H, HBCH₃).

¹¹B NMR (160.5 MHz, THF-*d*₈): δ = 60.8 (*h*_{1/2} = 800 Hz, BCH₃), -16.5 (d, ¹J_{BH} = 74.5 Hz, HBCH₃).

¹³C{¹H} NMR (125.8 MHz, THF-*d*₈): δ = 181.7 (q, ¹J_{CB} = 49.5 Hz, C-f), 144.5 (C-e), 134.5 (C-d), 134.4 (C-a), 128.4 (C-b), 120.8 (C-c), 10.6 (q, ¹J_{CB} = 40.8 Hz, HBCH₃), 4.7 (BCH₃).

Deprotonation of Li[6]

The deprotonation of Li[**6**] is possible at elevated temperatures with Li[C(SiMe₃)₃] and amide: a) Deprotonation of Li[**6**] with the extremely bulky methanide base is quantitative. b) The deprotonation with amide represents the final step of the DBA-catalyzed hydrogenation of imine Ph(H)₂C=N*t*Bu.⁵

Synthesis of Ph(H)₂C–N(Li)*t*Bu

n-BuLi (2.51 M in hexane, 2.2 mL, 5.5 mmol) was added dropwise at -78 °C to a solution of Ph(H)₂C–N(H)*t*Bu (1.0 mL, 5.5 mmol) in THF (15 mL). The colorless solution immediately adopted a pink color. The reaction mixture was allowed to warm to room temperature overnight, all volatiles were removed *in vacuo*, and the remaining orange solid was collected in a glovebox (1.000 g, 75%, obtained as [Li(thf)][Ph(H)₂C–N*t*Bu]). X-ray quality crystals of dimeric {[Li(thf)][Ph(H)₂C–N*t*Bu]}₂ were grown by slow evaporation of a THF solution of Ph(H)₂C–N(Li)*t*Bu.

Note: The amount of thf ligands can vary and should be confirmed by NMR spectroscopy before the amide salt is used. The compound is very sensitive towards air and moisture, but stable for weeks in an argon-filled glovebox. Upon prolonged storage (over months), the color of the solid changed to dark brown and ¹H NMR analysis showed a significant amount of Ph(H)₂C–N(H)*t*Bu. We therefore recommend to prepare the compound fresh before use.

¹H NMR (300.0 MHz, THF-*d*₈): δ = 7.23 – 7.14 (m, 2H, Ph-H-*o*), 7.09 – 7.00 (m, 2H, Ph-H-*m*), 6.97 – 6.89 (m, 1H, Ph-H-*p*), 3.76 (s, 2H, CH₂), 0.86 (s, 9H, C(CH₃)₃).

¹³C{¹H} NMR (75.4 MHz, THF-*d*₈): δ = 152.4 (Ph-C-*i*), 128.6 (Ph-C-*o*), 128.1 (Ph-C-*m*), 125.3 (Ph-C-*p*), 55.3 (CH₂), 53.8 (C(CH₃)₃), 32.6 (C(CH₃)₃).

Deprotonation with $[\text{Li}(\text{thf})_2][\text{C}(\text{SiMe}_3)_3]$

A freshly prepared solution of $\text{Li}[6]$ (0.049 mmol) in $\text{THF-}d_8$ (0.5 mL) was placed in a screw-capped vial, treated with neat solid $[\text{Li}(\text{thf})_2][\text{C}(\text{SiMe}_3)_3]$ (17 mg, 0.044 mmol), and stirred until a clear solution was formed. The reaction mixture was transferred to an NMR tube and the tube was flame-sealed. No reaction took place at room temperature. After heating the NMR tube at 115 °C for 35 h, NMR spectroscopy showed the quantitative formation of $\text{Li}_2[2]$ along with the protonation product TMS_3CH . Figure S4 shows the ^1H NMR spectrum recorded on the reaction mixture after temperature treatment.

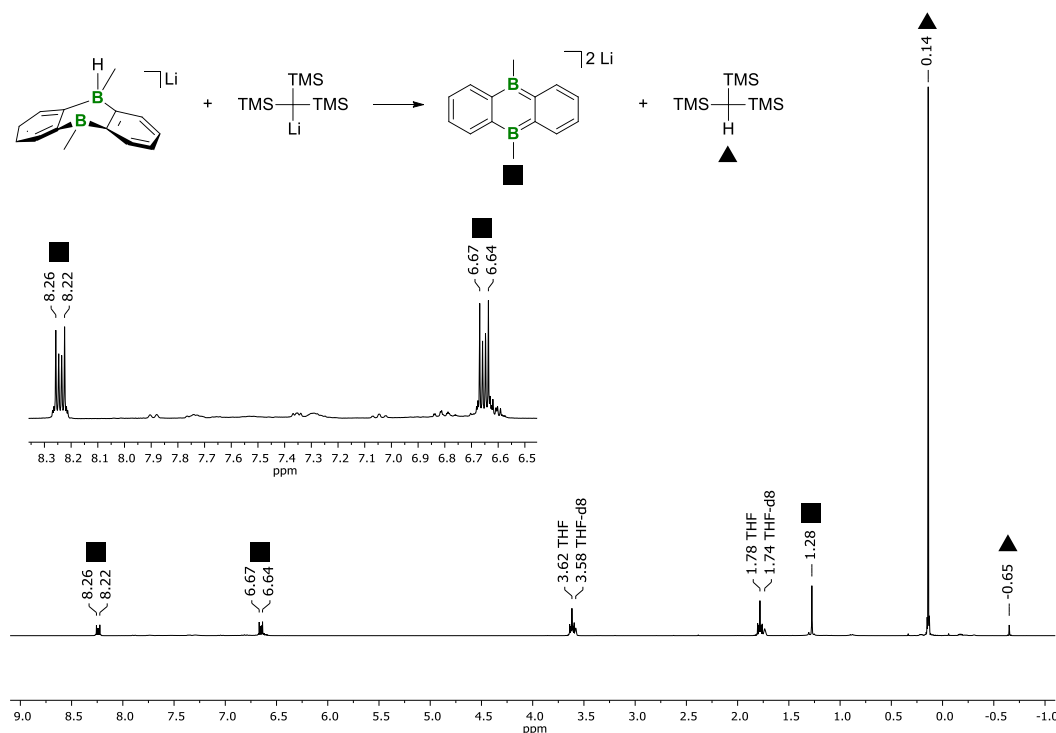


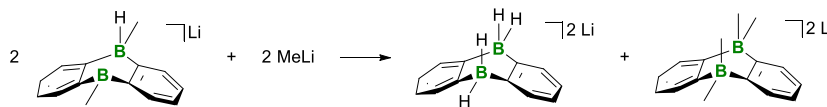
Figure S4. ^1H NMR spectrum (300.0 MHz, $\text{THF-}d_8$) recorded on the reaction mixture of $\text{Li}[6]$ and $[\text{Li}(\text{thf})_2][\text{C}(\text{SiMe}_3)_3]$ after 35 h at 115 °C.

Deprotonation with $\text{Ph}(\text{H})_2\text{C-N}(\text{Li})t\text{Bu}$

A freshly prepared solution of $\text{Li}[6]$ (0.059 mmol) in $\text{THF-}d_8$ (0.5 mL) was placed in a screw-capped vial, treated with neat solid $\text{Ph}(\text{H})_2\text{C-N}(\text{Li})t\text{Bu} \cdot 0.35 \text{ THF}$ (11 mg, 0.057 mmol), and stirred until a clear solution was formed. The reaction mixture was transferred to an NMR tube and the tube was flame-sealed. No deprotonation reaction took place at room temperature. After heating the NMR tube at 115 °C for 19 h, NMR spectroscopy showed the formation of $\text{Li}_2[2]$ along with the protonation product $\text{Ph}(\text{H})_2\text{C-N}(\text{H})t\text{Bu}$.

H/Me scrambling in mixtures of Li[6] and MeLi

In the course of the deprotonation experiments on Li[6], we observed substituent redistribution reactions when employing smaller Lewis bases (e.g., MeLi, see Scheme S1). Since this observation is reminiscent of the formation of Na₂[7] from Na₂[4] (*vide supra*), a more detailed investigation was performed.



Scheme S1. MeLi-induced substituent redistribution reactions starting from Li[6].

Substituent redistribution in Li[6]/MeLi mixtures

An NMR tube was charged with a freshly prepared THF solution (0.5 mL) of Li[6] (0.049 mmol). MeLi (1.6 M in Et₂O, 31 μ L, 0.050 mmol) was added, all volatiles were removed under reduced pressure, and the solid residue was re-dissolved in THF-*d*₈ (0.5 mL). The NMR tube was flame-sealed. NMR spectroscopy revealed the formation of a 1:1 mixture of Li₂[11]⁵ and Li₂[10].

An authentic sample of Li₂[10] was independently synthesized from **2** and MeLi:

MeLi (1.6 M in Et₂O, 48 μ L, 0.077 mmol) was added to an NMR tube charged with a THF solution (0.4 mL) of **2** (8 mg, 0.039 mmol). After removal of all volatiles, the solid residue was re-dissolved in THF-*d*₈ (0.5 mL), the NMR tube was flame-sealed, and NMR spectra were recorded. X-ray quality crystals of [Li(thf)₄][Li(thf)₂DBA-Me₄] were subsequently obtained by gas-phase diffusion of *n*-hexane into the THF-*d*₈ solution.

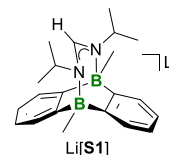
¹H NMR (500.2 MHz, THF-*d*₈): δ = 7.41 – 7.35 (m, 4H, H-a), 6.67 – 6.61 (m, 4H, H-b) –0.10 – (–0.15) (br, 12H, CH₃).

¹¹B NMR (160.5 MHz, THF-*d*₈): δ = –18.1.

¹³C {¹H} NMR (125.8 MHz, THF-*d*₈): δ = 165.1 (q, ¹J_{CB} = 46.1 Hz, C-e), 133.5 (C-a), 122.0 (C-b), 19.1 (q, ¹J_{CB} = 39.4 Hz, BCH₃).

Hydride abstraction from Li[6] with *i*PrN=C=N*i*Pr: Synthesis of Li[S1]

*i*PrN=C=N*i*Pr (15.5 μ L, 0.100 mmol) was added to an NMR tube charged with a freshly prepared THF solution (0.5 mL) of Li[6] (0.049 mmol). All volatiles were removed *in vacuo*, the solid residue was re-dissolved in THF-*d*₈ (0.5 mL), the NMR



tube was flame-sealed, and NMR spectra were recorded. X-ray quality crystals of [Li(12-c-4)₂][S1]·THF were obtained by slow evaporation of a THF solution of Li[S1] containing 12-crown-4.

¹H NMR (500.2 MHz, THF-*d*₈): δ = 7.19 – 7.15 (m, 4H, H-a), 6.88 (s, 1H, NCHN), 6.63 – 6.59 (m, 4H, H-b), 3.93 (sept, 2H, ³J_{HH} = 6.7 Hz, CH(CH₃)₂), 0.93 (d, 12H, ³J_{HH} = 6.7 Hz, CH(CH₃)₂), 0.32 (br s, 6H, BCH₃).

¹¹B NMR (160.5 MHz, THF-*d*₈): δ = -9.6.

¹³C{¹H} (125.8 MHz, THF-*d*₈): δ = 164.5 (br, C-e), 151.0 (NCHN), 126.5 (C-a), 122.1 (C-b), 49.1 (CH(CH₃)₂), 24.8 (CH(CH₃)₂), 6.1 (br, BCH₃).

3. Hydroboration reactions with DBA derivatives

3.1 General procedures and characterization data

General procedure for the hydroboration of unsaturated substrates with Li₂[**2**] (25 mol%) in an NMR tube:

Note: The reactions can be carried out equally well with 5 mol% of the catalyst. Herein, we consistently used 25 mol% in order to have a chance to detect some of the reaction intermediates by NMR spectroscopy.

A freshly prepared THF-*d*₈ solution (0.5 mL) of Li₂[**2**] (0.049 mmol) was transferred to an NMR tube. The respective substrate (0.20 mmol) and neat HBpin (40 μL, 0.28 mmol) were added sequentially at room temperature. The NMR tube was flame-sealed and the reaction progress was monitored by NMR spectroscopy. Those reactions that showed no progress at room temperature were heated in an oven at the temperature and for the time periods given in Table S3.

Table S3. Overview of the catalytic hydroboration reactions using Li₂[**2**] (25 mol%) and HBpin; the required reaction temperatures and times are also given.*

substrate	<i>m</i> / mg	<i>V</i> / μl	<i>T</i> / °C	<i>t</i> / h	yield / %**
Ph ₂ C=CH ₂	36	35	r.t.	21	93
Ph ₂ C=O	36	–	r.t.	< 0.1	64
<i>i</i> PrN=C=N <i>i</i> Pr	24	30	r.t.	< 0.1	–
<i>i</i> PrN=C=N <i>i</i> Pr***	24	30	100	23	–
Ph(H)C=NPh	36	–	r.t.	4	71
Ph(H)C=N <i>t</i> Bu****	32	35	100	88	–

*It has been confirmed that in the absence of Li₂[**2**] either no hydroboration occurs or the reaction proceeds much more slowly than reported here (cf. chapter 3.3).

**Given that 25 mol% of the DBA catalyst is present in the reaction mixtures, the maximum yield of hydroboration of substrates forming irreversible [4+2] cycloadducts with the catalyst is 75%. In cases where higher yields are obtained, the cycloadduct formation must be partially reversible. To illustrate this point, we emphasize that hydroboration of Ph₂C=CH₂ is 75% complete after 21 h at room temperature; to achieve yields > 90%, the reaction has to be continued for two more days. The yields correspond to the compound isolated after workup.

***68 μL HBpin (0.47 mmol) were used to obtain the doubly hydroborated product.

**** After 45 h at 100 °C, the conversion of Ph(H)C=N*t*Bu was 85% complete.

NMR-spectroscopic characterization of the hydroboration products



^1H NMR (300.0 MHz, THF- d_8): δ = 7.23 – 7.15 (m, 8H, Ph), 7.11 – 7.05 (m, 2H, Ph), 1.64 (s, 3H, CH_3), 1.18 (s, 12H, $\text{OC}(\text{CH}_3)_2$).

^{11}B NMR (96.3 MHz, THF- d_8): δ = 32.0 ($h_{1/2}$ = 240 Hz).

$^{13}\text{C}\{^1\text{H}\}$ NMR (75.4 MHz, THF- d_8): δ = 148.6, 129.1, 128.3, 125.7, 84.2, 26.0, 24.6; n.o. CB.

All volatiles were removed from the reaction mixture *in vacuo* and the residue was purified by flash chromatography (eluent cyclohexane/ethyl acetate 19:1). The colorless solid (56 mg, 93%) was reinvestigated by NMR spectroscopy in CDCl_3 to ensure full comparability with the literature data:⁹

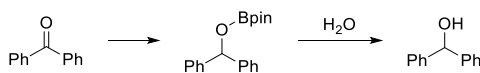
^1H NMR (400.1 MHz, CDCl_3): δ = 7.32 – 7.22 (m, 8H, Ph), 7.22 – 7.15 (m, 2H, Ph), 1.71 (s, 3H, CH_3), 1.22 (s, 12H, $\text{OC}(\text{CH}_3)_2$).

^{11}B NMR (128.4 MHz, CDCl_3): δ = 34.0 ($h_{1/2}$ = 250 Hz).

$^{13}\text{C}\{^1\text{H}\}$ NMR (100.6 MHz, CDCl_3): δ = 147.8, 128.7, 128.1, 125.5, 83.9, 25.9, 24.6; n.o. CB.

The NMR data in CDCl_3 are in accordance with the literature.⁹

HRMS: 308.19294 (found); 308.19421 (calc. $[\text{C}_{20}\text{H}_{25}\text{B}_1\text{O}_2]^+$).



Bpin-containing primary product:

^1H NMR (300.0 MHz, THF- d_8): δ = 7.38 – 7.31 (m, 4H, Ph), 7.29 – 7.22 (m, 4H, Ph), 7.21 – 7.16 (m, 2H, Ph), 6.17 (s, 1H, CH), 1.17 (s, 12H, $\text{OC}(\text{CH}_3)_2$).

^{11}B NMR (96.3 MHz, THF- d_8): δ = 22.5 ($h_{1/2}$ = 170 Hz).

$^{13}\text{C}\{^1\text{H}\}$ NMR (75.4 MHz, THF- d_8): δ = 144.3, 128.7, 127.7, 127.1, 83.2, 78.5, 24.7.

The NMR data in THF- d_8 are in accordance with the literature.¹⁰

The reaction mixture was transferred to a round-bottom flask. A few drops of HCl (10 % in water) were added and the solvent was evaporated. The residue was purified two times by flash chromatography (eluent cyclohexane/ethyl acetate 9:1 and 19:1) to obtain the free alcohol as a colorless solid (23.3 mg, 64 %).

Free alcohol:

^1H NMR (400.1 MHz, CDCl_3): δ = 7.39 – 7.30 (m, 8H, Ph), 7.29 – 7.23 (m, 2H, Ph), 5.83 (s, 1H, CH), 2.28 (s, 1H, OH).

$^{13}\text{C}\{^1\text{H}\}$ NMR (100.6 MHz, CDCl_3): δ = 143.9, 128.6, 127.7, 126.7, 76.4.

The NMR data in CDCl_3 are in accordance with the literature.¹¹

HRMS: 185.09589 (found); 185.09609 (calc. $[\text{C}_{13}\text{H}_{12}\text{O}_1+\text{H}]^+$).



^1H NMR (300.0 MHz, THF- d_8): δ = 7.80 (s, 1H, NCHN), 4.51 (sept, $^3J_{\text{HH}}$ = 6.7 Hz, 1H, $\text{CH}(\text{CH}_3)_2$), 3.23 (sept, $^3J_{\text{HH}}$ = 6.2 Hz, 1H, $\text{CH}(\text{CH}_3)_2$), 1.24 (s, 12H, $\text{OC}(\text{CH}_3)_2$), 1.21 (d, $^3J_{\text{HH}}$ = 6.7 Hz, 6H, $\text{CH}(\text{CH}_3)_2$), 1.05 (d, $^3J_{\text{HH}}$ = 6.2 Hz, 6H, $\text{CH}(\text{CH}_3)_2$).

^{11}B NMR (96.3 MHz, THF- d_8): δ = 23.2 ($h_{1/2}$ = 170 Hz).

$^{13}\text{C}\{^1\text{H}\}$ NMR (75.4 MHz, THF- d_8): 150.0 (NCHN), 83.3 ($\text{OC}(\text{CH}_3)_2$), 57.3 (NCH(CH_3) $_2$), 43.7 (NCH(CH_3) $_2$), 25.6 ($\text{CH}(\text{CH}_3)_2$), 24.6 ($\text{OC}(\text{CH}_3)_2$), 21.5 ($\text{CH}(\text{CH}_3)_2$).

X-ray quality crystals were obtained by sublimation from the reaction mixture at 10^{-3} mbar. The cell parameters were in line with literature data (CSD code: AKIFIL).¹² The crystals were picked manually and dissolved in C_6D_6 for comparison with published NMR data.

^1H NMR (300.0 MHz, C_6D_6): δ = 8.28 (s, 1H, NCHN), 5.00 (sept, $^3J_{\text{HH}}$ = 6.8 Hz, 1H, BNCH(CH_3) $_2$), 3.32 (sept, $^3J_{\text{HH}}$ = 6.2 Hz, 1H, NCH(CH_3) $_2$), 1.46 (d, $^3J_{\text{HH}}$ = 6.8 Hz, 6H, BNCH(CH_3)), 1.21 (d, $^3J_{\text{HH}}$ = 6.2 Hz, 6H, NCH(CH_3)), 1.03 (s, 12H, $\text{OC}(\text{CH}_3)_2$).

^{11}B NMR (96.3 MHz, C_6D_6): δ = 25.5 (s, $h_{1/2}$ = 120 Hz).

$^{13}\text{C}\{^1\text{H}\}$ NMR (75.4 MHz, C_6D_6): δ = 150.0 (NCHN), 82.7 ($\text{OC}(\text{CH}_3)_2$), 57.3 (BNCH(CH_3) $_2$), 43.7 (NCH(CH_3) $_2$), 25.7 (BNCH(CH_3) $_2$), 24.5 ($\text{OC}(\text{CH}_3)_2$), 21.9 (NCH(CH_3) $_2$).

The NMR data in C_6D_6 are in accordance with the literature.¹²

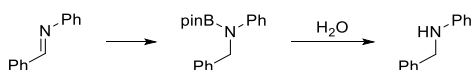


^1H NMR (300.0 MHz, THF- d_8): δ = 4.13 (s, 2H, CH_2), 3.30 (sept, $^3J_{\text{HH}}$ = 6.7 Hz, 2H, $\text{CH}(\text{CH}_3)_2$), 1.21 – 1.14 (m, 36H, $4 \times \text{OC}(\text{CH}_3)_2$ and $2 \times \text{CH}(\text{CH}_3)_2$).

^{11}B NMR (96.3 MHz, THF- d_8): δ = 22.6 ($h_{1/2}$ = 330 Hz).

$^{13}\text{C}\{^1\text{H}\}$ NMR (75.4 MHz, THF- d_8) δ = 81.9, 59.6, 47.1, 24.6, 23.0.

The NMR data in THF- d_8 are in accordance with the literature.¹⁰



Bpin-containing product:

^1H NMR (300.0 MHz, THF- d_8): δ = 7.27 – 7.19 (m, 6H, Ph), 7.11 – 7.04 (m, 2H, Ph), 6.83 – 6.74 (m, 2H, Ph), 4.70 (s, 2H, CH_2), 1.29 (s, 12H, $\text{OC}(\text{CH}_3)_2$).

^{11}B NMR (96.3 MHz, THF- d_8): δ = 23.2 ($h_{1/2}$ = 200 Hz).

$^{13}\text{C}\{^1\text{H}\}$ NMR (75.4 MHz, THF- d_8): δ = 146.9, 141.3, 128.8, 128.7, 127.0, 126.9, 121.5, 121.0, 83.4, 51.3, 24.7.

The NMR data in THF- d_8 are in accordance with the literature.^{10,13}

The reaction mixture was transferred to a round-bottom flask. A few drops of water were added, and the solvent was evaporated. The residue was purified two times by flash chromatography (eluent cyclohexane/CH₂Cl₂ 99:1 and 49:1) to obtain the free amine as a colorless oil (25.6 mg, 71 %).

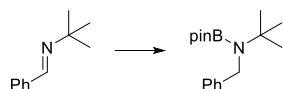
Free amine:

¹H NMR (400.1 MHz, CDCl₃): δ = 7.43 – 7.34 (m, 4H, Ph), 7.34 – 7.27 (m, 1H, Ph), 7.23 – 7.17 (m, 2H, Ph), 6.78 – 6.71 (m, 1H, Ph), 6.69 – 6.64 (m, 2H, Ph), 4.36 (s, 2H, CH₂), 4.04 (br s, 1H, NH),

¹³C{¹H} NMR (100.6 MHz, CDCl₃): 148.3, 139.6, 129.4, 128.8, 127.6, 127.4, 117.7, 113.0, 45.8.

The NMR data in CDCl₃ are in accordance with the literature.¹⁴

HRMS: 184.11206 (found); 184.11208 (calc. [C₁₃H₁₃N₁+H]⁺).



¹H NMR (300.0 MHz, THF-*d*₈): δ = 7.30 – 7.18 (m, 4H, Ph), 7.16 – 7.04 (m, 1H, Ph), 4.24 (s, 2H, CH₂), 1.22 (s, 12H, OC(CH₃)₂), 1.19 (s, 9H, C(CH₃)₃).

¹¹B NMR (96.3 MHz, THF-*d*₈): δ = 23.2 (*h*_{1/2} = 200 Hz).

The NMR data in THF-*d*₈ are comparable to those reported in the literature, although they were recorded in CDCl₃.¹⁵

3.2 Additional experimental data regarding the hydroboration reactions

Interaction between selected substrates and $\text{Li}_2[2]$:

In the course of $\text{Li}_2[2]$ -catalyzed hydroboration reactions, NMR signals assignable to [4+2] cycloadducts between $\text{Li}_2[2]$ and the substrates (except $\text{Ph}(\text{H})\text{C}=\text{N}t\text{Bu}$ and $i\text{PrN}(\text{Bpin})-\text{C}(\text{H})=\text{N}i\text{Pr}$) were observed (see Figure S5 for the exemplary case of $\text{Ph}(\text{H})\text{C}=\text{NPh}$ as substrate). In all these cases, the hydroboration reactions did not require elevated temperatures, but proceeded smoothly already at room temperature. In contrast, heating was necessary to achieve hydroboration of $\text{Ph}(\text{H})\text{C}=\text{N}t\text{Bu}$ and the second hydroboration of $i\text{PrN}=\text{C}=\text{N}i\text{Pr}$.

We therefore assumed that, whenever formed, the individual [4+2] cycloadducts are the actual catalysts (cf. Mechanism II in Figure 5), whereas in the cases of $\text{Ph}(\text{H})\text{C}=\text{N}t\text{Bu}$ and $i\text{PrN}(\text{Bpin})-\text{C}(\text{H})=\text{N}i\text{Pr}$, hydroboration involves the activation of HBpin by $\text{Li}_2[2]$ (cf. Mechanism I in Figure 4). To test this working hypothesis, we performed a number of control experiments:

Experiment 1: The pre-formed [4+2] cycloadduct between $\text{Li}_2[2]$ and $\text{Ph}(\text{H})\text{C}=\text{NPh}$ was successfully employed to catalyze the hydroboration of $\text{Ph}(\text{H})\text{C}=\text{NPh}$. The resonances of the cycloadduct $\text{Li}_2[12]$ were detectable over the whole time period (Figure S5).

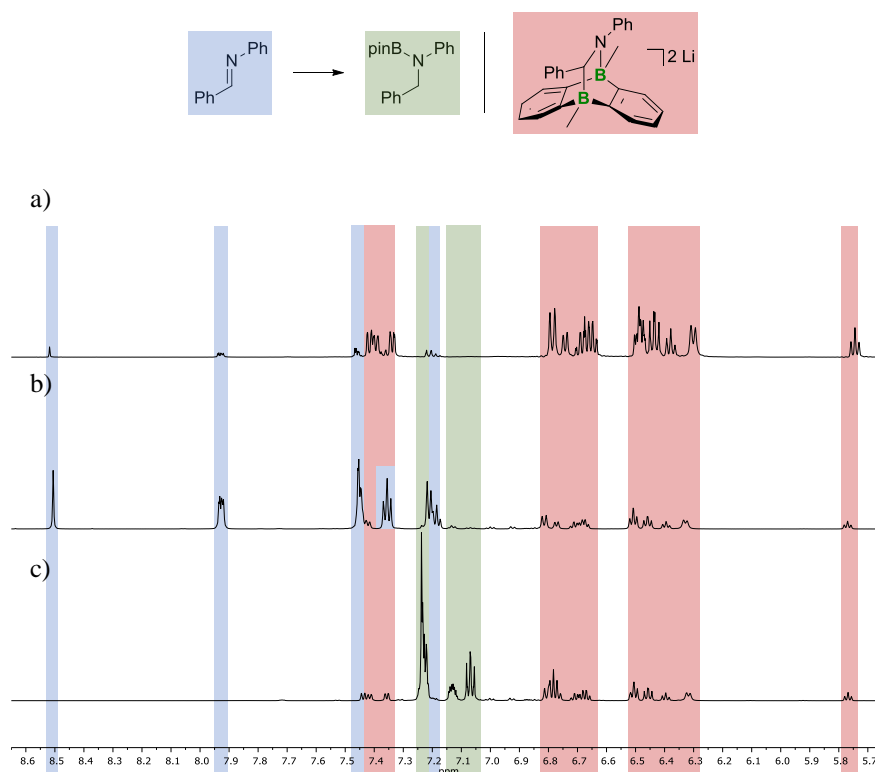


Figure S5. ^1H NMR spectra (500.2 MHz/600.3 MHz/600.3 MHz, $\text{THF}-d_8$) recorded on a) a 1:1 mixture of $\text{Li}_2[2]$ and $\text{Ph}(\text{H})\text{C}=\text{NPh}$ (containing traces of residual free $\text{Ph}(\text{H})\text{C}=\text{NPh}$, because a perfectly equimolar stoichiometry was not achieved), b) the same sample immediately after the addition of further $\text{Ph}(\text{H})\text{C}=\text{NPh}$ (3 equiv.) and of HBpin (5.6 equiv.), and c) the previous sample after storage at room temperature for 4 h.

Experiment 2: The [4+2] cycloadduct between $\text{Li}_2[\mathbf{2}]$ and benzophenone ($\text{Li}_2[\mathbf{13}]$) was successfully used to catalyze the hydroboration of $\text{Ph}(\text{H})\text{C}=\text{NPh}$. According to NMR spectroscopy (Figure S6), $\text{Ph}(\text{H})_2\text{C}-\text{N}(\text{Bpin})\text{Ph}$ was the only hydroboration product; the catalyst remained intact (room temperature, 3 d). This crossover experiment confirms that free benzophenone is not released during the catalytic cycle, because otherwise also $\text{Ph}_2(\text{H})\text{C}-\text{OBpin}$ should have been detectable. Spectrum b) shows unconsumed $\text{Ph}(\text{H})\text{C}=\text{NPh}$ along with the product; spectrum c) proves that the imine has been fully consumed and the relative amount of $\text{Ph}(\text{H})_2\text{C}-\text{N}(\text{Bpin})\text{Ph}$ has increased.

$\text{Li}_2[\mathbf{13}]$ was synthesized according to literature from $\text{Li}_2[\mathbf{2}]$ (10 mg, 0.049 mmol) and $\text{Ph}_2\text{C}=\text{O}$ (9 mg, 0.049 mmol) in $\text{THF-}d_8$ (0.5 mL).⁴ The solution was transferred to an NMR tube charged with $\text{Ph}(\text{H})\text{C}=\text{NPh}$ (18mg, 0.099 mmol). HBpin (14 μL , 0.097 mmol) was added and the NMR tube was flame-sealed.

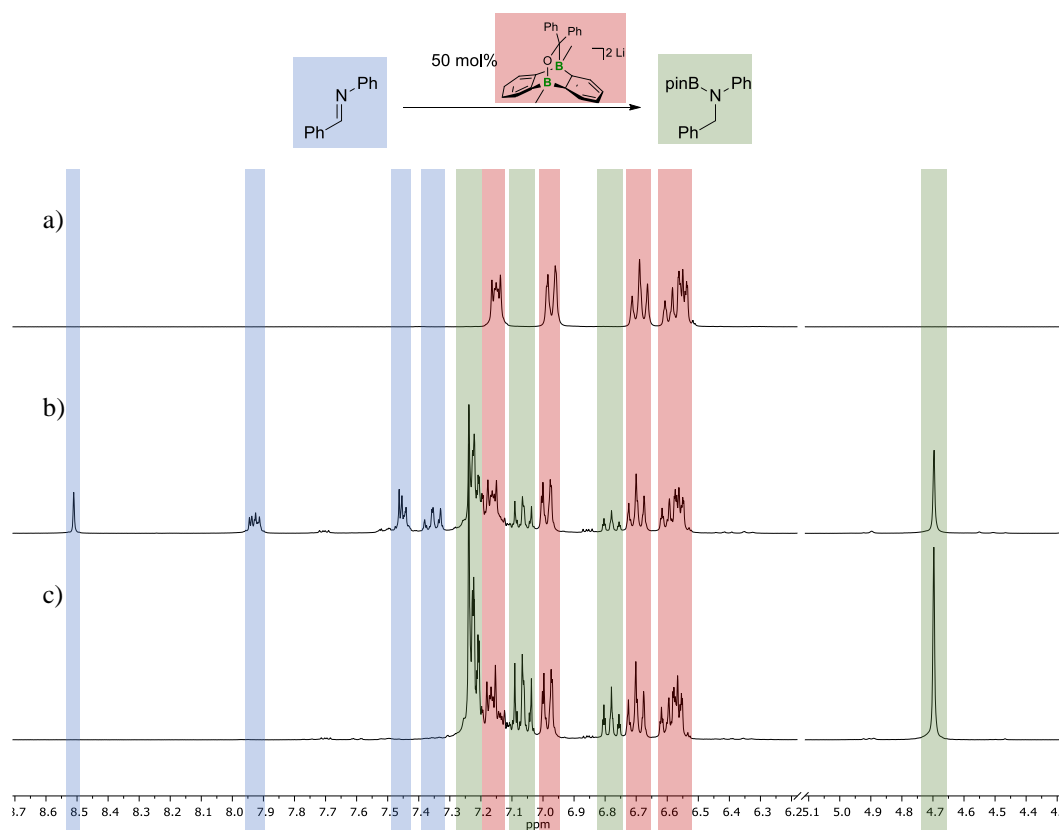


Figure S6. ^1H NMR spectra (300.0 MHz, $\text{THF-}d_8$) recorded on a) $\text{Li}_2[\mathbf{13}]$ without added $\text{Ph}(\text{H})\text{C}=\text{NPh}$ and HBpin, b) the same sample 40 min after the addition of $\text{Ph}(\text{H})\text{C}=\text{NPh}$ and HBpin, and c) the same sample 3 d later.

Experiment 3: A second crossover experiment revealed that also the less polar [4+2] cycloadduct between $\text{Li}_2[\mathbf{2}]$ and ethylene ($\text{Li}_2[\mathbf{14}]$) catalyzes the hydroboration of $\text{Ph}(\text{H})\text{C}=\text{NPh}$. The overall performance of the catalyst did not change significantly upon addition of 12-crown-4 or replacement of Li^+ with $[\text{nBu}_4\text{N}]^+$. To a first approximation, counter-cation effects are therefore negligible for reactions proceeding by Mechanism II. We take this as a justification for omitting the counter cations in corresponding quantum-chemical calculations.

$\text{Li}_2[\mathbf{14}]$ was synthesized according to literature from $\text{Li}_2[\mathbf{2}]$ (10 mg, 0.049 mmol) and exc. ethylene (1 atm) in $\text{THF-}d_8$ (0.5 mL).⁵ NMR spectra were recorded to confirm the successful [4+2] cycloaddition. The sample was evaporated to dryness *in vacuo* to ensure complete removal of unconsumed ethylene, the remaining solid was re-dissolved in $\text{THF-}d_8$ (0.5 mL), and the solution was transferred to an NMR tube charged with $\text{Ph}(\text{H})\text{C}=\text{NPh}$ (36 mg, 0.20 mmol). HBpin (40 μL , 0.28 mmol) was added and the NMR tube was flame-sealed. NMR spectroscopy revealed quantitative conversion of $\text{Ph}(\text{H})\text{C}=\text{NPh}$ to $\text{Ph}(\text{H})_2\text{C}-\text{N}(\text{Bpin})\text{Ph}$ within 1 d at room temperature without detectable loss of $\text{Li}_2[\mathbf{14}]$.

Preparation of [4+2] cycloadducts between $\text{Li}_2[\mathbf{2}]$ and all the unsaturated substrates

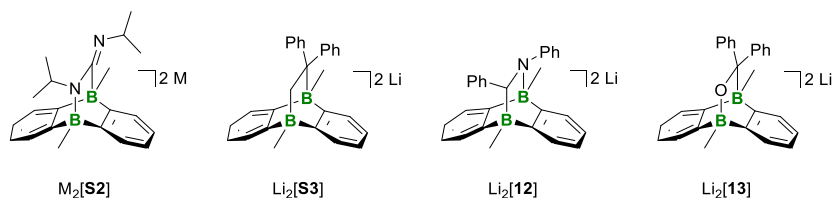
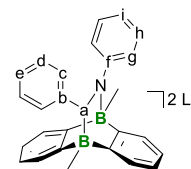


Figure S7. [4+2] cycloadducts $\text{Li}_2[\mathbf{S2}]$, $\text{Li}_2[\mathbf{S3}]$, $\text{Li}_2[\mathbf{12}]$, and $\text{Li}_2[\mathbf{13}]$.

The cycloadducts $\text{Li}_2[\mathbf{13}]$,⁴ and $\text{Li}_2[\mathbf{S3}]$ ⁵ have already been published by our group.

$\text{Li}_2[\mathbf{12}]$ A freshly prepared solution of $\text{Li}_2[\mathbf{2}]$ (0.074 mmol) in $\text{THF-}d_8$ (0.5 mL) was transferred to an NMR tube charged with $\text{Ph}(\text{H})\text{C}=\text{NPh}$ (13 mg, 0.072 mmol). The color of the solution immediately changed from dark red to light brown. The NMR tube was flame-sealed. NMR spectroscopy revealed the quantitative consumption of the starting materials and the selective formation of the cycloadduct.



Attempts at growing single crystals of the addition product $\text{Li}_2[\mathbf{12}]$ from THF in the presence of 12-crown-4 resulted in crystals of the *N*-protonated salt $[\text{Li}(\text{12-c-4})_2][\mathbf{12H}]$ (Figure S85). Our group has already reported a similar observation in the crystallization of the [4+2] cycloadduct between $\text{Ph}(\text{H})\text{C}=\text{N}t\text{Bu}$ and $\text{Li}_2[\mathbf{2}]$.⁵ We speculate that Li^+ coordination by the crown ether drastically increases the basicity of the tricyclic amine; although the crown ether had been stored over molecular sieves (3 Å) for months, it may still have contained trace amounts of water as proton source.

NMR data of Li₂[**12**]

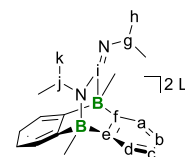
¹H NMR (500.2 MHz, THF-*d*₈): δ = 7.43 – 7.41 (m, 1H, DBA), 7.41 – 7.38 (m, 1H, DBA), 7.35 – 7.32 (m, 1H, DBA), 6.81 – 6.76 (m, 2H, H-g), 6.76 – 6.72 (m, 1H, DBA), 6.71 – 6.63 (m, 3H, DBA), 6.51 – 6.46 (m, 3H, 2x H-d and 1x DBA), 6.45 – 6.42 (m, 2H, H-h), 6.40 – 6.36 (m, 1H, H-e), 6.32 – 6.28 (m, 2H, H-c), 5.76 – 5.73 (m, 1H, H-i), 3.21 (s, 1H, H-a), 0.76 (s, 3H, NBCH₃), –0.08 (s, 3H, CBCH₃).

¹¹B NMR (160.5 MHz, THF-*d*₈): δ = –8.6 (NB), –13.9 (CB).

¹³C{¹H} NMR (125.8 MHz, THF-*d*₈): δ = 171.4 (br, CBC DBA), 167.5 (br, CBC DBA), 165.7 (br; 2x NBC DBA), 159.2 (C-f), 156.1 (C-b), 129.0 (DBA), 128.0 (DBA), 127.5 (C-c), 126.7 (C-h), 126.4 (DBA), 126.1 (DBA), 125.1 (C-d), 122.1 (DBA), 121.5 (DBA), 121.1 (DBA), 121.0 (DBA), 120.2 (C-e), 119.6 (C-g), 109.3 (C-i), 68.5 (br, C-a), 6.5 (br, NBCH₃), 2.9 (br, CBCH₃).

Note: An assignment of the DBA signals in the ¹H and ¹³C{¹H} NMR spectra was not possible due to extensive signal overlap.

Li₂[S2] *i*PrN=C=N*i*Pr (11 μL, 0.071 mmol) was added to a freshly prepared THF-*d*₈ solution (0.5 mL) of Li₂[**2**] (0.074 mmol) in an NMR tube. The NMR tube was flame-sealed. NMR spectroscopy revealed a quantitative conversion of the starting materials after 15 h at 50 °C and selective formation of the cycloadduct.

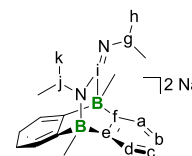


¹H NMR (500.2 MHz, THF-*d*₈): δ = 7.19 – 7.13 (m, 4H, H-a and H-d), 6.53 – 6.49 (m, 4H, H-b and H-c), 4.64 (n.r., 1H, H-g), 4.36 (n.r., 1H, H-j), 0.91 (d, ³J_{HH} = 5.9 Hz, 6H, H-h), 0.85 (d, ³J_{HH} = 6.6 Hz, 6H, H-k), 0.63 (br s, 3H, CBCH₃), 0.55 (s, 3H, NBCH₃).

¹¹B NMR (160.5 MHz, THF-*d*₈): δ = –8.4 (NB), –13.6 (CB).

¹³C{¹H} NMR (125.8 MHz, THF-*d*₈): δ = 203.8 (br, C-i), 168.4 (br, C-f), 167.9 (br, C-e), 126.6 (C-a), 125.6 (C-d), 120.8 (C-b or C-c), 120.4 (C-b or C-c), 49.6 (C-j), 46.9 (C-g), 28.1 (C-h), 24.2 (C-k), 5.9 (br, CBCH₃), 5.4 (br, NBCH₃).

Na₂[S2] *i*PrN=C=N*i*Pr (11 μL, 0.071 mmol) was added to a freshly prepared THF-*d*₈ solution (0.5 mL) of Li₂[**2**] (0.074 mmol) in an NMR tube. The NMR tube was flame-sealed. NMR spectroscopy revealed a quantitative conversion of the starting materials after 9 h at 50 °C and selective formation of the cycloadduct.



X-ray quality crystals of {[Na(18-c-6)(thf)₂]Na[S2]}₂ were grown by gas-phase diffusion of *n*-hexane into a THF solution of Na₂[S2] in the presence of 18-crown-6.

¹H NMR (500.2 MHz, THF-*d*₈): δ = 7.30 – 7.23 (m, 4H, H-a and H-d), 6.65 – 6.59 (m, 4H, H-b and H-c), 4.88 (sept, ³J_{HH} = 6.3 Hz, 1H, H-j), 4.60 (sept, ³J_{HH} = 5.9 Hz, 1H, H-g), 0.90 (m, 12H, H-h and H-k), 0.69 (s, 3H, CBCH₃), 0.58 (s, 3H, NBCH₃).

¹¹B NMR (160.5 MHz, THF-*d*₈): δ = –8.7 (NB), –13.6 (CB).

$^{13}\text{C}\{^1\text{H}\}$ NMR (125.8 MHz, THF- d_8): δ = 198.5 (q, $^1J_{\text{BC}} = 47.5$ Hz, C-i), 169.8 – 168.6 (C-e and C-f), 126.3 (C-a or C-d), 125.4 (C-a or C-d), 121.5 (C-b or C-c), 121.3 (C-b or C-c), 48.1 (C-j), 47.2 (C-g), 28.7 (C-h), 23.4 (C-k), 6.3 (q, $^1J_{\text{BC}} = 46.5$ Hz, CBCH₃), 5.4 (br, NBCH₃).

3.3 Control hydroboration experiments

Control reactions were performed to qualitatively compare the velocities of the uncatalyzed HBpin-hydroboration reactions with those of the corresponding Li₂[**2**]-catalyzed ones. Contrary to previous reports, we observed hydroboration of *i*PrN=C=NiPr even in the absence of the catalyst, but the reaction proceeded significantly slower than [DBA]²⁻-catalyzed one.^{16,17} Ph₂C=O slowly underwent uncatalyzed hydroboration at 50 °C, although previous publications have stated that such reactions with related compounds like acetophenone do not take place.^{18–20} One reason may be that we used the donor solvent THF-*d*₈ rather than the previously employed less polar solvents C₆H₆, CHCl₃, or CH₂Cl₂; adduct formation with HBpin may activate the compound. The control experiments performed are compiled in Table S4.

Procedure for the control experiments: Neat HBpin (40 μL, 0.28 mmol) was added to an NMR tube charged with a THF-*d*₈ solution (0.5 mL) of the respective substrate (0.2 mmol). The NMR tube was flame-sealed. The sample was kept at the temperatures listed in Table S4 and repeatedly analyzed at room temperature by NMR spectroscopy.

Table S4. Overview of the hydroboration reactions with HBpin and without catalytic amounts of Li₂[**2**]; the required reaction temperatures, times and conversions are also given.

substrate			<i>T</i> / °C	<i>t</i> / h	Conversion / %*
	<i>m</i> / mg	<i>V</i> / μL			
Ph ₂ C=CH ₂	36	35	100	18	–
Ph ₂ C=O	36	–	50	3	40
<i>i</i> PrN=C=NiPr	24	30	room temperature	24	54
Ph(H)C=NPh	36	–	100	35	29
Ph(H)C=N <i>t</i> Bu	32	35	100	35	traces

*Conversions were determined by comparing the integral values of the starting material vs. product resonances in the ¹H NMR spectrum.

4. NMR spectra of the DBA derivatives

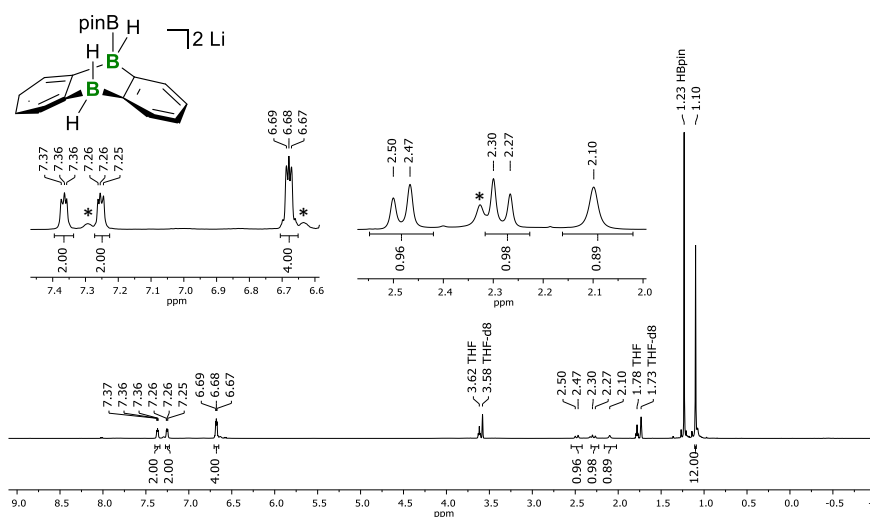


Figure S8. $^1\text{H}\{^{11}\text{B}\}$ NMR spectrum (500.2 MHz, $\text{THF-}d_8$) recorded on the reaction mixture of $\text{Li}_2[1]$ and HBpin. Asterisks mark resonances of $\text{Li}_2[8]$.

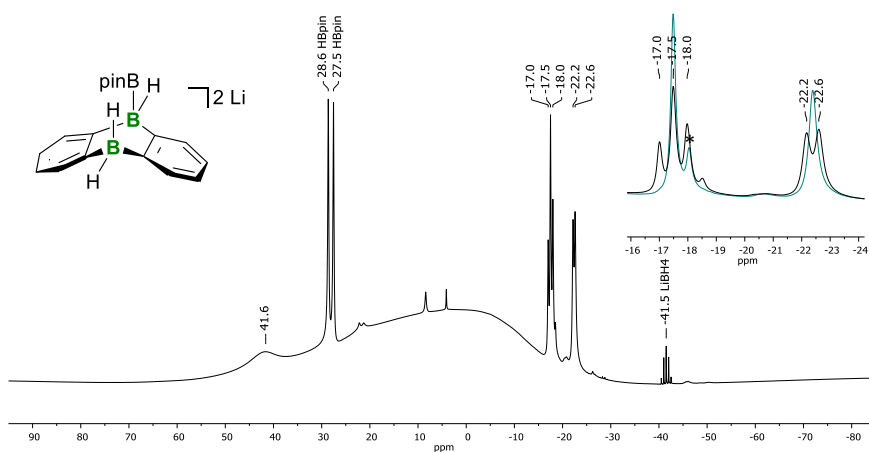


Figure S9. ^{11}B NMR spectrum (160.5 MHz, $\text{THF-}d_8$) and $^{11}\text{B}\{^1\text{H}\}$ NMR spectrum (160.5 MHz, $\text{THF-}d_8$) recorded on the reaction mixture of $\text{Li}_2[1]$ and HBpin. Blue line: $^{11}\text{B}\{^1\text{H}\}$ NMR spectrum (160.5 MHz, $\text{THF-}d_8$) recorded on the reaction mixture of $\text{Li}_2[1]$ and HBpin. The asterisk marks the resonance of $\text{Li}_2[8]$.

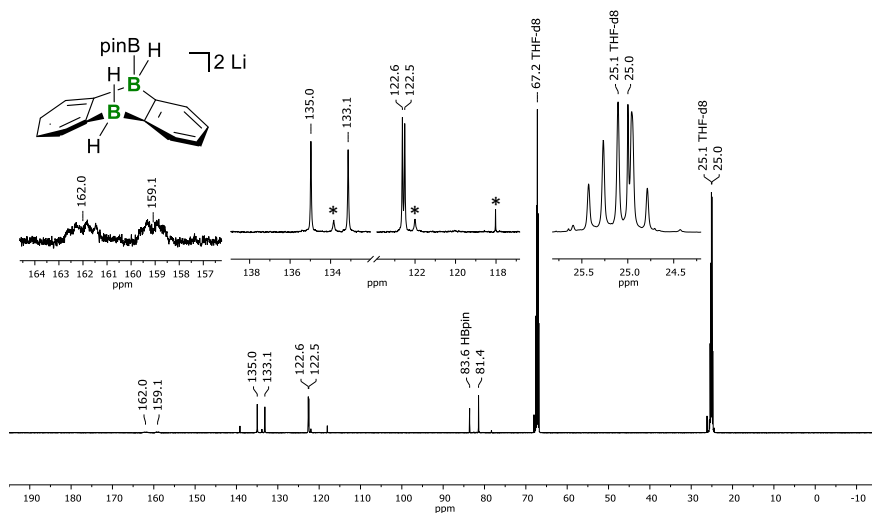


Figure S10. $^{13}\text{C}\{^1\text{H}\}$ NMR spectrum (125.8 MHz, $\text{THF-}d_8$) recorded on the reaction mixture of $\text{Li}_2[1]$ and HBpin. Asterisks mark resonances of $\text{Li}_2[8]$.

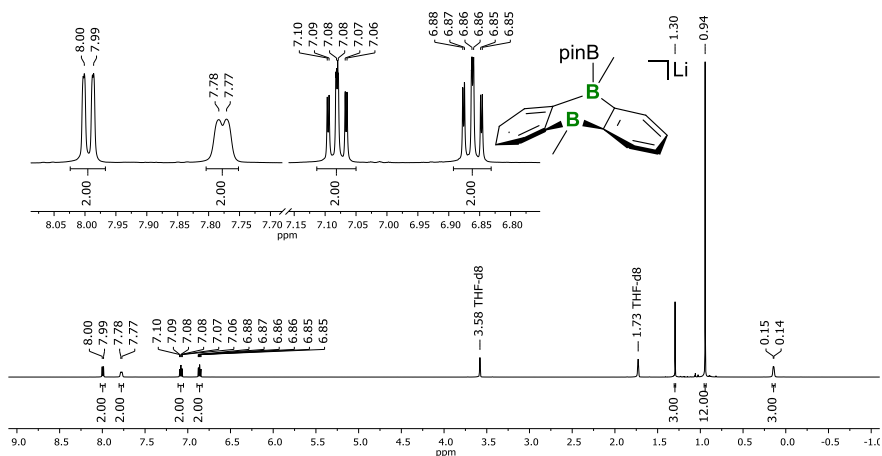


Figure S11. ^1H NMR spectrum (500.2 MHz, $\text{THF-}d_8$) of $\text{Li}[5]$.

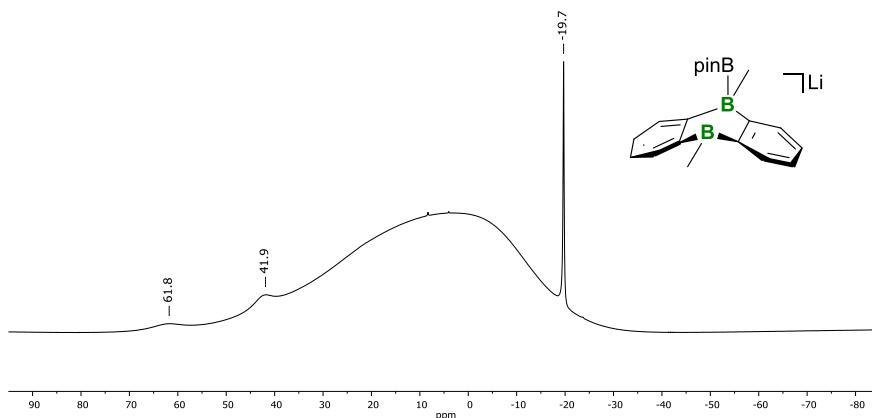


Figure S12. ^{11}B NMR spectrum (160.5 MHz, $\text{THF-}d_8$) of $\text{Li}[5]$.

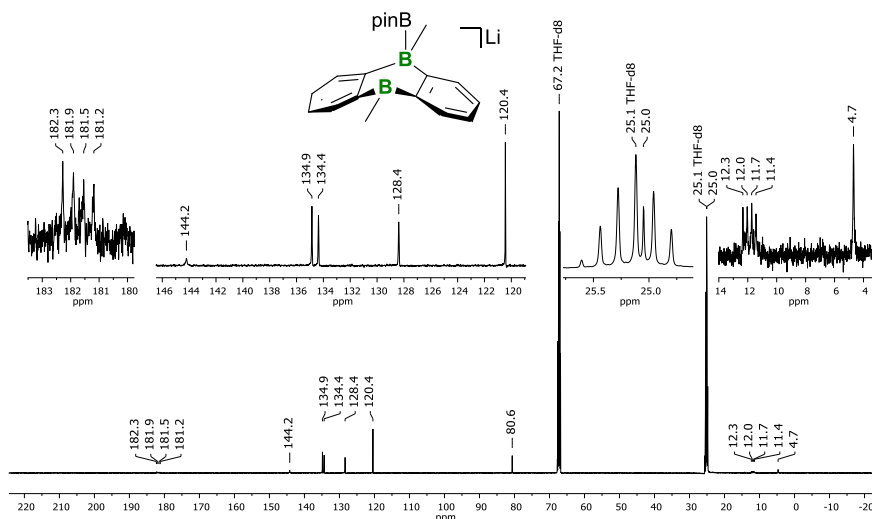


Figure S13. $^{13}\text{C}\{^1\text{H}\}$ NMR spectrum (125.8 MHz, $\text{THF-}d_8$) of $\text{Li}[5]$.

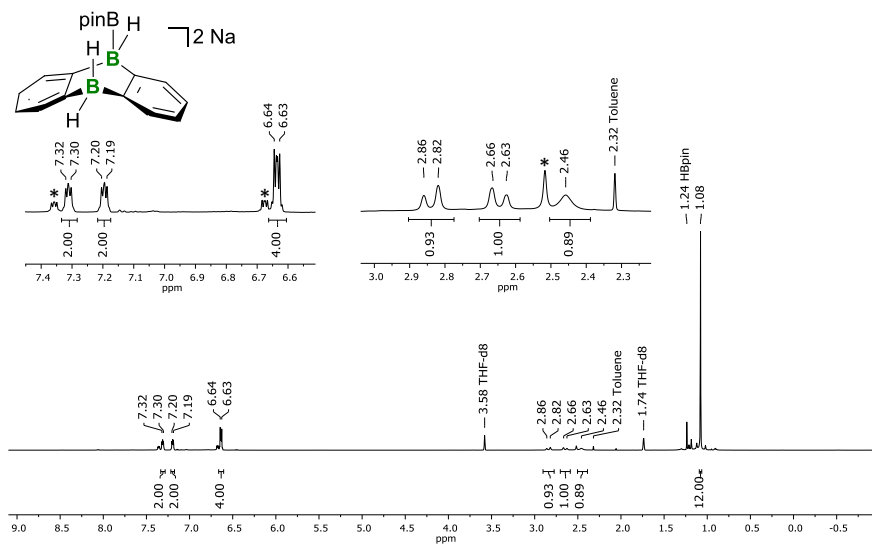


Figure S14. $^1\text{H}\{^{11}\text{B}\}$ NMR spectrum (500.2 MHz, $\text{THF-}d_8$) recorded on the reaction mixture of $\text{Na}_2[1]$ and HBpin . Asterisks mark resonances of $\text{Na}_2[8]$.

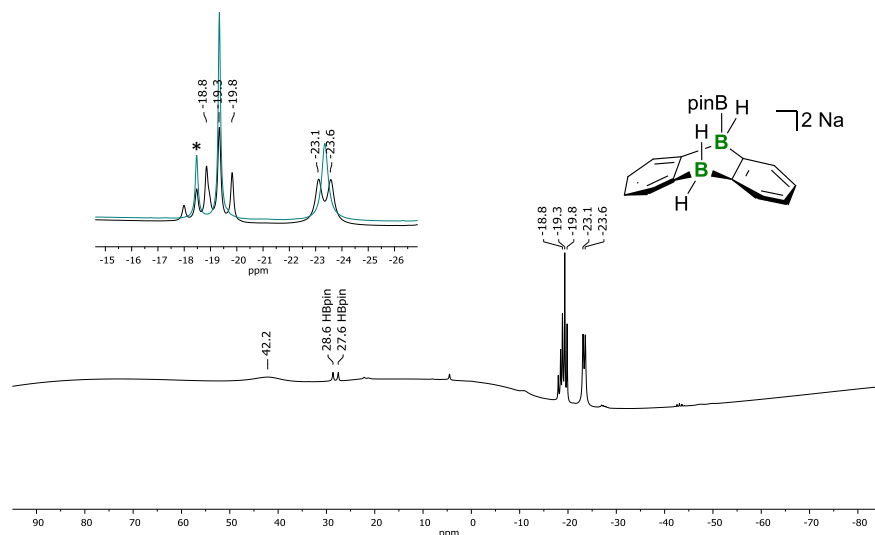


Figure S15. ^{11}B NMR spectrum (160.5 MHz, THF-d_8) recorded on the reaction mixture of $\text{Na}_2[1]$ and HBpin. Blue line: $^{11}\text{B}\{^1\text{H}\}$ NMR spectrum (160.5 MHz, THF-d_8) recorded on the reaction mixture of $\text{Na}_2[1]$ and HBpin. The asterisk marks the resonance of $\text{Na}_2[8]$.

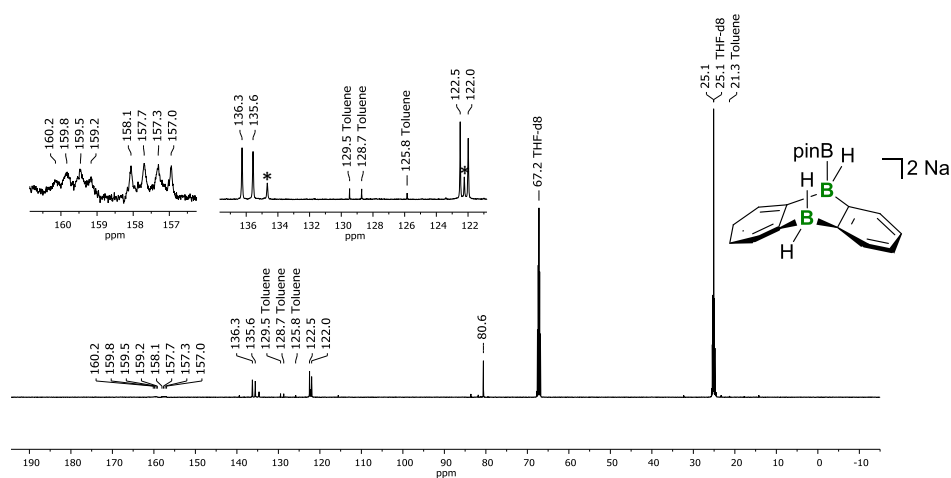


Figure S16. $^{13}\text{C}\{^1\text{H}\}$ NMR spectrum (125.8 MHz, THF-d_8) recorded on the reaction mixture of $\text{Na}_2[1]$ and HBpin. Asterisks mark resonances of $\text{Na}_2[8]$.

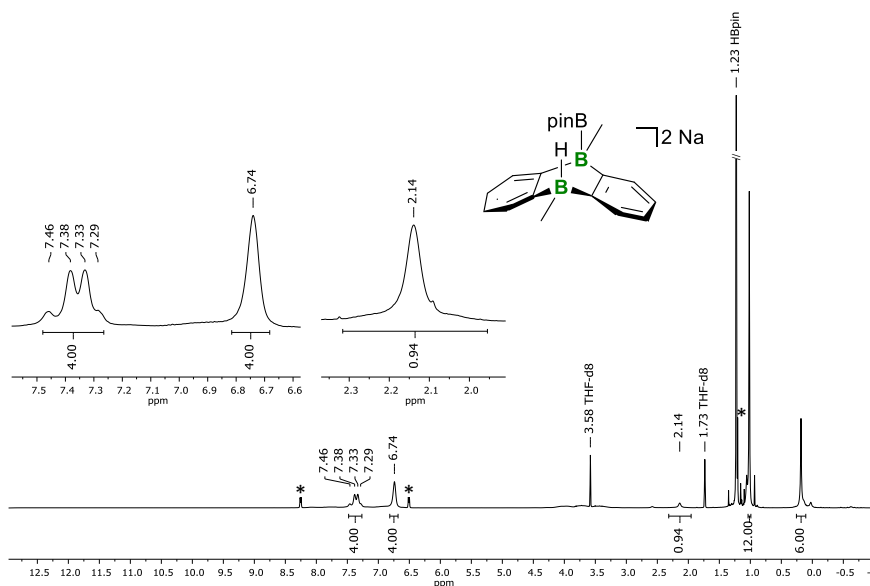


Figure S17. $^1\text{H}\{^{11}\text{B}\}$ NMR spectrum (500.2 MHz, THF-d_8) recorded on the reaction mixture of $\text{Na}_2[2]$ and HBpin. Asterisks mark resonances of the starting material $\text{Na}_2[2]$.

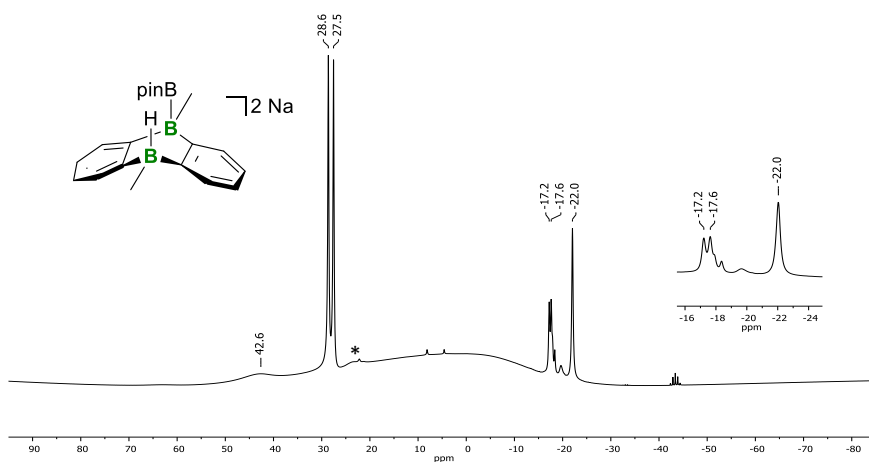


Figure S18. ^{11}B NMR spectrum (160.5 MHz, THF-d_8) recorded on the reaction mixture of $\text{Na}_2[2]$ and HBpin. The asterisk marks the resonance of $\text{Na}_2[2]$.

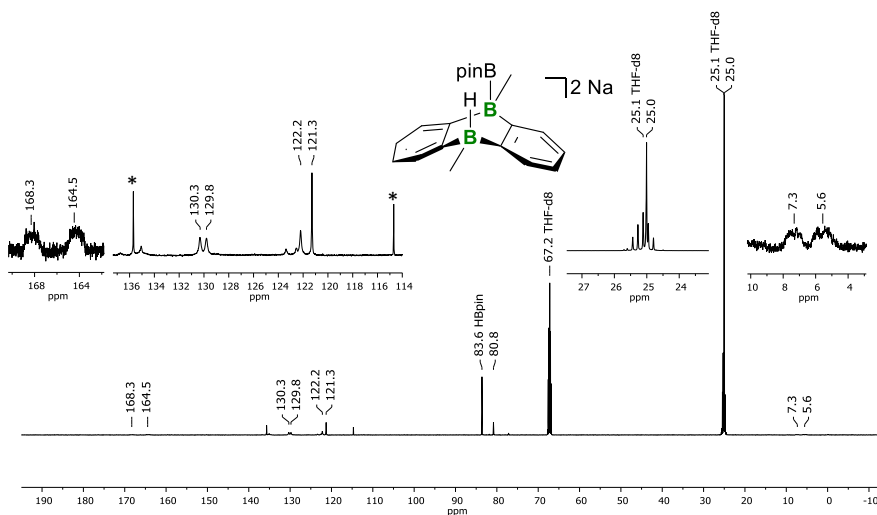


Figure S19. $^{13}\text{C}\{^1\text{H}\}$ NMR spectrum (125.8 MHz, THF-d_8) recorded on the reaction mixture of $\text{Na}_2[2]$ and HBpin. Asterisks mark resonances of the starting material $\text{Na}_2[2]$.

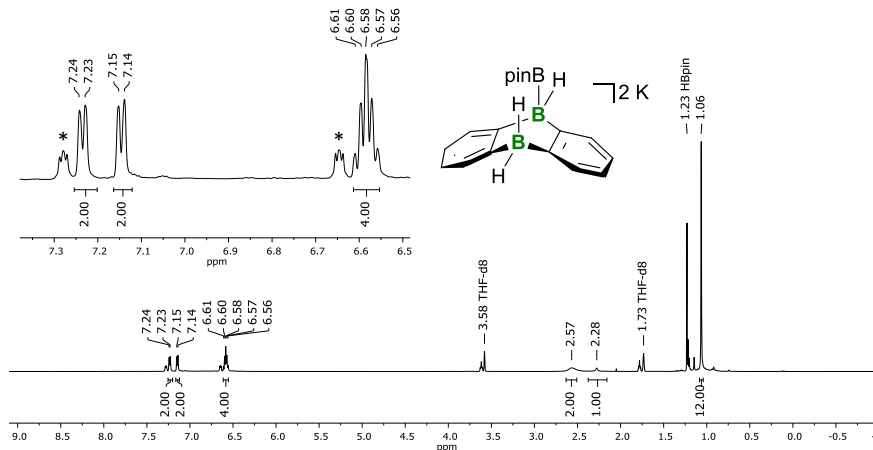


Figure S20. $^1\text{H}\{^{11}\text{B}\}$ NMR spectrum (500.2 MHz, $\text{THF-}d_8$) recorded on the reaction mixture of $\text{K}_2[1]$ and HBpin. Asterisks mark resonances of $\text{K}_2[8]$.

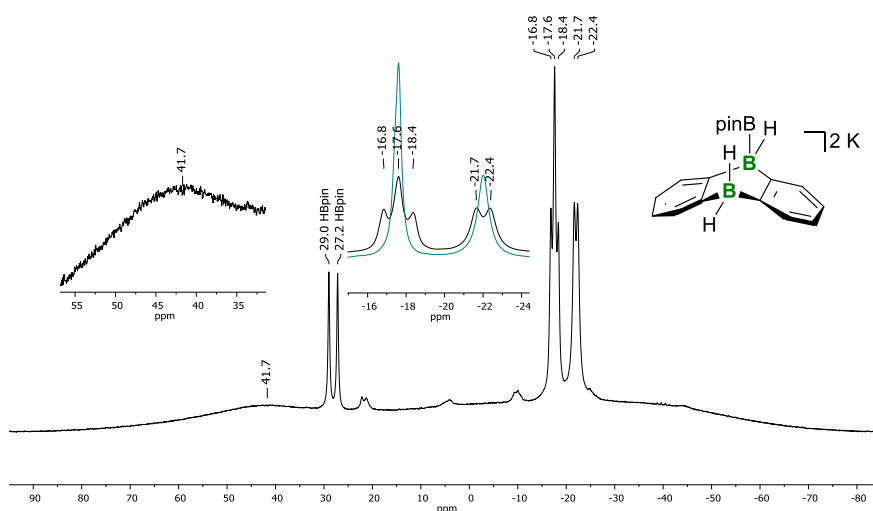


Figure S21. ^{11}B NMR spectrum (96.3 MHz, $\text{THF-}d_8$) recorded on the reaction mixture of $\text{K}_2[1]$ and HBpin. Blue line: $^{11}\text{B}\{^1\text{H}\}$ NMR spectrum (96.3 MHz, $\text{THF-}d_8$) recorded on the reaction mixture of $\text{K}_2[1]$ and HBpin.

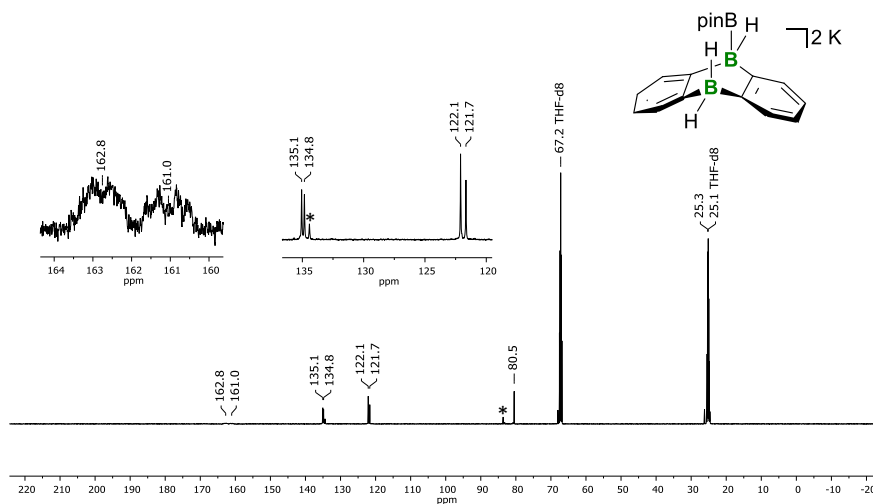


Figure S22. $^{13}\text{C}\{^1\text{H}\}$ NMR spectrum (125.8 MHz, $\text{THF-}d_8$) recorded on the reaction mixture of $\text{K}_2[1]$ and HBpin. Asterisks mark resonances of $\text{K}_2[8]$ and HBpin.

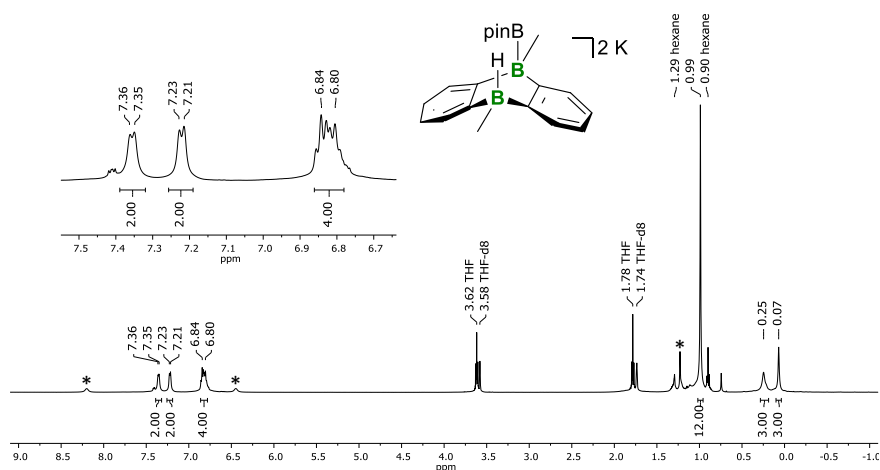


Figure S23. ^1H NMR spectrum (500.2 MHz, $\text{THF-}d_8$) recorded on the reaction mixture of $\text{K}_2[2]$ and HBpin. Asterisks mark resonances of the starting material $\text{K}_2[2]$.

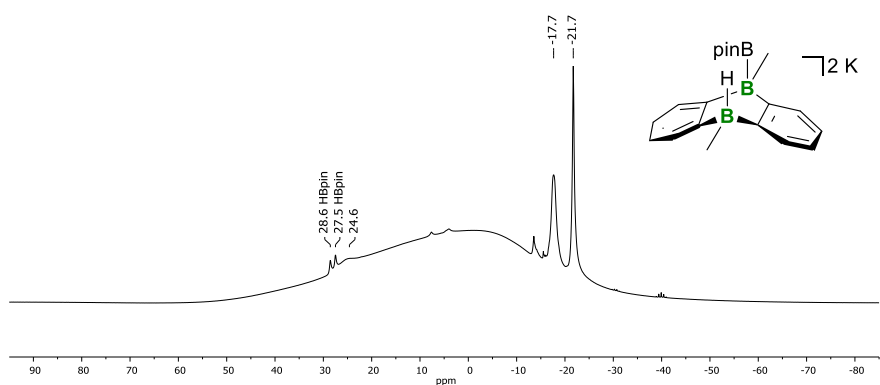


Figure S24. ^{11}B NMR spectrum (160.5 MHz, $\text{THF-}d_8$) recorded on the reaction mixture of $\text{K}_2[2]$ and HBpin.

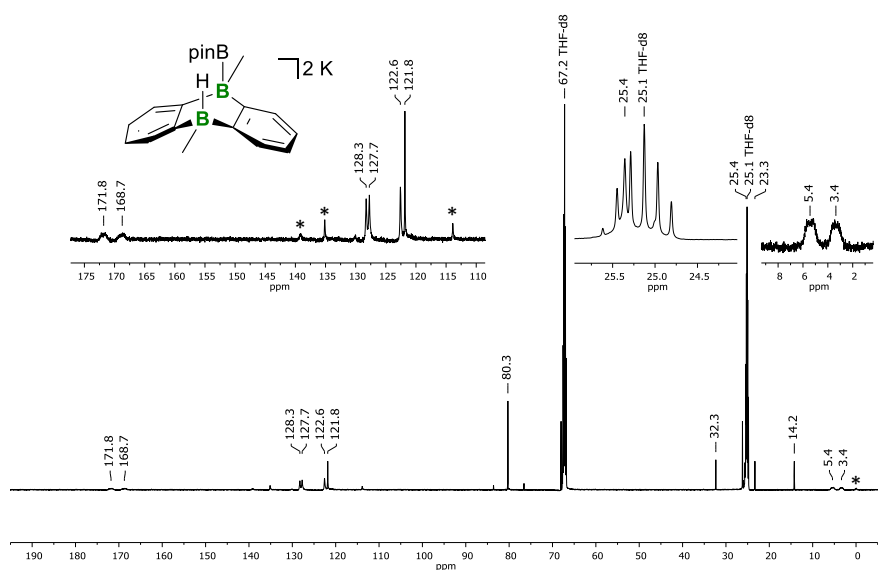


Figure S25. $^{13}\text{C}\{^1\text{H}\}$ NMR spectrum (125.8 MHz, $\text{THF-}d_8$) recorded on the reaction mixture of $\text{K}_2[2]$ and HBpin. Asterisks mark resonances of the starting material $\text{K}_2[2]$.

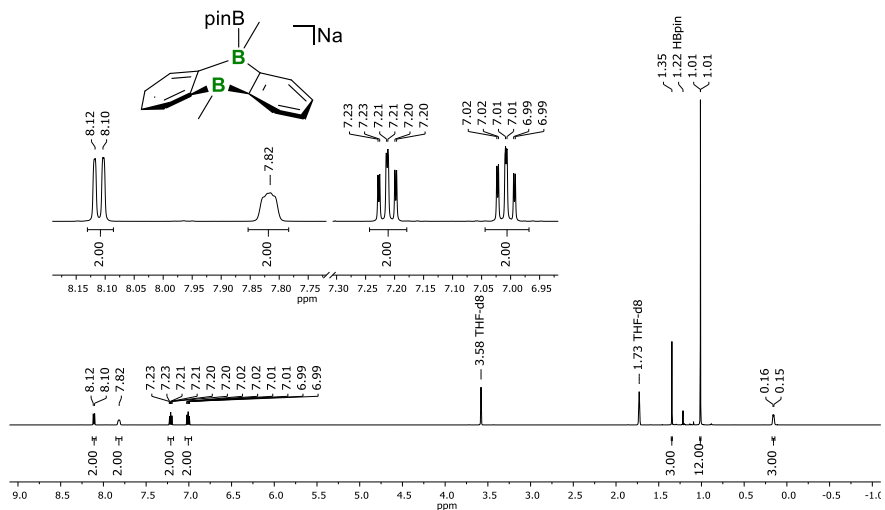


Figure S26. ^1H NMR spectrum (500.2 MHz, THF-d_8) of Na[5].

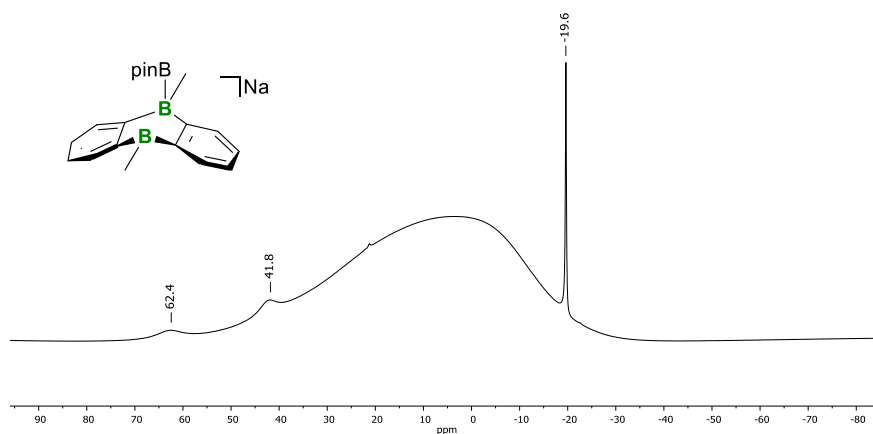


Figure S27. ^{11}B NMR spectrum (160.5 MHz, THF-d_8) of Na[5].

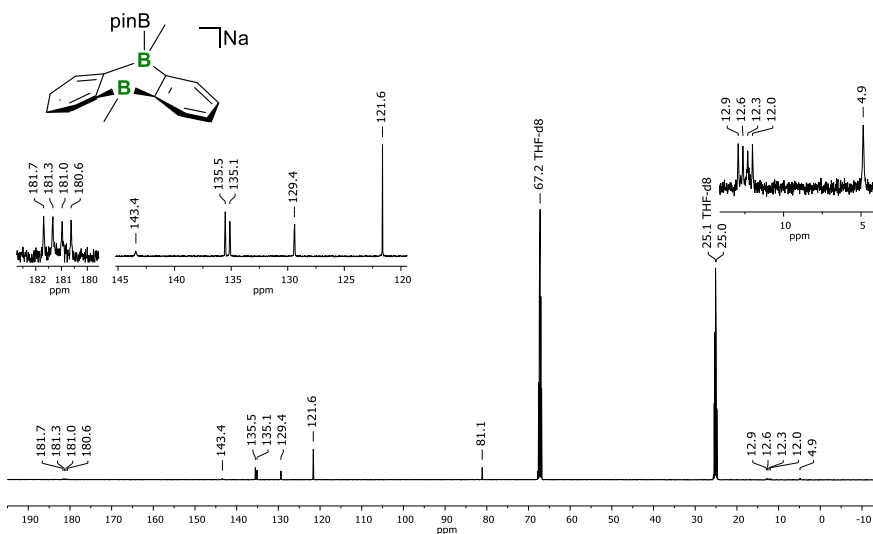


Figure S28. $^{13}\text{C}\{^1\text{H}\}$ NMR spectrum (125.8 MHz, THF-d_8) of Na[5].

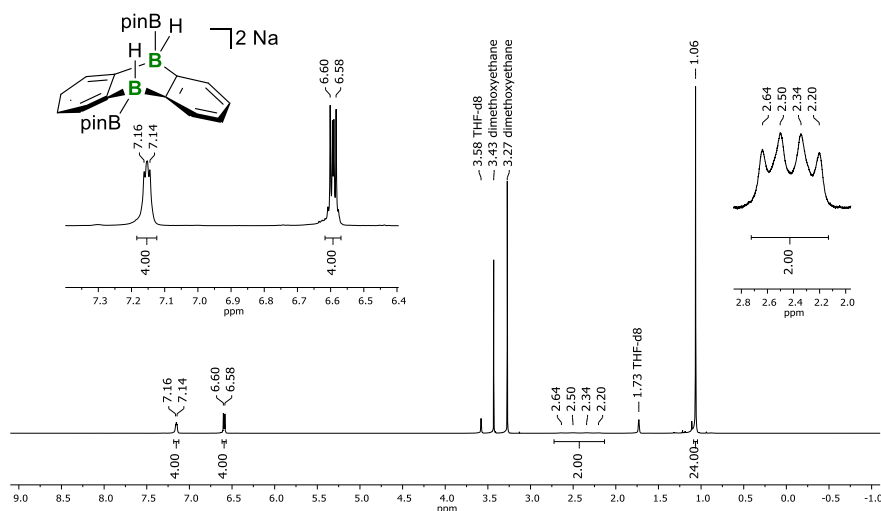


Figure S29. ^1H NMR spectrum (500.2 MHz, $\text{THF-}d_8$) of re-dissolved crystals of $[\text{Na}(\text{dme})_2][\mathbf{7}]$.

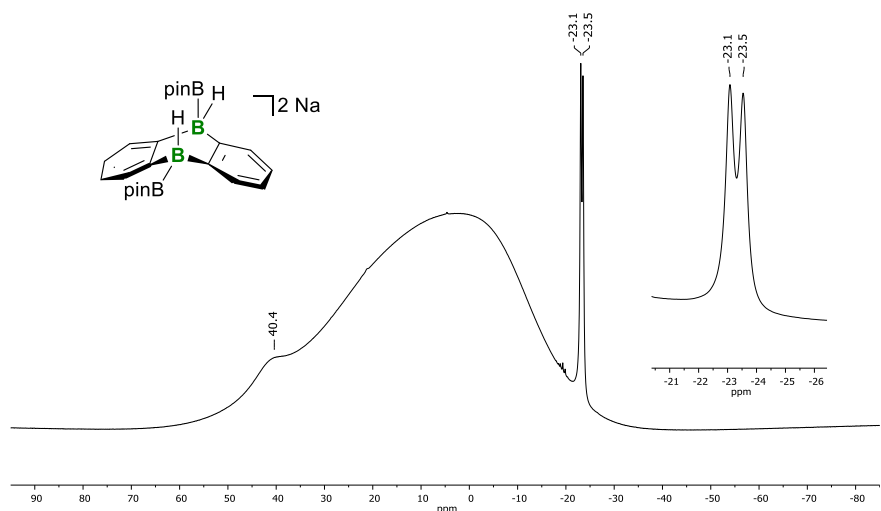


Figure S30. ^{11}B NMR spectrum (160.5 MHz, $\text{THF-}d_8$) of re-dissolved crystals of $[\text{Na}(\text{dme})_2][\mathbf{7}]$.

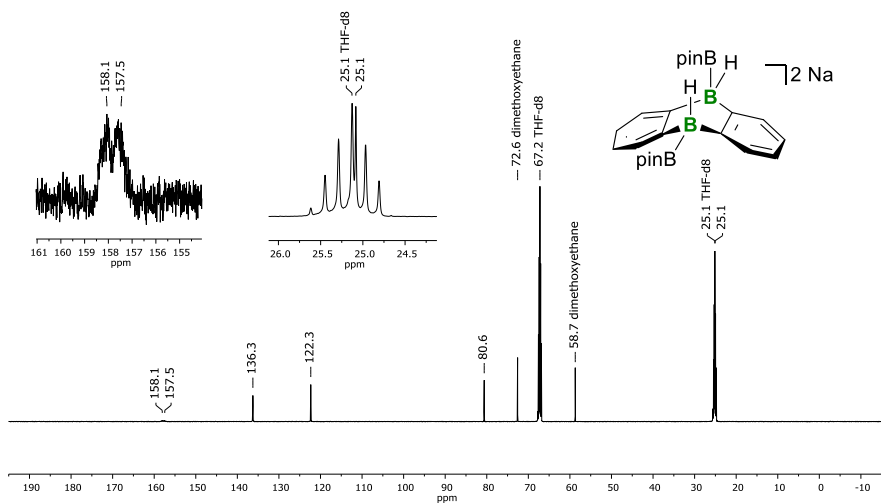


Figure S31. $^{13}\text{C}\{^1\text{H}\}$ NMR spectrum (125.8 MHz, $\text{THF-}d_8$) of re-dissolved crystals of $[\text{Na}(\text{dme})_2][\mathbf{7}]$.

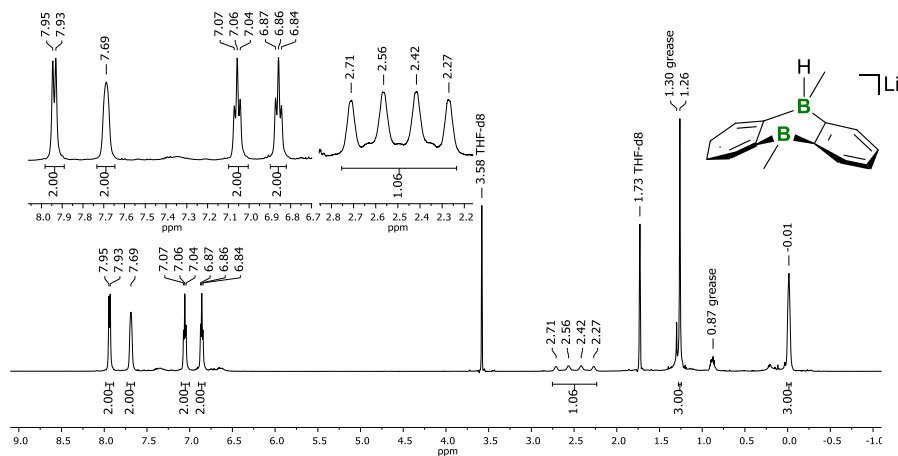


Figure S32. ^1H NMR spectrum (500.2 MHz, THF-d_8) of $\text{Li}[6]$.

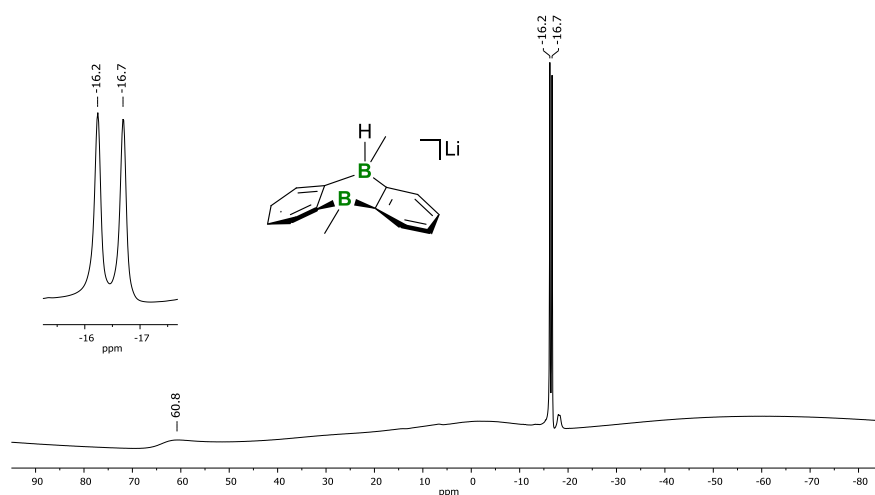


Figure S33. ^{11}B NMR spectrum (160.5 MHz, THF-d_8) of $\text{Li}[6]$.

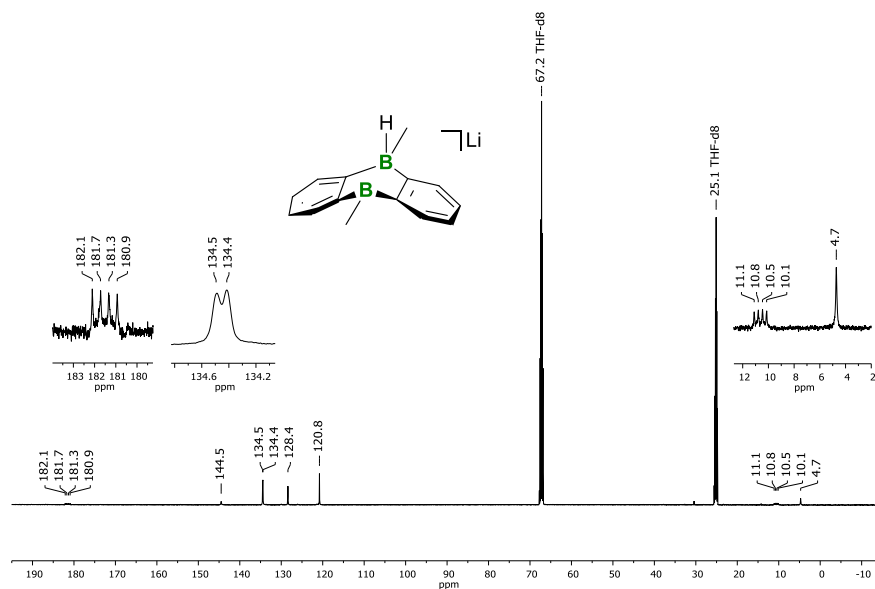


Figure S34. $^{13}\text{C}\{^1\text{H}\}$ NMR spectrum (125.8 MHz, THF-d_8) of $\text{Li}[6]$.

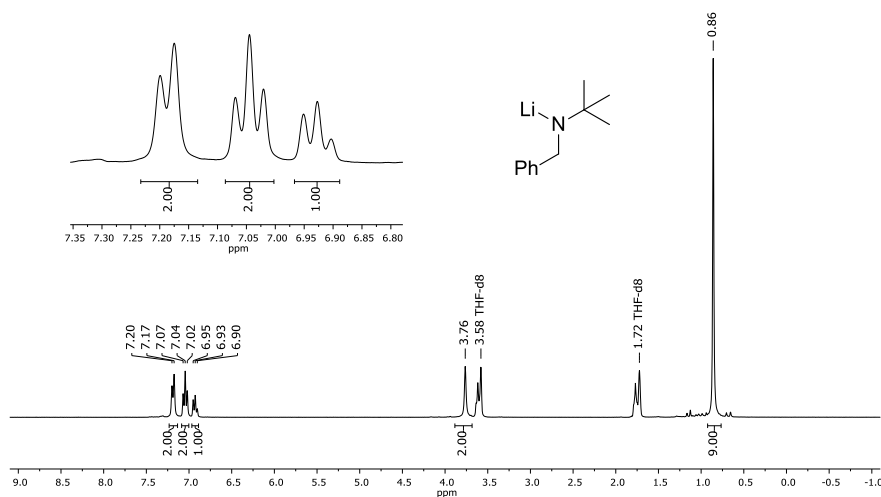


Figure S35. ^1H NMR spectrum (300.0 MHz, THF-d_8) of $\text{Ph}(\text{H})_2\text{C-N}(\text{Li})t\text{Bu}$.

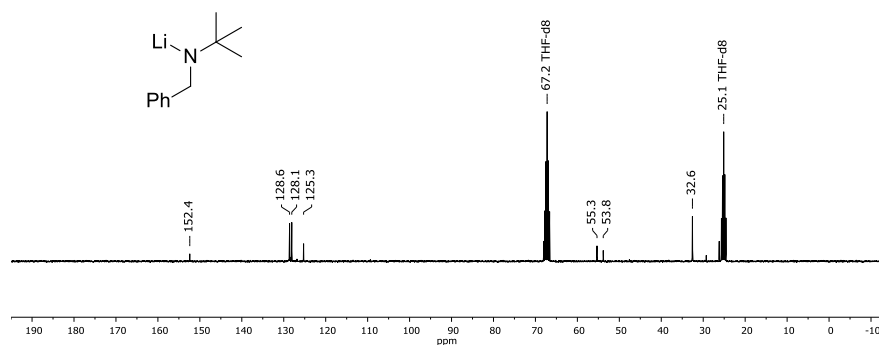


Figure S36. $^{13}\text{C}\{^1\text{H}\}$ NMR spectrum (75.4 MHz, THF-d_8) of $\text{Ph}(\text{H})_2\text{C-N}(\text{Li})t\text{Bu}$.

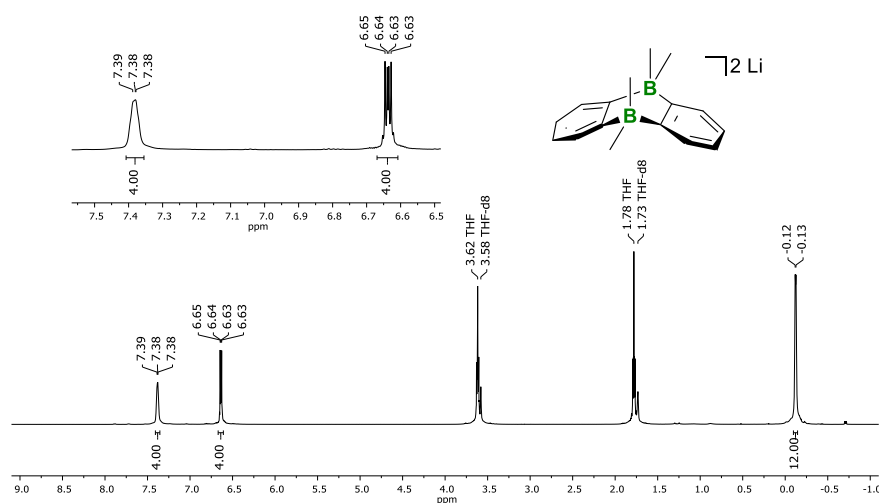


Figure S37. ^1H NMR spectrum (500.2 MHz, THF-d_8) of $\text{Li}_2[\mathbf{10}]$.

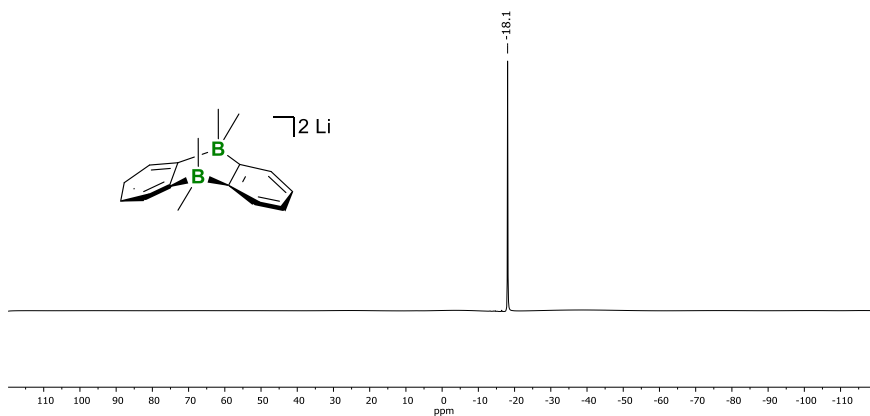


Figure S38. ^{11}B NMR spectrum (160.5 MHz, $\text{THF-}d_8$) of $\text{Li}_2[\mathbf{10}]$.

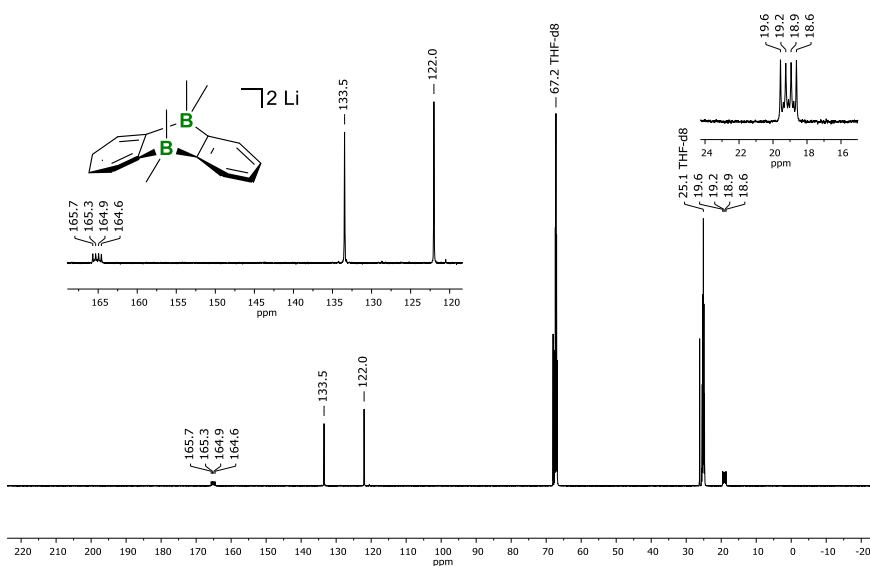


Figure S39. $^{13}\text{C}\{^1\text{H}\}$ NMR spectrum (125.8 MHz, $\text{THF-}d_8$) of $\text{Li}_2[\mathbf{10}]$.

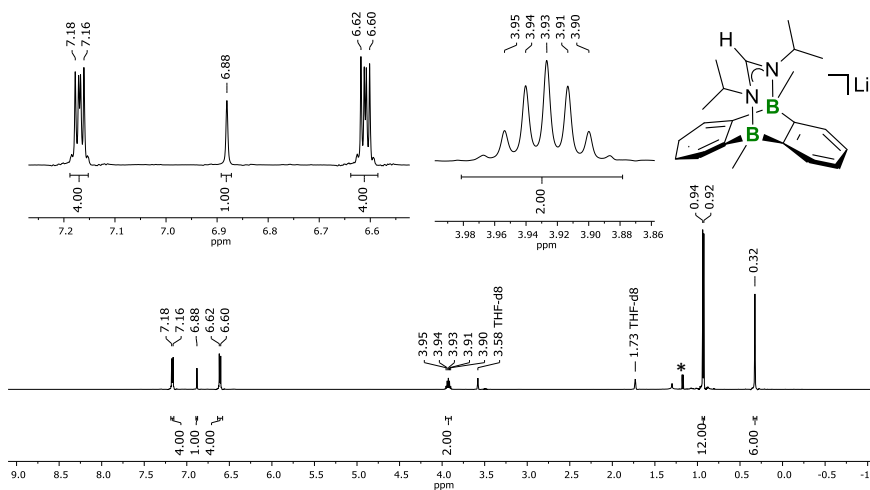


Figure S40. ^1H NMR spectrum (500.2 MHz, $\text{THF-}d_8$) of $\text{Li}[\mathbf{S1}]$. The asterisk marks a resonance of residual $i\text{PrN}=\text{C}=\text{NiPr}$.

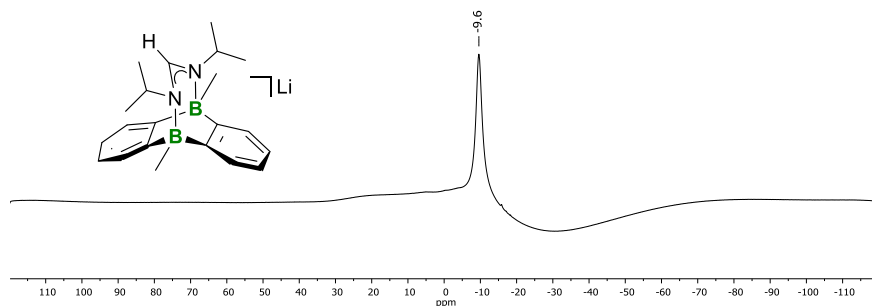


Figure S41. ^{11}B NMR spectrum (160.5 MHz, $\text{THF-}d_8$) of $\text{Li}[\text{S1}]$.

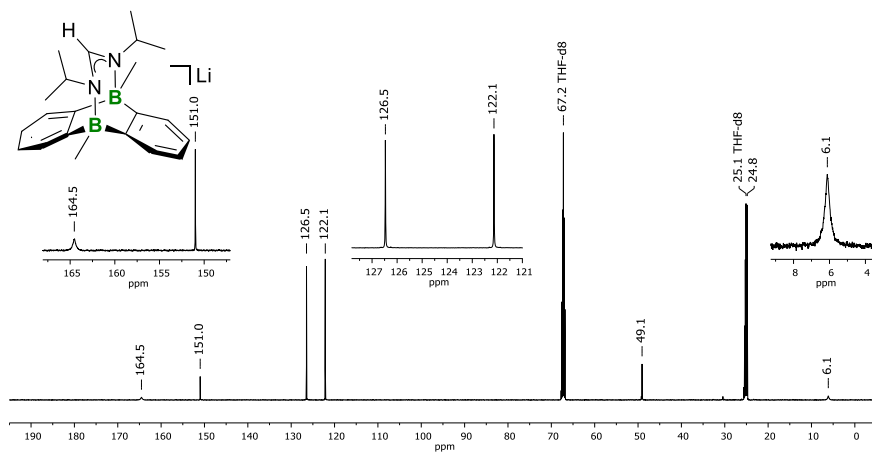


Figure S42. $^{13}\text{C}\{^1\text{H}\}$ NMR spectrum (125.8 MHz, $\text{THF-}d_8$) of $\text{Li}[\text{S1}]$.

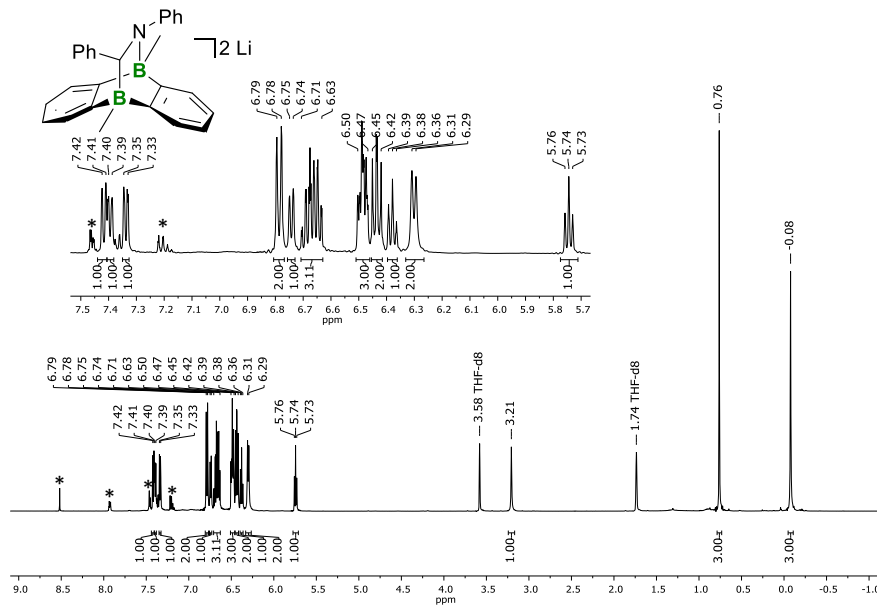


Figure S49. ^1H NMR spectrum (500.2 MHz, $\text{THF-}d_8$) of $\text{Li}_2[\mathbf{12}]$. Asterisks marks resonances of residual $\text{Ph}(\text{H})\text{C}=\text{NPh}$.

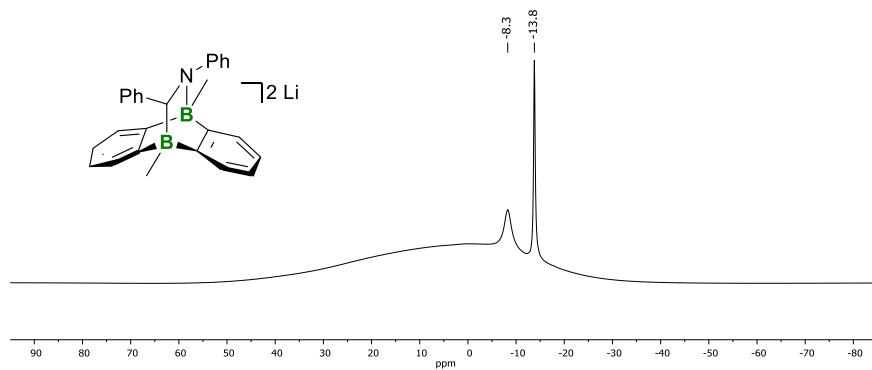


Figure S50. ^{11}B NMR spectrum (160.5 MHz, $\text{THF-}d_8$) of $\text{Li}_2[\mathbf{12}]$.

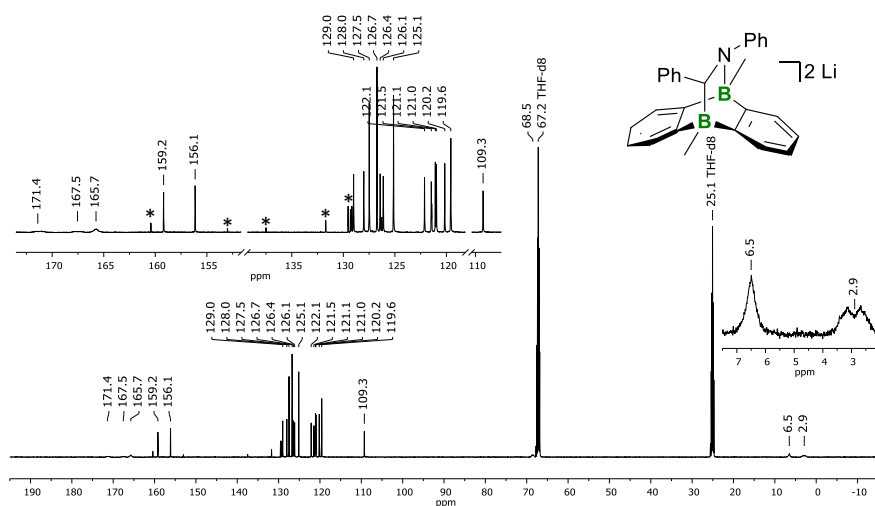


Figure S51. $^{13}\text{C}\{^1\text{H}\}$ NMR spectrum (125.8 MHz, $\text{THF-}d_8$) of $\text{Li}_2[\mathbf{12}]$. Asterisks mark resonances of residual $\text{Ph}(\text{H})\text{C}=\text{NPh}$.

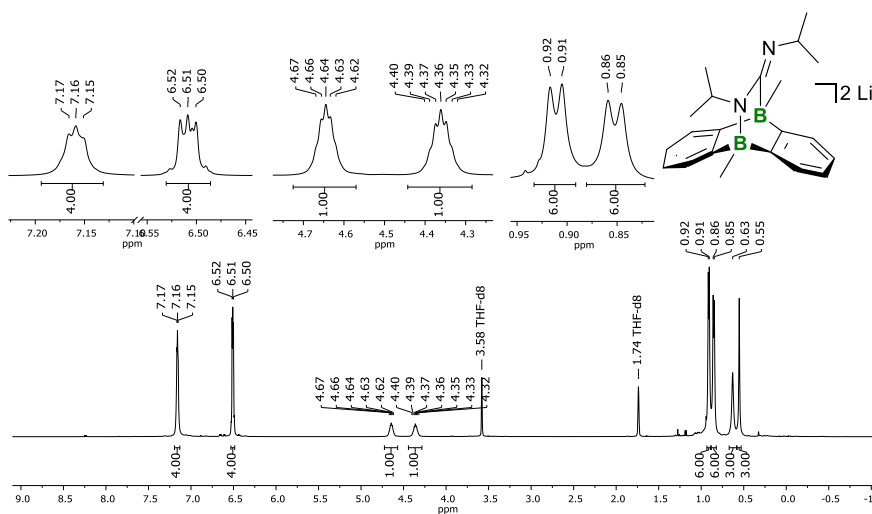


Figure S52. ^1H NMR spectrum (500.2 MHz, $\text{THF-}d_8$) of $\text{Li}_2[\mathbf{S2}]$.

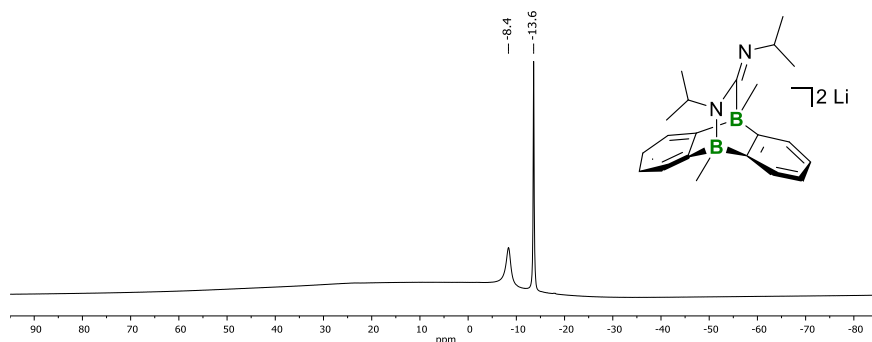


Figure S53. ^{11}B NMR spectrum (160.5 MHz, $\text{THF-}d_8$) of $\text{Li}_2[\text{S2}]$.

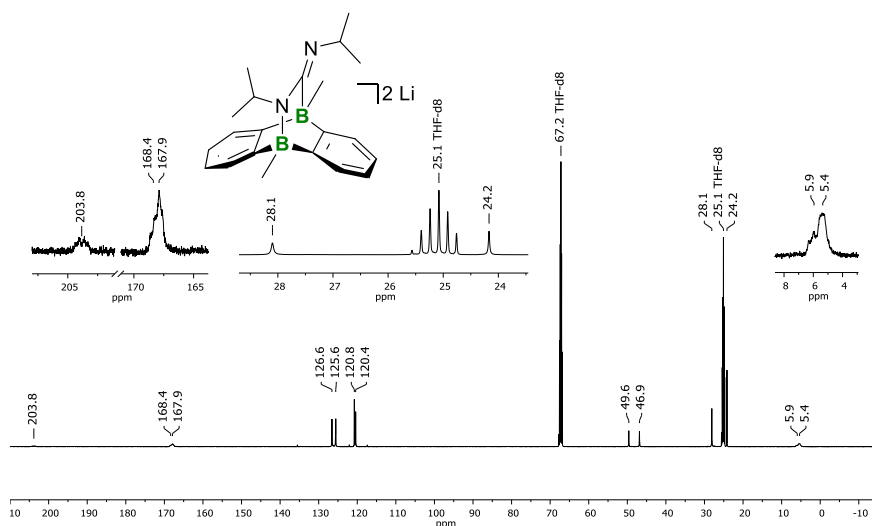


Figure S54. $^{13}\text{C}\{^1\text{H}\}$ NMR spectrum (125.8 MHz, $\text{THF-}d_8$) of $\text{Li}_2[\text{S2}]$.

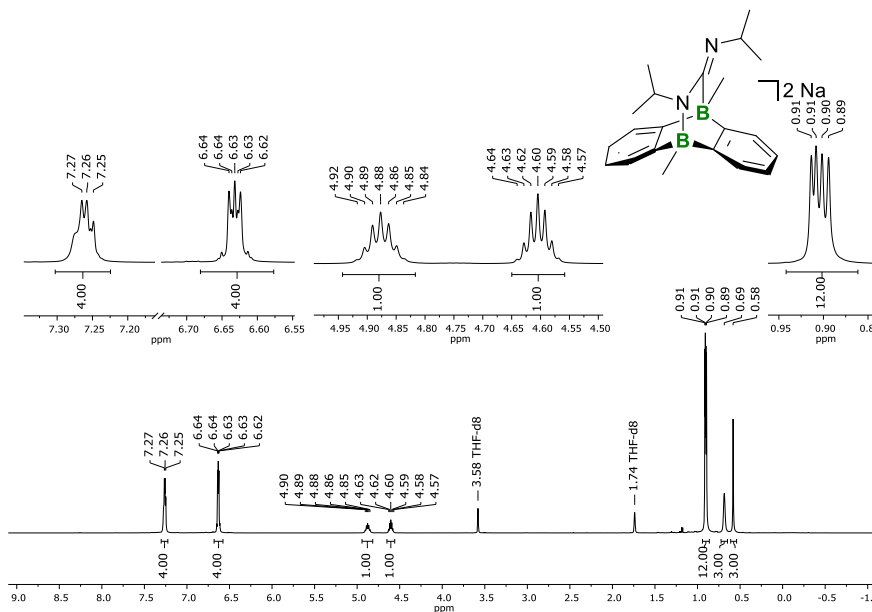


Figure S55. ^1H NMR spectrum (500.2 MHz, $\text{THF-}d_8$) of $\text{Na}_2[\text{S2}]$.

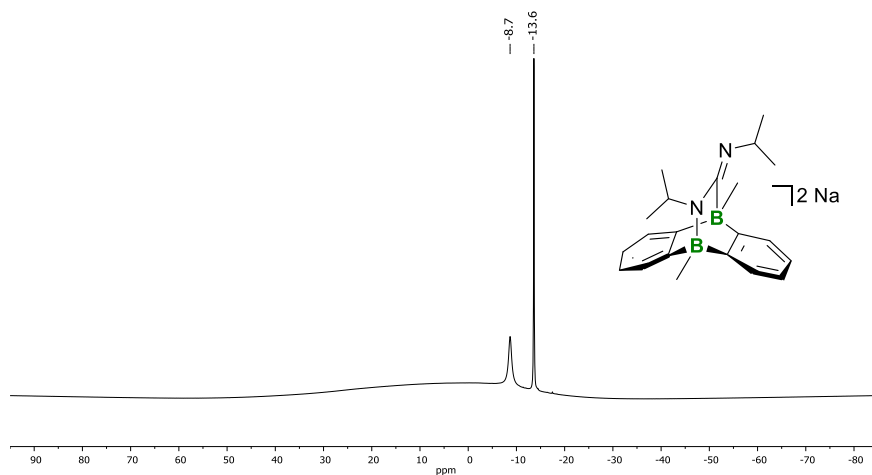


Figure S56. ^{11}B NMR spectrum (160.5 MHz, $\text{THF-}d_8$) of $\text{Na}_2[\text{S2}]$.

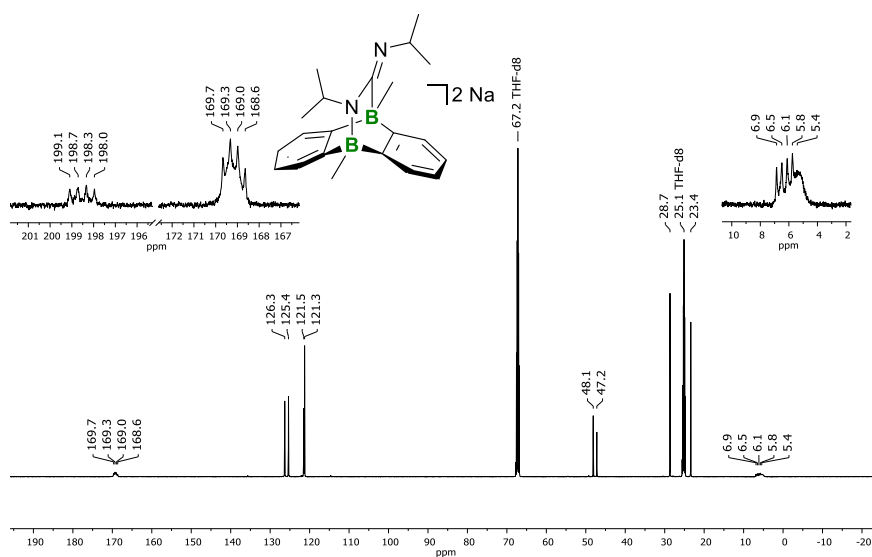


Figure S57. $^{13}\text{C}\{^1\text{H}\}$ NMR spectrum (125.8 MHz, $\text{THF-}d_8$) of $\text{Na}_2[\text{S2}]$.

5. NMR spectra of the hydroboration reactions

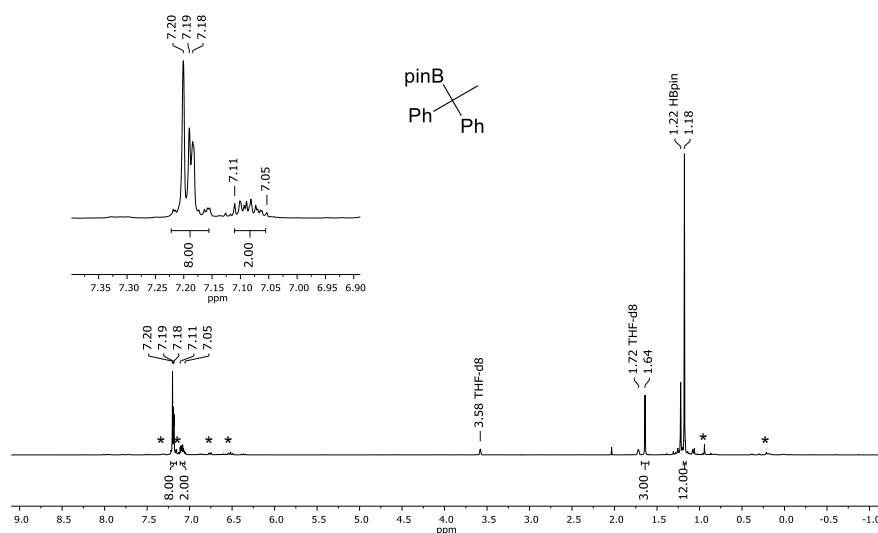


Figure S58. ^1H NMR spectrum (300.0 MHz, $\text{THF-}d_8$) recorded on the reaction mixture of $\text{Li}_2[\text{2}]$, $\text{Ph}_2\text{C}=\text{CH}_2$, and HBpin after 3 d at room temperature. Asterisks mark resonances of the catalyst $\text{Li}_2[\text{S3}]$.

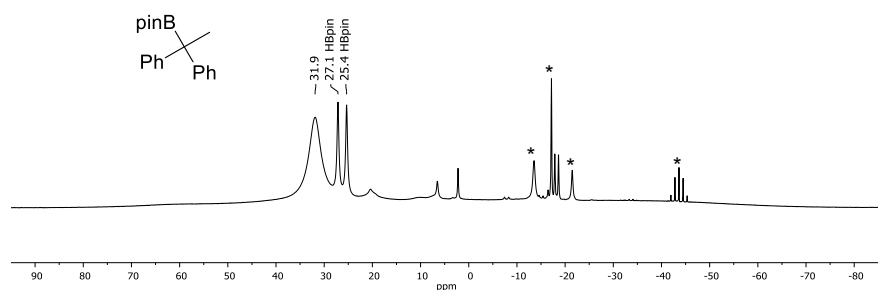


Figure S59. ^{11}B NMR spectrum (96.3 MHz, $\text{THF-}d_8$) recorded on the reaction mixture of $\text{Li}_2[\text{2}]$, $\text{Ph}_2\text{C}=\text{CH}_2$, and HBpin after 3 d at room temperature. Asterisks mark the resonances of the catalyst $\text{Li}_2[\text{S3}]$, Li[5] , and LiBH_4 , respectively.

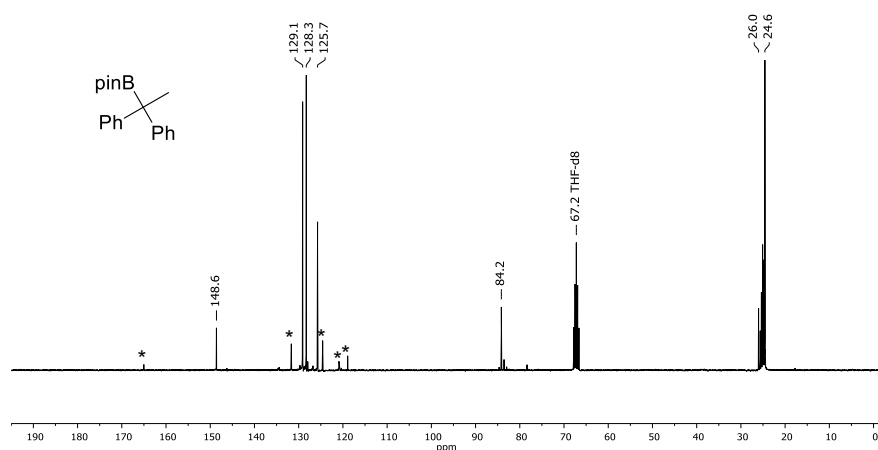


Figure S60. $^{13}\text{C}\{^1\text{H}\}$ NMR spectrum (75.4 MHz, $\text{THF-}d_8$) recorded on the reaction mixture of $\text{Li}_2[\text{2}]$, $\text{Ph}_2\text{C}=\text{CH}_2$, and HBpin after 3 d at room temperature. Asterisks mark the resonances of the catalyst $\text{Li}_2[\text{S3}]$.

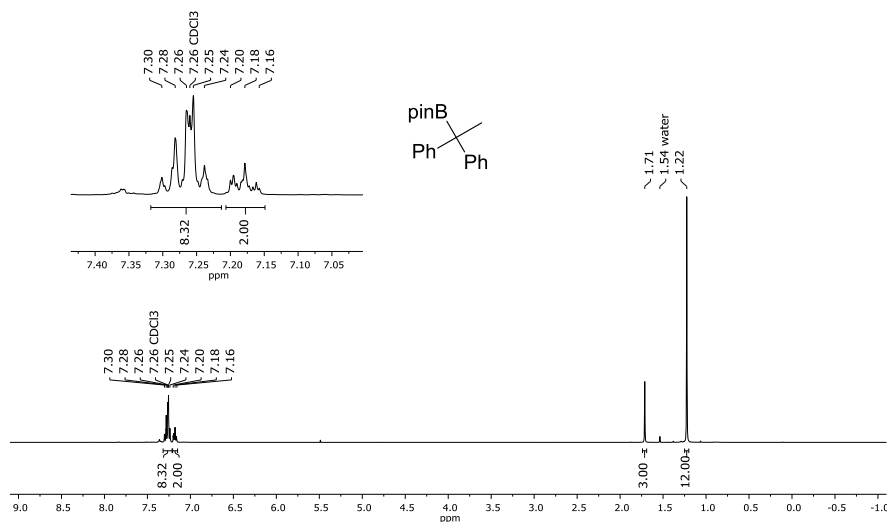


Figure S61. ¹H NMR spectrum (400.0 MHz, CDCl₃) of Ph₂C(Me)Bpin.

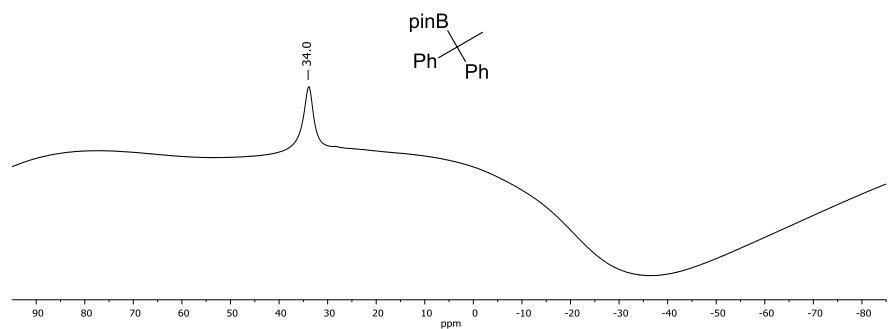


Figure S62. ¹¹B NMR spectrum (128.4 MHz, CDCl₃) of Ph₂C(Me)Bpin.

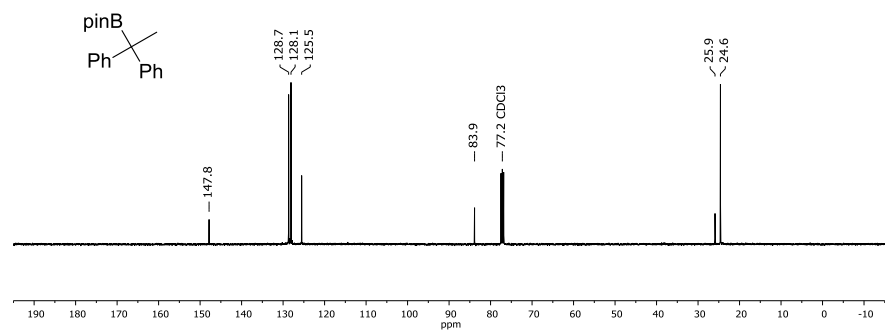


Figure S63. ¹³C{¹H} NMR spectrum (100.6 MHz, CDCl₃) of Ph₂C(Me)Bpin.

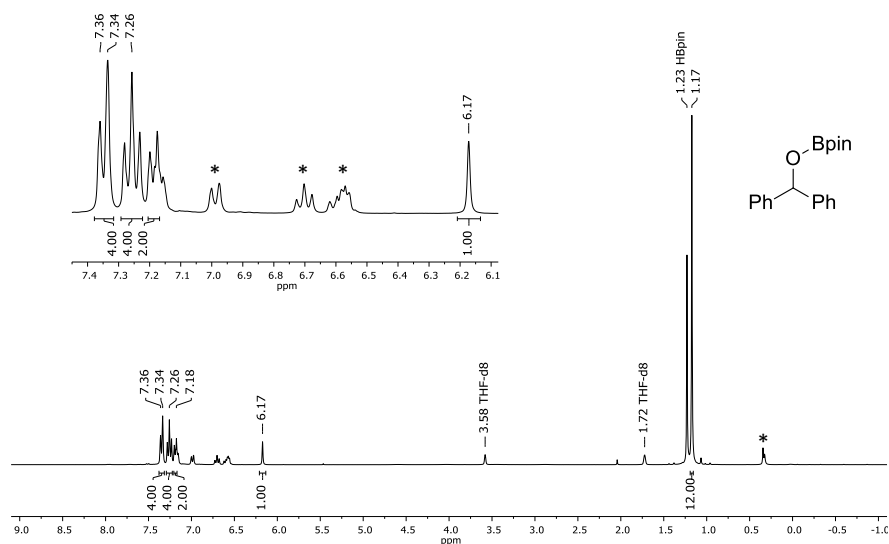


Figure S64. ^1H NMR spectrum (300.0 MHz, THF-d_8) recorded on the reaction mixture of $\text{Li}_2[\mathbf{2}]$, $\text{Ph}_2\text{C=O}$, and HBpin immediately after flame-sealing the NMR tube. Asterisks mark resonances of the catalyst $\text{Li}_2[\mathbf{13}]$.

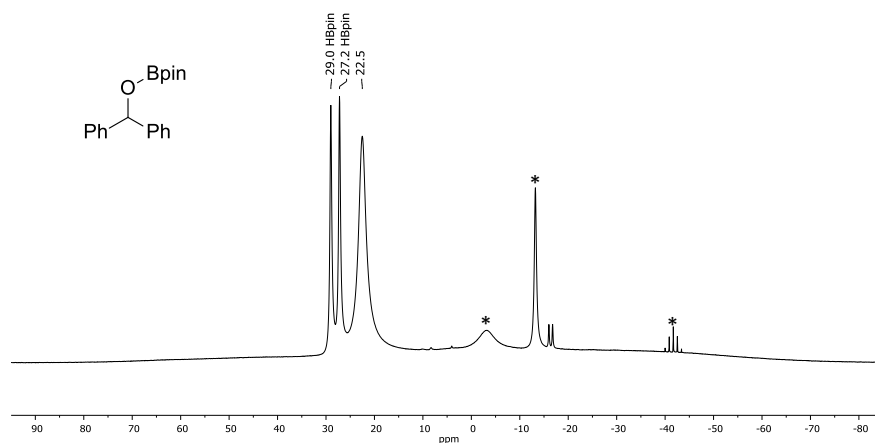


Figure S65. ^{11}B NMR spectrum (96.3 MHz, THF-d_8) recorded on the reaction mixture of $\text{Li}_2[\mathbf{2}]$, $\text{Ph}_2\text{C=O}$, and HBpin immediately after flame-sealing the NMR tube. Asterisks mark the resonances of the catalyst $\text{Li}_2[\mathbf{13}]$ and those of LiBH_4 .

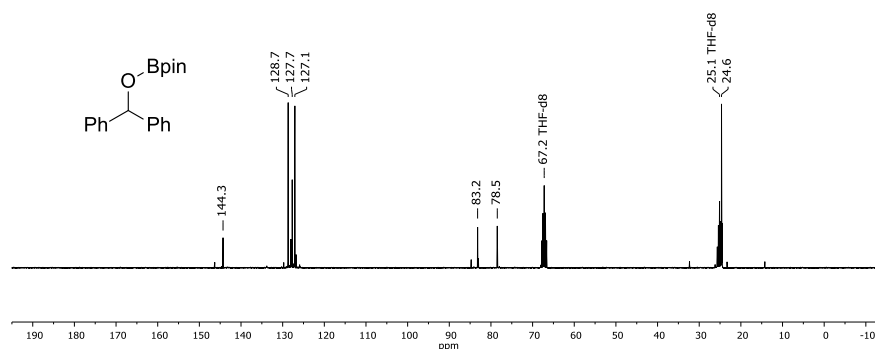


Figure S66. $^{13}\text{C}\{^1\text{H}\}$ NMR spectrum (75.4 MHz, THF-d_8) recorded on the reaction mixture of $\text{Li}_2[\mathbf{2}]$, $\text{Ph}_2\text{C=O}$, and HBpin immediately after flame-sealing the NMR tube.

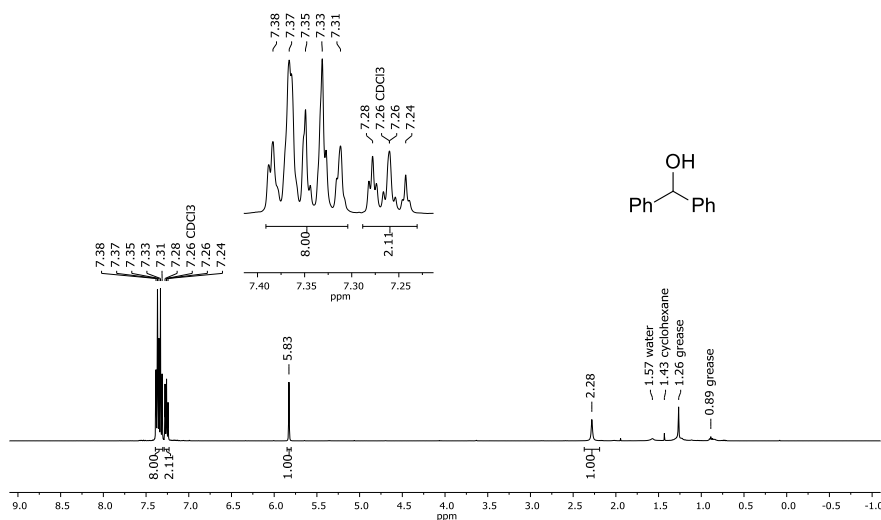


Figure S67. ^1H NMR spectrum (400.0 MHz, CDCl_3) of $\text{Ph}_2\text{C}(\text{H})\text{OH}$.

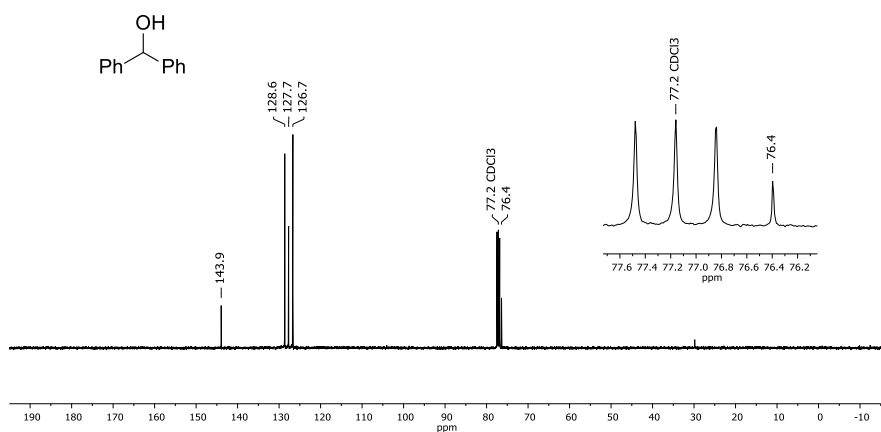


Figure S68. $^{13}\text{C}\{^1\text{H}\}$ NMR spectrum (100.6 MHz, CDCl_3) of $\text{Ph}_2\text{C}(\text{H})\text{OH}$.

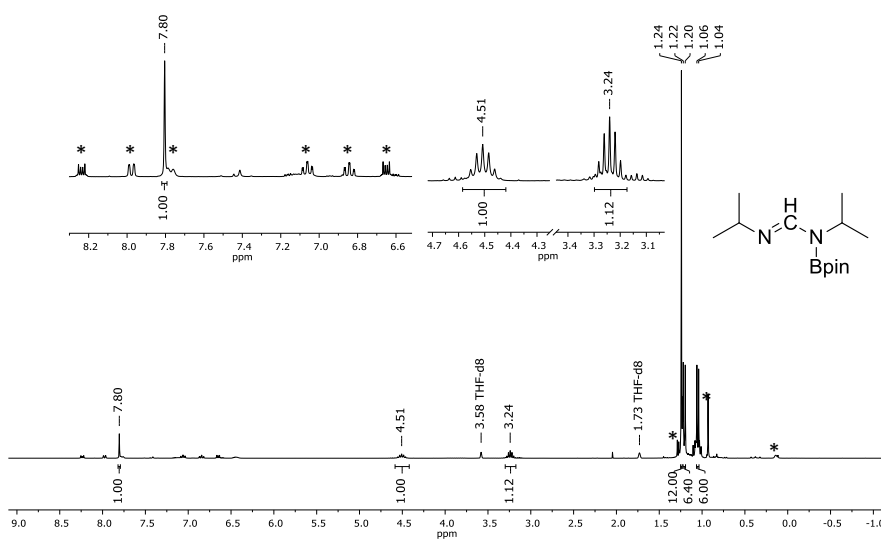


Figure S69. ^1H NMR spectrum (300.0 MHz, $\text{THF-}d_8$) recorded on the crude reaction mixture of $\text{Li}_2[\mathbf{2}]$, $i\text{PrN}=\text{C}=\text{N}i\text{Pr}$, and HBpin immediately after flame-sealing the NMR tube. Asterisks mark resonances of $\text{Li}[\mathbf{5}]$ and $\text{Li}_2[\mathbf{2}]$.

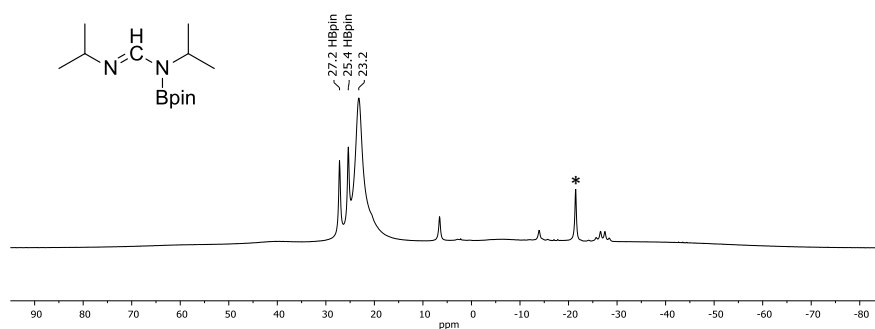


Figure S70. ^{11}B NMR spectrum (96.3 MHz, $\text{THF-}d_8$) recorded on the crude reaction mixture of $\text{Li}_2[\mathbf{2}]$, $i\text{PrN}=\text{C}=\text{NiPr}$, and HBpin immediately after flame-sealing the NMR tube. The asterisk marks a resonance of $\text{Li}[\mathbf{5}]$.

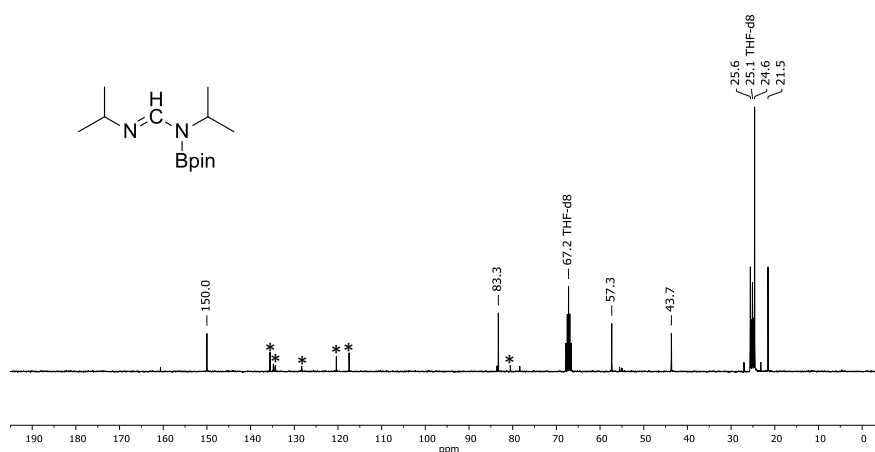


Figure S71. $^{13}\text{C}\{^1\text{H}\}$ NMR spectrum (75.4 MHz, $\text{THF-}d_8$) recorded on the reaction mixture of $\text{Li}_2[\mathbf{2}]$, $i\text{PrN}=\text{C}=\text{NiPr}$, and HBpin immediately after flame-sealing the NMR tube. Asterisks mark resonances of $\text{Li}[\mathbf{5}]$ and $\text{Li}_2[\mathbf{2}]$.

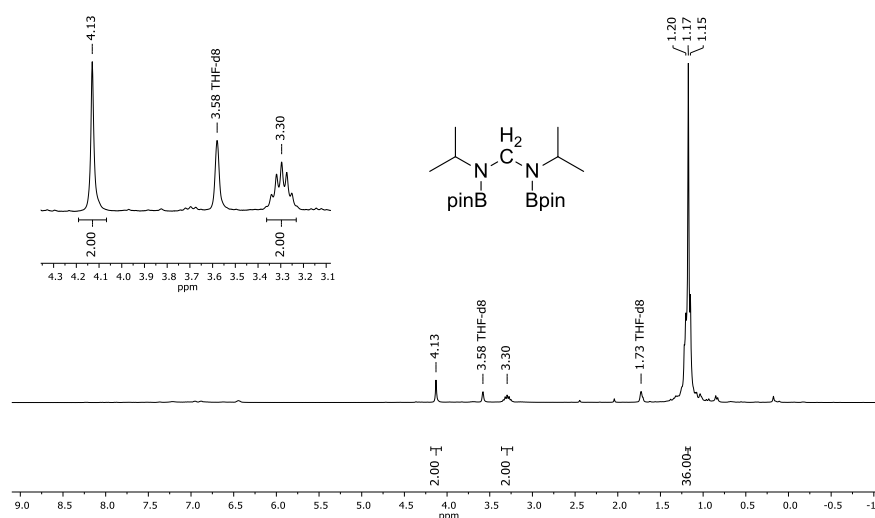


Figure S72. ^1H NMR spectrum (300.0 MHz, $\text{THF-}d_8$) recorded on the reaction mixture of $\text{Li}_2[\mathbf{2}]$, $i\text{PrN}=\text{C}=\text{NiPr}$, and 2.4 equiv. HBpin after 23 h at 100°C .

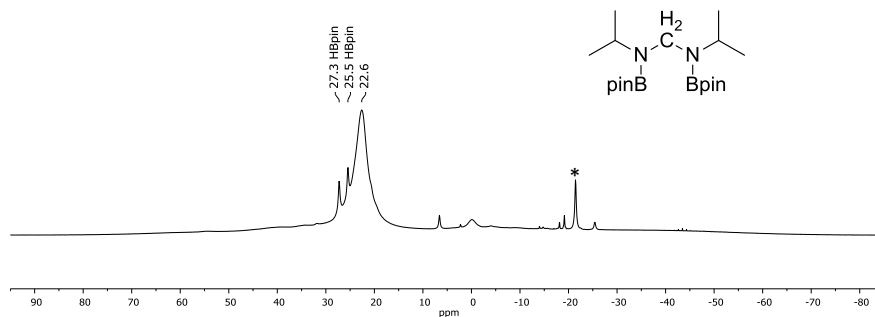


Figure S73. ^{11}B NMR spectrum (96.3 MHz, $\text{THF-}d_8$) recorded on the reaction mixture of $\text{Li}_2[\mathbf{2}]$, $i\text{PrN}=\text{C}=\text{NiPr}$, and 2.4 equiv. HBpin after 23 h at 100°C . The asterisk marks a resonance of $\text{Li}[\mathbf{5}]$.

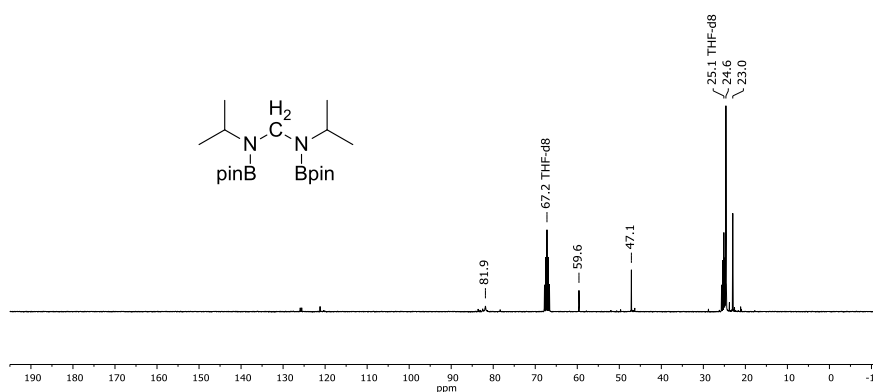


Figure S74. $^{13}\text{C}\{^1\text{H}\}$ NMR spectrum (75.4 MHz, $\text{THF-}d_8$) recorded on the reaction mixture of $\text{Li}_2[\mathbf{2}]$, $i\text{PrN}=\text{C}=\text{NiPr}$, and 2.4 equiv. HBpin after 23 h at 100°C .

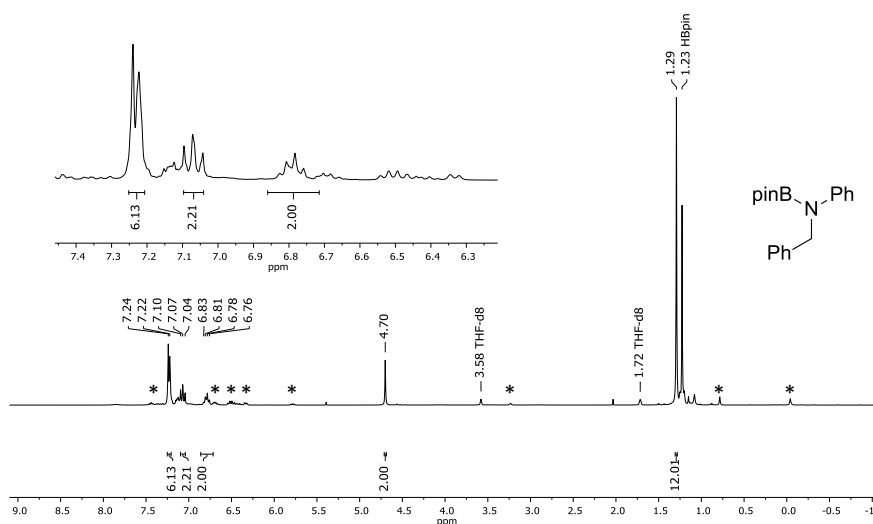


Figure S75. ^1H NMR spectrum (300.0 MHz, $\text{THF-}d_8$) recorded on the reaction mixture of $\text{Li}_2[\mathbf{2}]$, $\text{Ph}(\text{H})\text{C}=\text{NPh}$, and HBpin after 4 h at room temperature. Asterisks mark resonances of the catalyst $\text{Li}_2[\mathbf{12}]$.

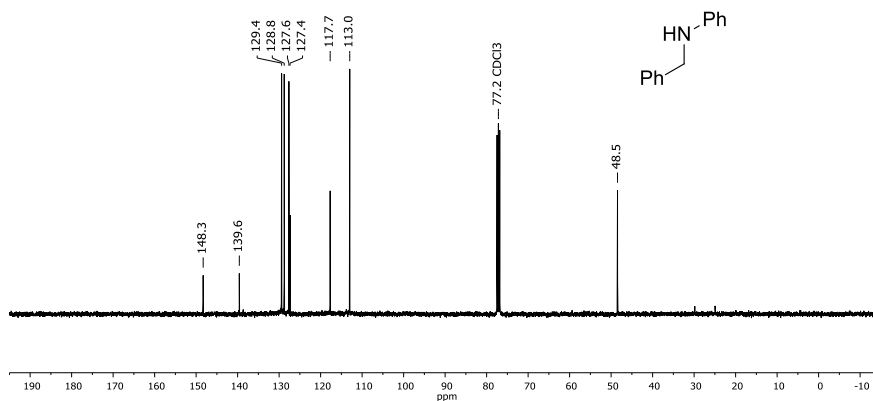


Figure S79. $^{13}\text{C}\{^1\text{H}\}$ NMR spectrum of $\text{Ph}(\text{H})_2\text{C}-\text{N}(\text{H})\text{Ph}$.

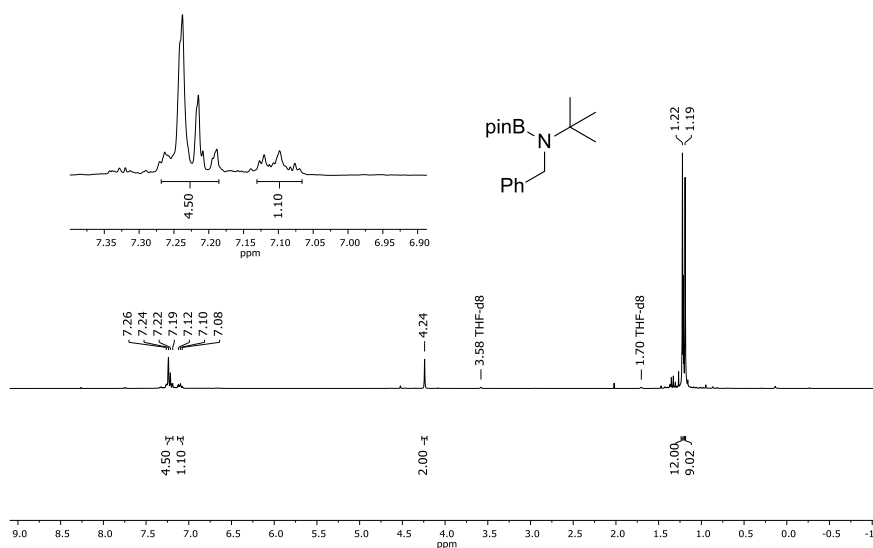


Figure S80. ^1H NMR spectrum (300.0 MHz, $\text{THF}-d_8$) recorded on the crude reaction mixture of $\text{Li}_2[\mathbf{2}]$, $\text{Ph}(\text{H})\text{C}=\text{N}t\text{Bu}$, and HBpin after 88 h at 100 °C.

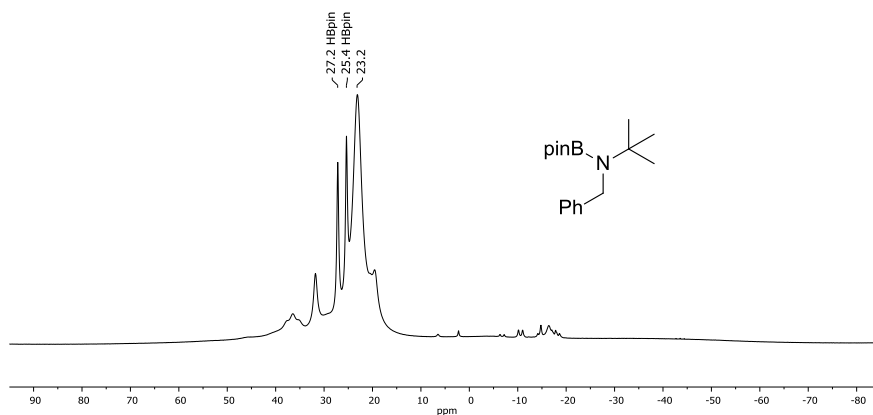


Figure S81. ^{11}B NMR spectrum (96.3 MHz, $\text{THF}-d_8$) recorded on the crude reaction mixture of $\text{Li}_2[\mathbf{2}]$, $\text{Ph}(\text{H})\text{C}=\text{N}t\text{Bu}$, and HBpin after 88 h at 100 °C.

6. X-ray crystal structure analyses

Data for all structures were collected on a STOE IPDS II two-circle diffractometer with a Genix Microfocus tube with mirror optics using $\text{MoK}\alpha$ radiation ($\lambda = 0.71073 \text{ \AA}$). The data were scaled using the frame-scaling procedure in the *X-AREA* program system.²¹ The structures were solved by direct methods using the program *SHELXS* and refined against F^2 with full-matrix least-squares techniques using the program *SHELXL*.²²

[Na(dme)]₂[**7**]: The compound is located on a center of inversion. The H atom bonded to B was isotropically refined.

[Na(thf)₂]₂[**5**]: In both thf ligands, one methylene group is disordered over two sets of sites with site occupation factors of 0.58(4) and 0.67(5) for the major occupied sites. The displacement parameters of the disordered atoms were restrained to an isotropic behavior. The crystal was twinned with a fractional contribution of 0.426(4) for the minor domain.

[Li(thf)₂]₂[**5**]: There are seven crystallographically independent formula units in the asymmetric unit. In five thf ligands, one methylene group is disordered over two sets of sites with site occupation factors of 0.53(3), 0.51(2), 0.71(3), 0.68(3), and 0.60(3) for the major occupied sites. In one thf ligand, two methylene groups are disordered over two sets of sites with a site occupation factor of 0.68(4) for the major occupied sites. The displacement parameters of the disordered atoms were restrained to an isotropic behavior. The geometric parameters of the thf ligand containing O31F were restrained to be equal to those of the thf ligand containing O41E.

[Li(12-c-4)₂]₂[**12H**]: N1 and C8 are mutually disordered with equal occupancies. Refinement for both atoms was done with an N and a C atom sharing the same coordinates and the same displacement parameters. The coordinates of the H atoms bonded to the disordered C and N atoms were refined.

{[Na(18-c-6)(thf)₂]₂Na[**S2**]}₂: In one thf ligand, one methylene group is disordered over two sets of sites with a site occupation factor of 0.69(3) for the major occupied sites. In one thf ligand, all four methylene groups are disordered over two sets of sites with a site occupation factor of 0.512(10) for the major occupied sites. The displacement parameters of the disordered atoms were restrained to an isotropic behavior. The anions and the two Na⁺ cations form a centrosymmetric dimer.

{[Li(thf)]₂[Ph(H)₂C–N*t*Bu]}₂: There are three independent formula units in the asymmetric unit. In three thf ligands, one methylene group is disordered over two sets of sites with a site occupation factor of 0.61(2), 0.52(2), and 0.75(3) for the major occupied sites. In one thf ligand, two methylene groups are disordered over two sets of sites with a site occupation factor of 0.62(2) for the major occupied sites. The displacement parameters of the disordered atoms were restrained to an isotropic behavior.

[Li(12-c-4)₂]₂[**6**]·C₆H₆: In one crown-ether ligand, all methylene groups are disordered over two sets of sites with a site occupation factor of 0.619(7) for the major occupied sites. The C₆H₆ molecule is located on a center of inversion and is disordered over two sets of sites with a site occupation factor of 0.65(2) for the major occupied sites. The displacement parameters of the C₆H₆ atoms were restrained to an

isotropic behavior. Bond distances in the C₆H₆ molecule were restrained to be similar. The boron-bonded H(1) atom was freely refined.

[Li(thf)₄][Li(thf)₂][**10**]: In one thf ligand, three methylene groups are disordered over two sets of sites with a site occupation factor of 0.51(4) for the major occupied sites. In three thf ligands, two methylene groups are disordered over two sets of sites with a site occupation factor of 0.66(3), 0.52(3), and 0.70(4) for the major occupied sites. In one thf ligand, one methylene group is disordered over two sets of sites with a site occupation factor of 0.62(5) for the major occupied sites. The displacement parameters of bonded atoms in all thf ligands including the Li⁺ ions were restrained to be similar. The absolute structure could not be determined reliably: Flack-x-parameter 0.4(10).

[Li(12-c-4)₂][**S1**]·THF: One thf ligand is disordered over a center of inversion with equal occupancies. Anion and cation are located on a two-fold rotation axis.

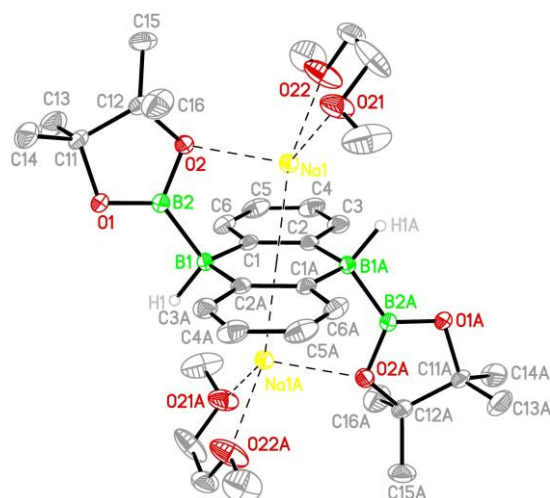


Figure S82. Molecular structure of $[\text{Na}(\text{dme})_2][7]$ in the solid state. Displacement ellipsoids are drawn at the 30% probability level; carbon-bonded hydrogen atoms are omitted for clarity. Selected bond lengths (\AA), atom \cdots atom distances (\AA), bond angles ($^\circ$), and dihedral angles ($^\circ$): $\text{B}(1)\text{--H}(1) = 1.18(2)$, $\text{B}(1)\text{--B}(2) = 1.711(3)$, $\text{B}(1)\text{--C}(1) = 1.633(3)$, $\text{B}(1)\text{--C}(2\text{A}) = 1.635(3)$, $\text{C}(1)\text{--C}(2) = 1.417(3)$; $\text{O}(2)\cdots\text{Na}(1) = 2.3359(16)$, $\text{Na}(1)\cdots\text{COG} = 2.3276(8)$; $\text{B}(2)\text{--B}(1)\text{--H}(1) = 108.9(11)$, $\text{C}(1)\text{--B}(1)\text{--C}(2\text{A}) = 113.84(16)$; $\text{B}(2)\text{B}(1)\text{H}(1)//\text{O}(1)\text{B}(2)\text{O}(2) = 19(2)$, $\text{C}(1)\text{B}(1)\text{C}(2\text{A})//\text{C}(1)\text{C}(2)\text{C}(1\text{A})\text{C}(2\text{A}) = 1.8(4)$. COG = centroid of the B_2C_4 ring. Symmetry transformation used to generate equivalent atoms: A: $-x+1, -y+1, -z$.

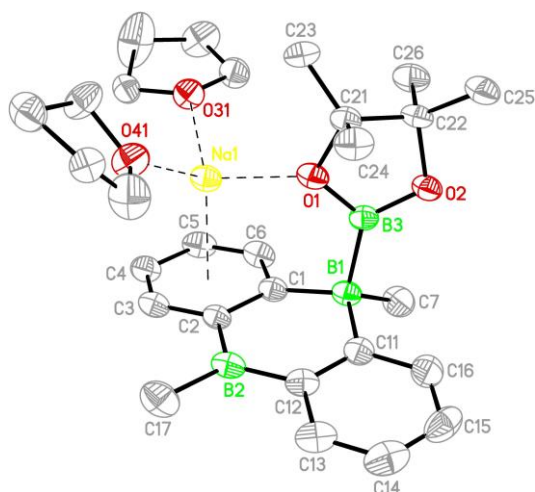


Figure S83. Molecular structure of $[\text{Na}(\text{thf})_2][5]$ in the solid state. Displacement ellipsoids are drawn at the 30% probability level; hydrogen atoms are omitted for clarity. Selected bond lengths (\AA), atom \cdots atom distances (\AA), bond angles ($^\circ$), and dihedral angles ($^\circ$): $\text{B}(1)\text{--B}(3) = 1.731(9)$, $\text{B}(1)\text{--C}(1) = 1.589(10)$, $\text{B}(1)\text{--C}(7) = 1.663(10)$, $\text{B}(1)\text{--C}(11) = 1.623(10)$, $\text{B}(2)\text{--C}(2) = 1.574(9)$, $\text{B}(2)\text{--C}(12) = 1.514(11)$, $\text{B}(2)\text{--C}(17) = 1.615(11)$, $\text{C}(1)\text{--C}(2) = 1.441(8)$, $\text{C}(11)\text{--C}(12) = 1.429(9)$; $\text{O}(1)\cdots\text{Na}(1) = 2.288(5)$, $\text{Na}(1)\cdots\text{COG} = 2.514(4)$; $\text{B}(3)\text{--B}(1)\text{--C}(7) = 108.2(6)$, $\text{C}(1)\text{--B}(1)\text{--C}(11) = 112.7(6)$, $\text{C}(2)\text{--B}(2)\text{--C}(12) = 120.0(6)$; $\text{B}(3)\text{B}(1)\text{C}(7)//\text{O}(1)\text{B}(3)\text{O}(2) = 33.2(7)$, $\text{C}(1)\text{B}(1)\text{C}(11)//\text{C}(1)\text{C}(2)\text{C}(11)\text{C}(12) = 13.5(4)$. COG = centroid of the C_6 ring.

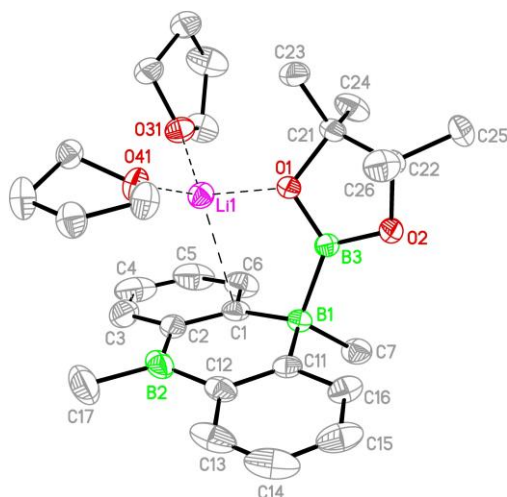


Figure S84. Molecular structure of one of the seven crystallographically independent $[\text{Li}(\text{thf})_2][\mathbf{5}]$ molecules in the solid state. Displacement ellipsoids are drawn at the 30% probability level; hydrogen atoms are omitted for clarity. Selected bond lengths (Å), atom⋯atom distances (Å), and bond angles (°; included in {} are the corresponding values of the other six independent molecules): $\text{B}(1)\text{--}\text{B}(3) = 1.718(4)$ {1.721(4)/1.717(4)/1.716(5)/1.720(4)/1.718(5)/1.725(5)}, $\text{B}(1)\text{--}\text{C}(1) = 1.609(4)$ {1.616(4)/1.613(4)/1.616(4)/1.613(4)/1.613(4)/1.617(4)}, $\text{B}(1)\text{--}\text{C}(7) = 1.648(4)$ {1.664(4)/1.664(4)/1.650(4)/1.648(4)/1.656(4)/1.652(4)}, $\text{B}(1)\text{--}\text{C}(11) = 1.611(4)$ {1.604(4)/1.612(4)/1.617(4)/1.615(4)/1.607(5)/1.610(5)}, $\text{B}(2)\text{--}\text{C}(2) = 1.557(5)$ {1.557(5)/1.558(5)/1.541(5)/1.559(5)/1.554(5)/1.552(5)}, $\text{B}(2)\text{--}\text{C}(12) = 1.546(5)$ {1.555(5)/1.550(4)/1.562(5)/1.549(5)/1.540(5)/1.549(5)}, $\text{B}(2)\text{--}\text{C}(17) = 1.579(5)$ {1.570(5)/1.578(5)/1.581(5)/1.580(5)/1.583(5)/1.586(5)}, $\text{C}(1)\text{--}\text{C}(2) = 1.418(4)$ {1.425(4)/1.416(4)/1.420(4)/1.417(4)/1.417(4)/1.417(4)}, $\text{C}(11)\text{--}\text{C}(12) = 1.424(4)$ {1.424(4)/1.421(4)/1.422(4)/1.423(4)/1.430(4)/1.428(4)}, $\text{O}(1)\cdots\text{Li}(1) = 1.927(5)$ {1.921(5)/1.922(5)/1.918(5)/1.928(5)/1.909(5)/1.921(5)}; $\text{B}(3)\text{--}\text{B}(1)\text{--}\text{C}(7) = 107.2(2)$ {101.1(2)/100.2(2)/106.0(2)/107.2(2)/105.2(3)/106.6(2)}, $\text{C}(1)\text{--}\text{B}(1)\text{--}\text{C}(11) = 112.6(2)$ {113.1(2)/112.5(2)/112.2(2)/112.3(2)/112.3(3)/112.5(3)}, $\text{C}(2)\text{--}\text{B}(2)\text{--}\text{C}(12) = 119.6(3)$ {118.6(3)/118.9(3)/119.0(3)/119.0(3)/118.8(3)/119.1(3)}.

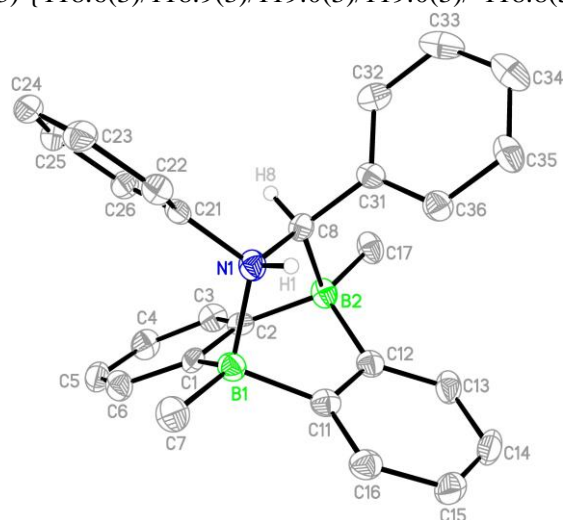


Figure S85. Molecular structure of $[\text{Li}(12\text{-c-}4)_2][\mathbf{12H}]$ in the solid state. Displacement ellipsoids are drawn at the 30% probability level; the $[\text{Li}(12\text{-c-}4)_2]^+$ ion and all carbon-bonded hydrogen atoms except H(8) are omitted for clarity. Selected bond lengths (Å) and bond angles (°): $\text{B}(1)\text{--}\text{C}(1) = 1.598(8)$, $\text{B}(1)\text{--}\text{C}(7) = 1.617(8)$, $\text{B}(1)\text{--}\text{C}(11) = 1.629(8)$, $\text{B}(1)\text{--}\text{N}(1) = 1.697(7)$, $\text{B}(2)\text{--}\text{C}(2) = 1.613(8)$, $\text{B}(2)\text{--}\text{C}(12) = 1.611(9)$, $\text{B}(2)\text{--}\text{C}(17) = 1.611(8)$, $\text{C}(1)\text{--}\text{C}(2) = 1.422(7)$, $\text{C}(11)\text{--}\text{C}(12) = 1.426(7)$, $\text{N}(1)\text{--}\text{C}(8) = 1.523(6)$,

$N(1)-C(21) = 1.480(7)$, $N(1)-H(1) = 0.94(6)$; $C(1)-B(1)-C(11) = 108.3(4)$, $C(2)-B(2)-C(12) = 108.4(4)$.

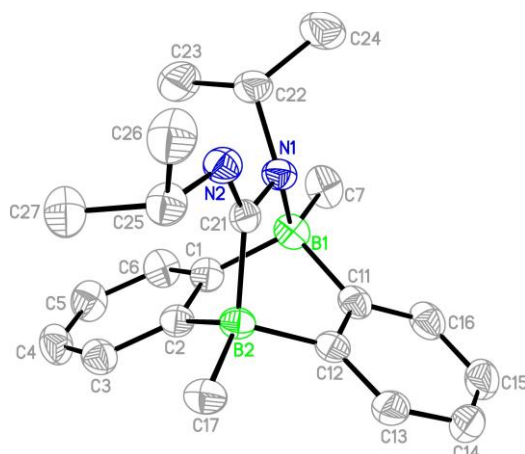


Figure S86. Molecular structure of $\{[Na(18-c-6)(thf)_2]Na[S2]\}_2$ in the solid state. Displacement ellipsoids are drawn at the 50% probability level; the $[Na(18-c-6)(thf)_2]^+$ and Na^+ ions and all hydrogen atoms are omitted for clarity. Selected bond lengths (\AA) and bond angles ($^\circ$): $B(1)-C(1) = 1.623(3)$, $B(1)-C(7) = 1.625(3)$, $B(1)-C(11) = 1.632(3)$, $B(1)-N(1) = 1.639(2)$, $B(2)-C(2) = 1.640(3)$, $B(2)-C(12) = 1.635(3)$, $B(2)-C(17) = 1.635(3)$, $B(2)-C(21) = 1.675(2)$, $N(1)-C(21) = 1.409(2)$, $N(2)-C(21) = 1.316(2)$; $C(1)-B(1)-C(11) = 106.09(15)$, $C(2)-B(2)-C(12) = 107.06(14)$, $N(1)-C(21)-N(2) = 116.52(15)$.

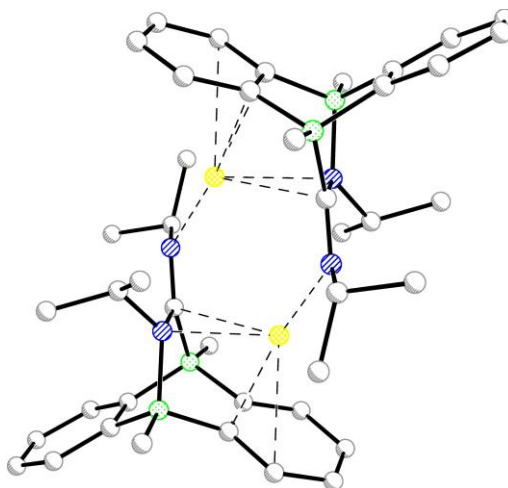


Figure S87. Description of the solid-state structure of $[Na(18-c-6)(thf)_2]_2\{Na[S2]\}_2$ (the $[Na(18-c-6)(thf)_2]^+$ ions are omitted for clarity): The crystal lattice consists of centrosymmetric dimers, in which two $[DBA]^{2-}$ entities are connected by two naked Na^+ ions located between them. The cations are coordinated by the N atom of the imine unit of one anionic fragment and the DBA-bridging C and N atoms of the second anionic fragment; the octahedral ligand sphere is completed by short contacts to one phenylene ring of the second fragment. Symmetry transformation used to generate equivalent atoms: $-x+1, -y, -z$.

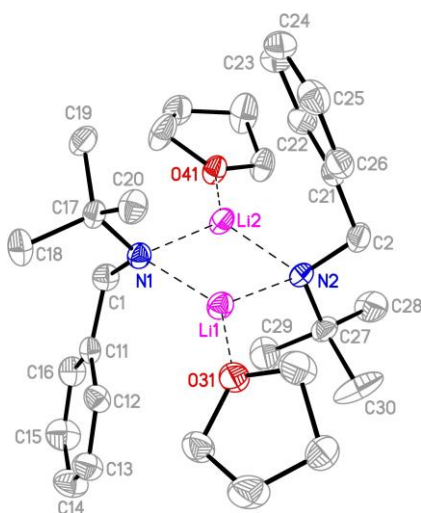


Figure S88. Molecular structure of one of the three crystallographically independent moieties of $[\text{Li}(\text{thf})][\text{Ph}(\text{H})_2\text{C}-\text{N}t\text{Bu}]_2$ in the solid state. Displacement ellipsoids are drawn at the 30% probability level; hydrogen atoms are omitted for clarity. Selected bond lengths (\AA) and bond angles ($^\circ$; included in $\{\}$) are the corresponding values of the other two independent molecules): $\text{N}(1)-\text{Li}(1) = 2.000(4)$ $\{2.003(4)/2.003(4)\}$, $\text{N}(1)-\text{Li}(2) = 2.012(4)$ $\{2.004(4)/2.042(5)\}$, $\text{N}(1)-\text{C}(1) = 1.455(3)$ $\{1.455(3)/1.470(3)\}$, $\text{N}(2)-\text{Li}(1) = 2.041(4)$ $\{2.033(4)/2.021(4)\}$, $\text{N}(2)-\text{Li}(2) = 2.000(4)$ $\{2.003(4)/2.024(4)\}$, $\text{N}(2)-\text{C}(2) = 1.451(3)$ $\{1.453(3)/1.460(3)\}$; $\text{C}(1)-\text{N}(1)-\text{C}(17) = 113.77(18)$ $\{113.10(17)/113.32(19)\}$, $\text{C}(2)-\text{N}(2)-\text{C}(27) = 112.29(18)$ $\{111.99(19)/111.70(18)\}$.

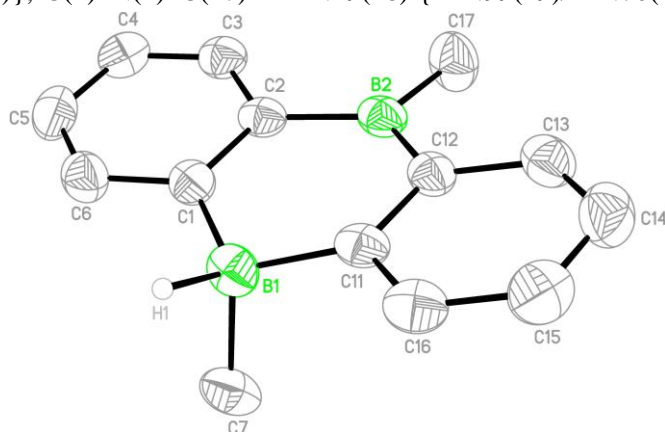


Figure S89. Molecular structure of $[\text{Li}(12\text{-c-}4)_2][\mathbf{6}] \cdot \text{C}_6\text{H}_6$ in the solid state. Displacement ellipsoids are drawn at the 50% probability level; the $[\text{Li}(12\text{-c-}4)_2]^+$ ion, the C_6H_6 molecule, and all carbon-bonded hydrogen atoms are omitted for clarity. Selected bond lengths (\AA) and bond angles ($^\circ$): $\text{B}(1)-\text{H}(1) = 1.29(2)$, $\text{B}(1)-\text{C}(1) = 1.611(4)$, $\text{B}(1)-\text{C}(7) = 1.647(4)$, $\text{B}(1)-\text{C}(11) = 1.609(4)$, $\text{B}(2)-\text{C}(2) = 1.562(4)$, $\text{B}(2)-\text{C}(12) = 1.555(4)$, $\text{B}(2)-\text{C}(17) = 1.581(4)$, $\text{C}(1)-\text{C}(2) = 1.424(3)$, $\text{C}(11)-\text{C}(12) = 1.419(3)$; $\text{H}(1)-\text{B}(1)-\text{C}(7) = 100.7(10)$, $\text{C}(1)-\text{B}(1)-\text{C}(11) = 112.7(2)$, $\text{C}(2)-\text{B}(2)-\text{C}(12) = 119.0(2)$.

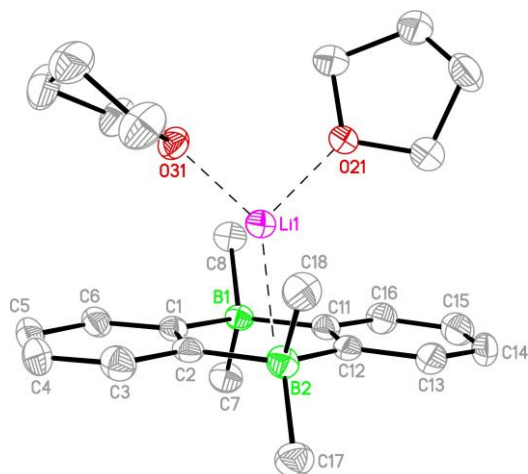


Figure S90. Molecular structure of $[\text{Li}(\text{thf})_4][\text{Li}(\text{thf})_2][\mathbf{10}]$ in the solid state. Displacement ellipsoids are drawn at the 30% probability level; the $[\text{Li}(\text{thf})_4]^+$ ion and all hydrogen atoms are omitted for clarity. Selected bond lengths (\AA), atom \cdots atom distances (\AA), and bond angles ($^\circ$): $\text{B}(1)\text{--C}(1) = 1.641(7)$, $\text{B}(1)\text{--C}(7) = 1.641(8)$, $\text{B}(1)\text{--C}(8) = 1.672(7)$, $\text{B}(1)\text{--C}(11) = 1.644(7)$, $\text{B}(2)\text{--C}(2) = 1.652(7)$, $\text{B}(2)\text{--C}(12) = 1.637(8)$, $\text{B}(2)\text{--C}(17) = 1.643(8)$, $\text{B}(2)\text{--C}(18) = 1.679(8)$, $\text{C}(1)\text{--C}(2) = 1.424(6)$, $\text{C}(11)\text{--C}(12) = 1.405(7)$; $\text{Li}(1)\cdots\text{COG} = 1.968(9)$; $\text{C}(1)\text{--B}(1)\text{--C}(11) = 112.0(4)$, $\text{C}(7)\text{--B}(1)\text{--C}(8) = 106.8(4)$, $\text{C}(2)\text{--B}(2)\text{--C}(12) = 111.8(4)$, $\text{C}(17)\text{--B}(2)\text{--C}(18) = 107.4(4)$. COG = centroid of the B_2C_4 ring.

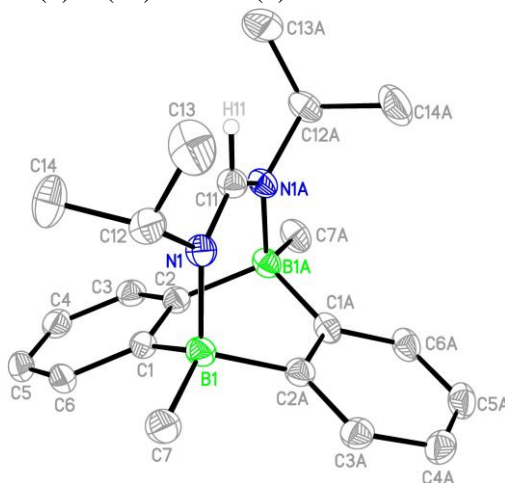


Figure S91. Molecular structure of $[\text{Li}(12\text{-c-}4)_2][\mathbf{S1}]\cdot\text{THF}$ in the solid state. Displacement ellipsoids are drawn at the 30% probability level; the $[\text{Li}(12\text{-c-}4)_2]^+$ ion, the non-coordinating THF molecule, and all hydrogen atoms (except for H(11)) are omitted for clarity. Selected bond lengths (\AA) and bond angles ($^\circ$): $\text{B}(1)\text{--C}(1) = 1.611(4)$, $\text{B}(1)\text{--C}(2\text{A}) = 1.633(4)$, $\text{B}(1)\text{--C}(7) = 1.629(4)$, $\text{B}(1)\text{--N}(1) = 1.644(3)$, $\text{C}(1)\text{--C}(2) = 1.429(3)$, $\text{N}(1)\text{--C}(11) = 1.326(2)$, $\text{N}(1)\text{--C}(12) = 1.485(3)$; $\text{C}(1)\text{--B}(1)\text{--C}(2\text{A}) = 109.6(2)$, $\text{C}(7)\text{--B}(1)\text{--N}(1) = 110.3(2)$, $\text{C}(11)\text{--N}(1)\text{--C}(12) = 115.0(2)$, $\text{N}(1)\text{--C}(11)\text{--N}(1\text{A}) = 129.6(3)$. Symmetry transformation used to generate equivalent atoms: A: $-x+1, y, -z+3/2$.

Table S5. Selected crystallographic data for [Na(dme)]₂[**7**], [Na(thf)₂][**5**], and [Li(thf)₂][**5**].

compound	[Na(dme)] ₂ [7]	[Na(thf) ₂][5]	[Li(thf) ₂][5]
internal code	wa2936	wa2943	wa3054
CCDC	2207512	2207513	2207514
formula	C ₃₂ H ₅₄ B ₄ Na ₂ O ₈	C ₂₈ H ₄₂ B ₃ NaO ₄	C ₂₈ H ₄₂ B ₃ LiO ₄
M _r	655.97	498.03	481.98
T (K)	173(2)	173(2)	173(2)
radiation, λ (Å)	MoKα, 0.71073	MoKα, 0.71073	MoKα, 0.71073
crystal system	triclinic	monoclinic	monoclinic
space group	<i>P</i> −1	<i>P</i> 2 ₁ /n	<i>P</i> 2 ₁ /n
<i>a</i> (Å)	9.5043(6)	9.6203(8)	29.1123(6)
<i>b</i> (Å)	10.1028(7)	16.4732(10)	15.8326(3)
<i>c</i> (Å)	11.4194(8)	18.2301(13)	43.5324(10)
α (°)	84.951(5)	90	90
β (°)	81.475(5)	90.025(6)	102.002(2)
γ (°)	62.613(5)	90	90
<i>V</i> (Å ³)	962.59(12)	2889.1(4)	19626.5(7)
<i>Z</i>	1	4	28
<i>D</i> _{calcd} (g cm ^{−3})	1.132	1.145	1.142
<i>F</i> (000)	352	1072	7280
μ (mm ^{−1})	0.096	0.085	0.071
crystal size (mm)	0.26 x 0.26 x 0.13	0.23 x 0.19 x 0.19	0.29 x 0.26 x 0.26
crystal shape, color	colorless block	colorless block	colorless block
reflections collected	11702	31985	203002
independent reflections	3583	5111	34632
<i>R</i> _{int}	0.0210	0.1179	0.0783
data/restraints/parameters	3583 / 0 / 212	5111 / 24 / 347	34632 / 135 / 2345
<i>R</i> ₁ , <i>wR</i> ₂ (<i>I</i> > 2 σ(<i>I</i>))	0.0595, 0.1464	0.0994, 0.2288	0.0801, 0.2172
<i>R</i> ₁ , <i>wR</i> ₂ (all data)	0.0667, 0.1530	0.1373, 0.2655	0.1499, 0.2751
GOF on <i>F</i> ²	1.050	1.129	1.032
largest difference peak and hole (e Å ^{−3})	0.648, −0.485	0.307, −0.321	0.446, −0.327

Table S6. Selected crystallographic data for [Li(12-c-4)₂][**12H**], {[Na(18-c-6)(thf)₂]Na[**S2**]}₂, and {[Li(thf)][Ph(H)₂C–N*t*Bu]}₂.

compound	[Li(12-c-4) ₂][12H]	{[Na(18-c-6)(thf) ₂]Na[S2]} ₂	{[Li(thf)][Ph(H) ₂ C–N <i>t</i> Bu]} ₂
internal code	wa2906	wa2700	wa3085
CCDC	2207515	2207516	2207517
formula	C ₄₃ H ₅₈ B ₂ LiNO ₈	C ₈₂ H ₁₃₆ B ₄ N ₄ Na ₄ O ₁₆	C ₃₀ H ₄₈ Li ₂ N ₂ O ₂
M _r	745.46	1569.14	482.58
T(K)	173(2)	173(2)	173(2)
radiation, λ(Å)	MoKα, 0.71073	MoKα, 0.71073	MoKα, 0.71073
crystal system	monoclinic	triclinic	monoclinic
space group	<i>P</i> 2 ₁ / <i>c</i>	<i>P</i> –1	<i>P</i> 2 ₁ / <i>c</i>
<i>a</i> (Å)	10.9511(10)	10.2466(4)	18.6111(6)
<i>b</i> (Å)	24.516(3)	14.7968(6)	16.4244(4)
<i>c</i> (Å)	15.2282(15)	15.6728(6)	30.4468(9)
α (°)	90	108.371(3)	90
β (°)	95.506(8)	95.677(3)	101.989(2)
γ (°)	90	90.320(3)	90
<i>V</i> (Å ³)	4069.6(7)	2242.39(16)	9103.9(5)
<i>Z</i>	4	1	12
<i>D</i> _{calcd} (g cm ^{–3})	1.217	1.162	1.056
<i>F</i> (000)	1600	848	3168
μ (mm ^{–1})	0.081	0.094	0.064
crystal size (mm)	0.28 x 0.13 x 0.13	0.24 x 0.19 x 0.13	0.29 x 0.27 x 0.24
crystal shape, color	colorless needle	colorless block	colorless block
reflections collected	31138	44204	91907
independent reflections	7152	8385	16084
<i>R</i> _{int}	0.1295	0.0329	0.0558
data/restraints/ parameters	7152 / 0 / 502	8385 / 60 / 543	16084 / 60 / 1022
<i>R</i> ₁ , <i>wR</i> ₂ (<i>I</i> > 2 σ(<i>I</i>))	0.1106, 0.2115	0.0571, 0.1515	0.0742, 0.1949
<i>R</i> ₁ , <i>wR</i> ₂ (all data)	0.1892, 0.2467	0.0647, 0.1570	0.1004, 0.2124
GOF on <i>F</i> ²	1.117	1.071	1.055
largest difference peak and hole (e Å ^{–3})	0.261, –0.271	0.668, –0.263	0.456, –0.314

Table S7. Selected crystallographic data for [Li(12-c-4)₂][**6**]·C₆H₆, [Li(thf)₄][Li(thf)₂][**10**], and [Li(12-c-4)₂][**S1**].THF.

compound	[Li(12-c-4) ₂][6].C ₆ H ₆	[Li(thf) ₄][Li(thf) ₂][10]	[Li(12-c-4) ₂][S1].THF
internal code	wa2944	wa2804	wa2840
CCDC	2207518	2207519	2207520
formula	C ₃₃ H ₅₀ B ₂ LiO ₈	C ₄₀ H ₆₈ B ₂ Li ₂ O ₆	C ₄₁ H ₆₉ B ₂ LiN ₂ O ₉
M _r	603.29	680.44	762.54
T (K)	173(2)	173(2)	173(2)
radiation, λ (Å)	MoKα, 0.71073	MoKα, 0.71073	MoKα, 0.71073
crystal system	triclinic	orthorhombic	monoclinic
space group	<i>P</i> −1	<i>P</i> 2 ₁ 2 ₁ 2 ₁	<i>C</i> 2/ <i>c</i>
<i>a</i> (Å)	8.5527(5)	13.1281(9)	12.6287(12)
<i>b</i> (Å)	12.4941(7)	16.9849(16)	21.7373(13)
<i>c</i> (Å)	16.5866(11)	18.6450(10)	17.0233(15)
α (°)	75.533(5)	90	90
β (°)	75.852(5)	90	110.611(7)
γ (°)	84.925(5)	90	90
<i>V</i> (Å ³)	1663.45(18)	4157.5(5)	4374.0(7)
<i>Z</i>	2	4	4
<i>D</i> _{calcd} (g cm ^{−3})	1.204	1.087	1.158
<i>F</i> (000)	650	1488	1656
μ (mm ^{−1})	0.083	0.069	0.079
crystal size (mm)	0.18 x 0.16 x 0.04	0.26 x 0.24 x 0.19	0.18 x 0.17 x 0.05
crystal shape, color	colorless plate	colorless block	colorless plate
reflections collected	18475	17711	20437
independent reflections	6225	7334	4131
<i>R</i> _{int}	0.0341	0.0487	0.0733
data/restraints/ parameters	6225 / 142 / 503	7334 / 420 / 546	4131 / 0 / 263
<i>R</i> ₁ , <i>wR</i> ₂ (<i>I</i> > 2 σ(<i>I</i>))	0.0642, 0.1187	0.0711, 0.1496	0.0639, 0.1386
<i>R</i> ₁ , <i>wR</i> ₂ (all data)	0.1030, 0.1379	0.1151, 0.1694	0.1104, 0.1657
GOF on <i>F</i> ²	1.197	1.053	1.050
largest difference peak and hole (e Å ^{−3})	0.246, −0.179	0.272, −0.145	0.212, −0.228

7. Additional details on quantum chemical calculations

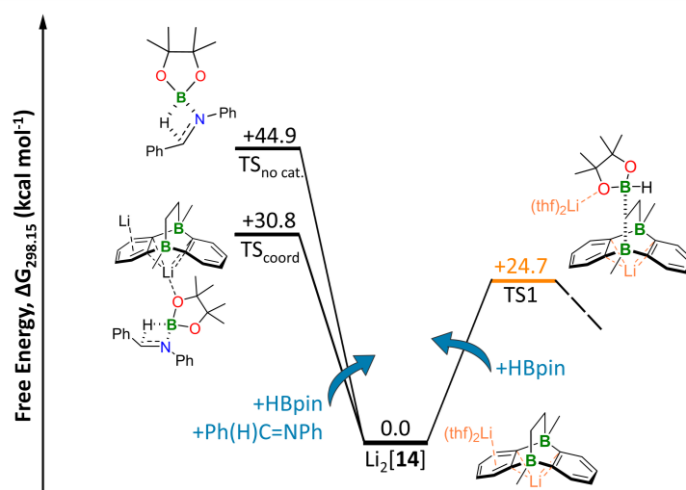


Figure S92. *Syn*-addition of HBpin to Ph(H)C=NPh as alternative hydroboration mechanism. Left: The hydroboration reaction without catalyst is characterized by a high barrier (TS_{no cat.}). Coordination of HBpin by Li₂[14] stabilizes the transition state of the *syn*-addition by about -14 kcal mol⁻¹ (TS_{coord.}), but the barrier is still too high if experimental reaction conditions are considered. The stabilization of TS_{coord.} is resulting from the electron withdrawing effect of the Li⁺ cation which renders the B center of HBpin more electrophilic. Solvation effects are included via the SMD model, but no explicit thf are taken into account. Right: Proposed rate determining step of Mechanism II, including explicit thf molecules (orange).

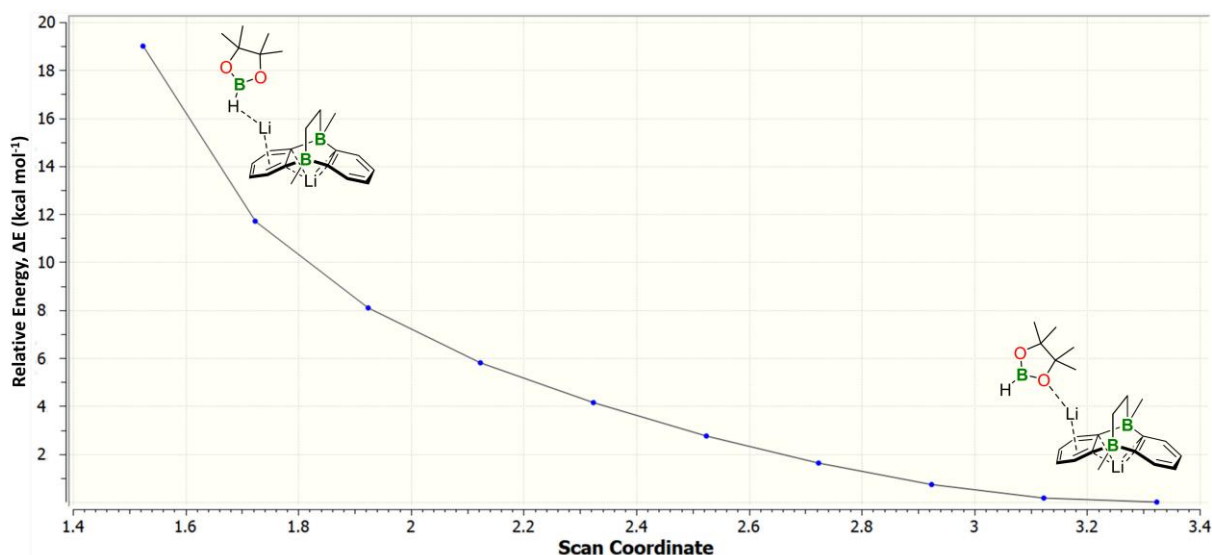


Figure S93. Interaction of HBpin with Li₂[14]. Relaxed scan of the H(Bpin)-Li distance.

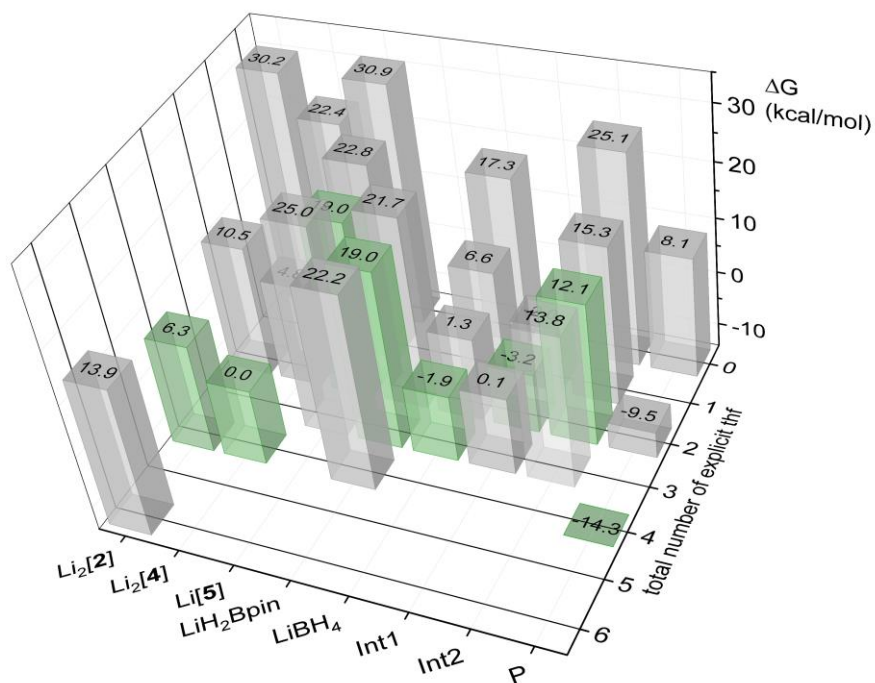


Figure S94. Solvent coordination number for each intermediate determined by free energy calculations. Marked in green: Lowest energy path with optimal coordination number.

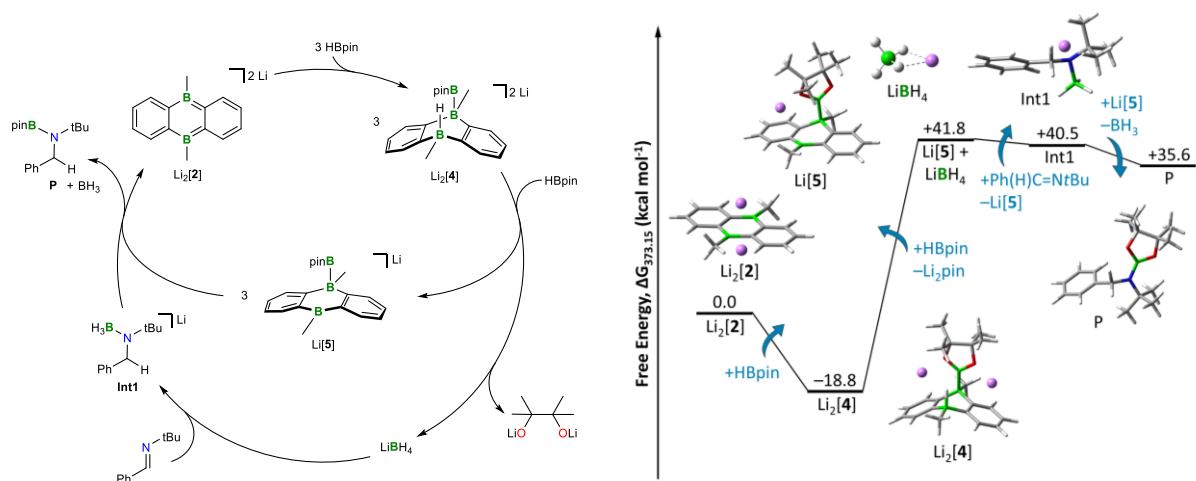


Figure S95. Initial hypothesis for the hydroboration mechanism. Three equivalents of Li₂[4] reduce one equivalent HBpin to Li[BH₄] and Li₂[pin]. The formation of Li₂[pin] is exceedingly endergonic. Thus, this mechanism is thermodynamically not possible and can be excluded. Explicit thf molecules are omitted for clarity.

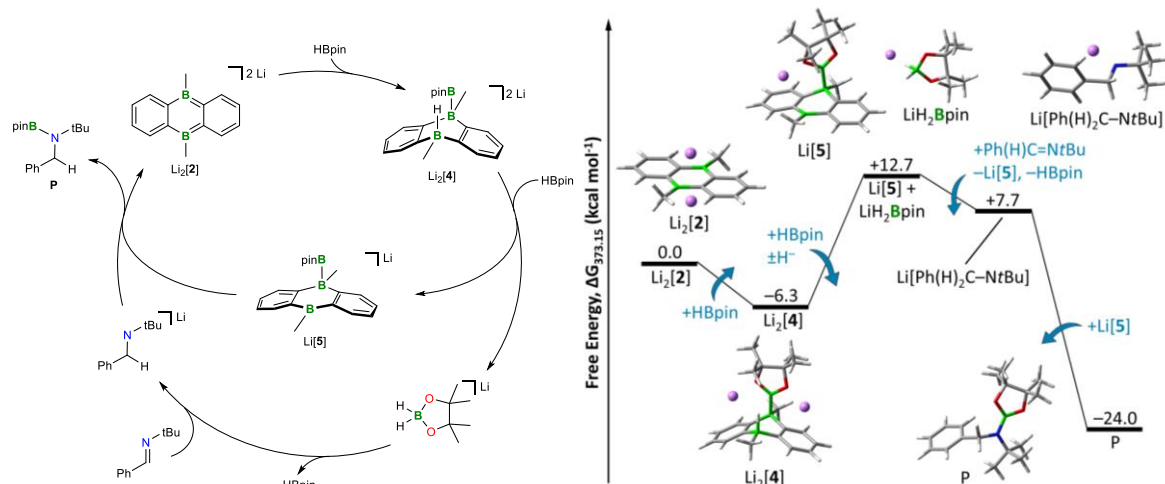


Figure S96. Second hypothetical mechanism without HBpin decomposition. Excess HBpin acts as a hydride shuttle to transport the activated hydride of $\text{Li}_2[4]$ to the substrate which is subsequently reduced. This mechanism does not explain the formation of $[\text{BH}_4]^-$ and can be excluded. Explicit thf molecules are omitted for clarity.

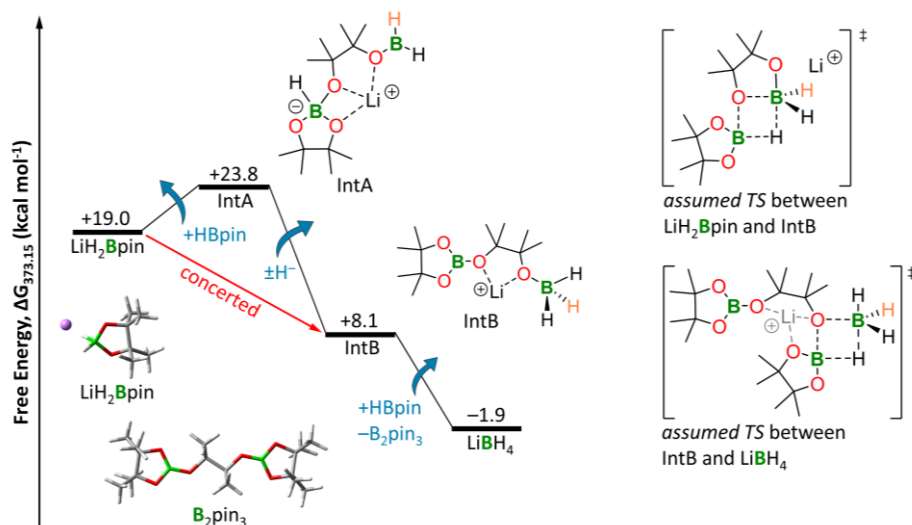


Figure S97. Decomposition of $\text{Li}[\text{H}_2\text{Bpin}]$. There are two possible ways of starting the decomposition reaction. One way is the formation of **IntA** which is the result of the O atom of $\text{Li}[\text{H}_2\text{Bpin}]$ nucleophilically attacking excess HBpin from solution. Subsequently, the hydride from the destabilized tetracoordinate B center is transferred to the terminal B center, forming **IntB**. Another way is a concerted σ -bond metathesis in which **IntB** is formed directly. In the last step, we assume a second σ -bond metathesis which leads to the formation of the stable side product B_2pin_3 and $\text{Li}[\text{BH}_4]$. Explicit thf molecules are omitted for clarity.

Table S8. Hydride Affinities. Free Energies of Hydride Transfer from $\text{Li}[\text{BH}_4]$ to X at 100°C .

X	$\text{Li}[\text{HX}]$	$\Delta G_{373.15}$ (kcal mol^{-1})
$\text{BH}_3 \cdot \text{thf}$	$\text{Li}[\text{BH}_4]$	0.0
Li[5]	Li₂[4]	+11.5
$\text{Ph}(\text{H})_2\text{C}-\text{N}(\text{BH}_2)t\text{Bu}$	Int1	+23.1
$\text{Ph}(\text{H})\text{C}=\text{N}t\text{Bu}$	$\text{Li}[\text{Ph}(\text{H})_2\text{C}-\text{N}t\text{Bu}]$	+25.5
HBpin	$\text{Li}[\text{H}_2\text{Bpin}]$	+30.5

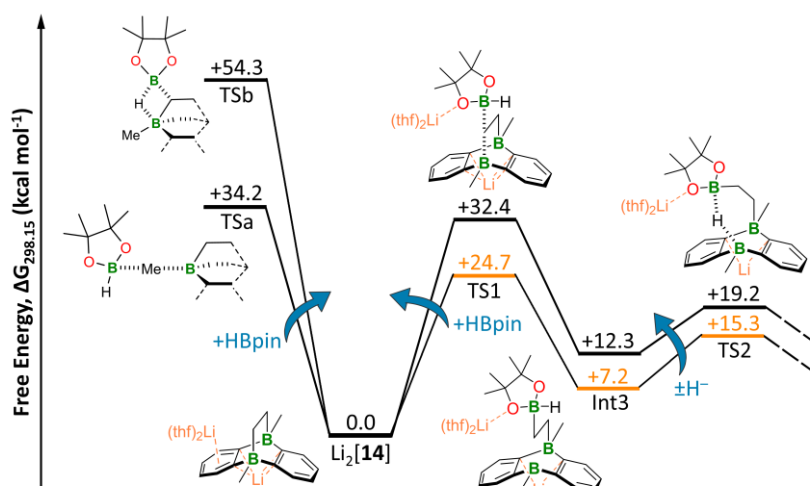


Figure S98. Left: Alternative nucleophilic attacks on HBpin. Right: Comparison of environment modelling (including explicit solvent and counterions, orange) vs SMD calculation without THF and counterions (black). **TSb** geometry was obtained via a relaxed scan (see Figure S98).

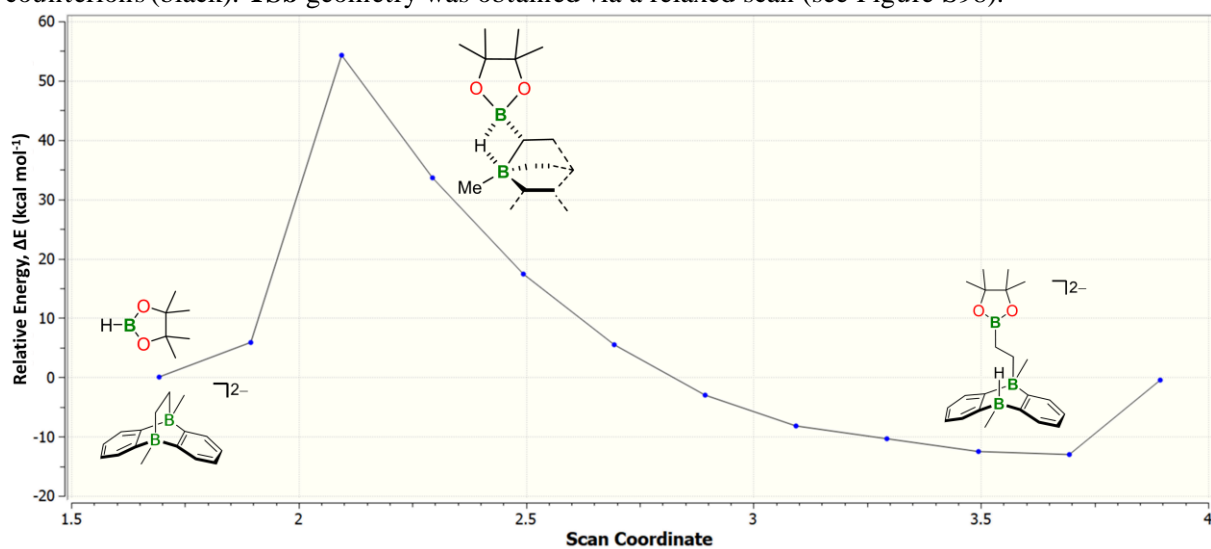


Figure S99. **TSb**: HBpin activation via σ -bond metathesis. Relaxed scan of the C(Bpin)–B(DBA) distance.

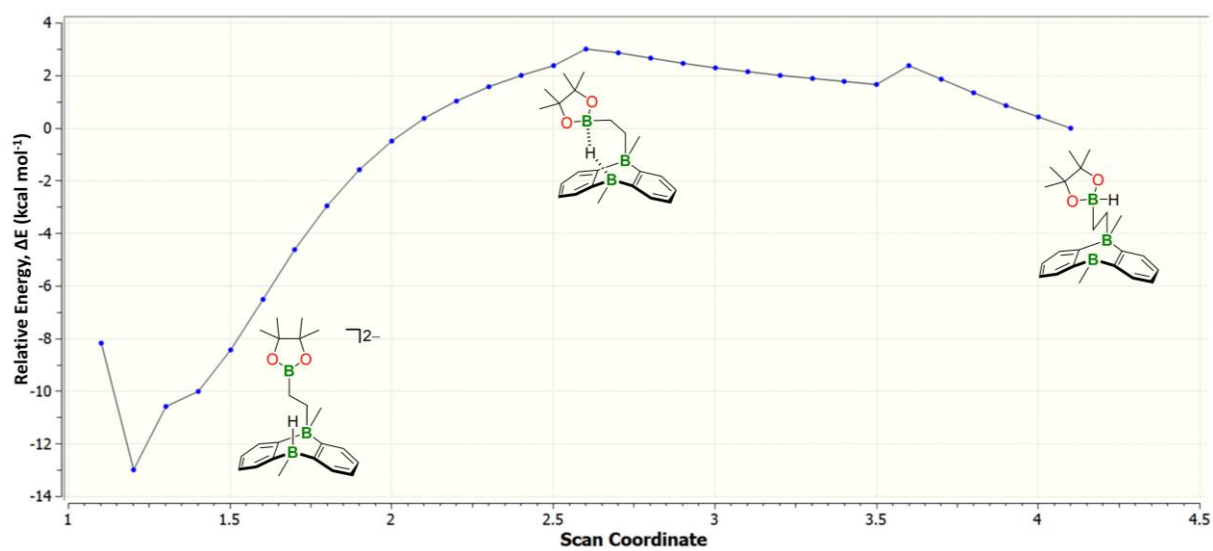


Figure S100. **TS2**: Intramolecular hydride transfer. Relaxed scan of the H(Bpin)–B(DBA) distance.

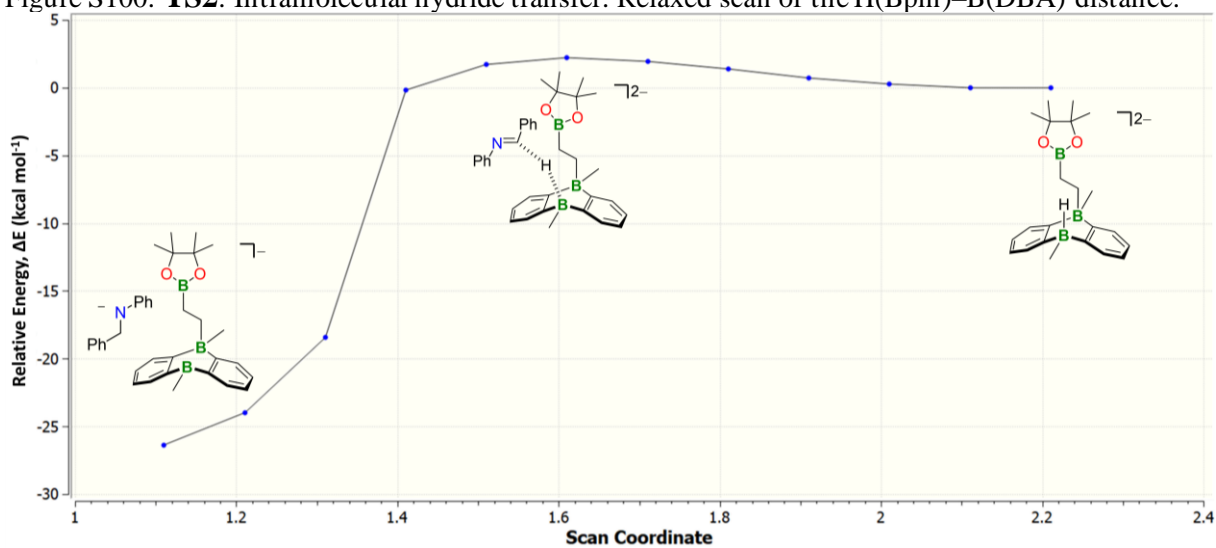


Figure S101. **TS3**: Intermolecular hydride transfer to Ph(H)C=NPh. Relaxed scan of the H(DBA)–C(H)Ph distance.

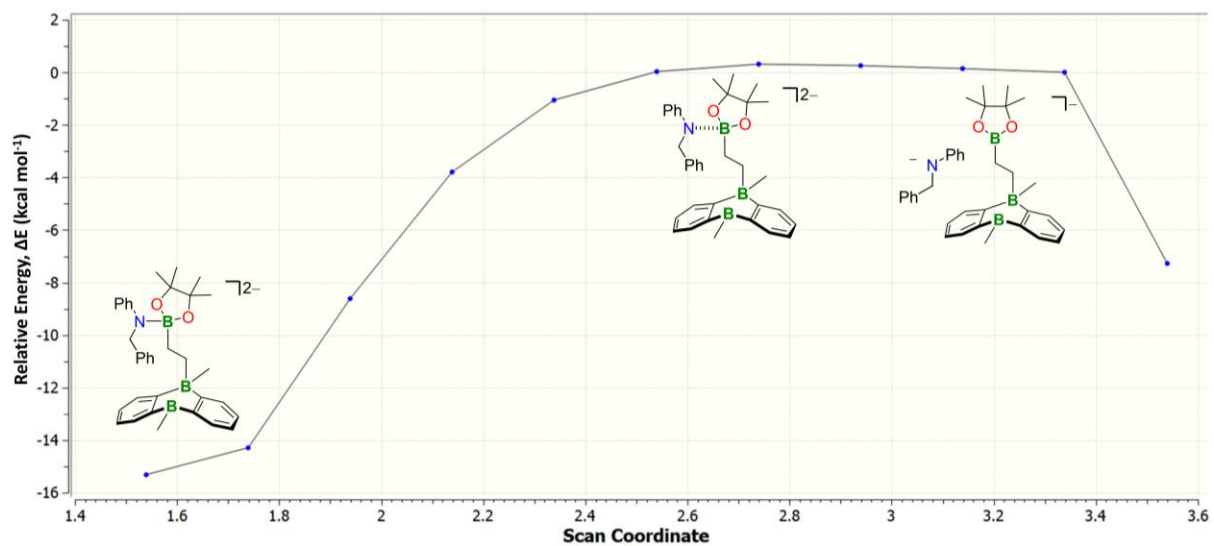


Figure S102. **TS4**: Nucleophilic attack of $[\text{Ph}(\text{H})_2\text{C}-\text{NPh}]^-$ on the B(pin) center. Relaxed scan of the N-B(pin) distance.

8. References

- 1 G. R. Fulmer, A. J. M. Miller, N. H. Sherden, H. E. Gottlieb, A. Nudelman, B. M. Stoltz, J. E. Bercaw and K. I. Goldberg, *Organometallics*, 2010, **29**, 2176–2179.
- 2 E. Januszewski, A. Lorbach, R. Grewal, M. Bolte, J. W. Bats, H.-W. Lerner and M. Wagner, *Chem. Eur. J.*, 2011, **17**, 12696–12705.
- 3 A. Lorbach, M. Bolte, H. Li, H.-W. Lerner, M. C. Holthausen, F. Jäkle and M. Wagner, *Angew. Chem. Int. Ed.*, 2009, **48**, 4584–4588.
- 4 E. von Grotthuss, S. E. Prey, M. Bolte, H.-W. Lerner and M. Wagner, *Angew. Chem. Int. Ed.*, 2018, **57**, 16491–16495.
- 5 E. von Grotthuss, S. E. Prey, M. Bolte, H.-W. Lerner and M. Wagner, *J. Am. Chem. Soc.*, 2019, **141**, 6082–6091.
- 6 E. von Grotthuss, M. Diefenbach, M. Bolte, H.-W. Lerner, M. C. Holthausen and M. Wagner, *Angew. Chem. Int. Ed.*, 2016, **55**, 14067–14071.
- 7 M. V. George, D. J. Peterson and H. Gilman, *J. Am. Chem. Soc.*, 1960, **82**, 403–406.
- 8 C. Kleeberg and C. Borner, *Eur. J. Inorg. Chem.*, 2013, **2013**, 2799–2806.
- 9 P. K. Verma, S. A. S. and K. Geetharani, *Org. Lett.*, 2018, **20**, 7840–7845.
- 10 D. Mukherjee, S. Shirase, T. P. Spaniol, K. Mashima and J. Okuda, *Chem. Commun.*, 2016, **52**, 13155–13158.
- 11 M. Kuriyama, R. Shimazawa and R. Shirai, *J. Org. Chem.*, 2008, **73**, 1597–1600.
- 12 C. Weetman, M. S. Hill and M. F. Mahon, *Chem. Eur. J.*, 2016, **22**, 7158–7162.
- 13 J. R. Lawson, L. C. Wilkins and R. L. Melen, *Chem. Eur. J.*, 2017, **23**, 10997–11000.
- 14 P. Eisenberger, A. M. Bailey and C. M. Crudden, *J. Am. Chem. Soc.*, 2012, **134**, 17384–17387.
- 15 N. Sarkar, S. Bera and S. Nembenna, *J. Org. Chem.*, 2020, **85**, 4999–5009.
- 16 M. Fleige, J. Möbus, T. Vom Stein, F. Glorius and D. W. Stephan, *Chem. Commun.*, 2016, **52**, 10830–10833.
- 17 A. Ramos, A. Antiñolo, F. Carrillo-Hermosilla, R. Fernández-Galán and D. García-Vivó, *Chem. Commun.*, 2019, **55**, 3073–3076.
- 18 D. Wu, R. Wang, Y. Li, R. Ganguly, H. Hirao and R. Kinjo, *Chem*, 2017, **3**, 134–151.
- 19 B. X. Leong, J. Lee, Y. Li, M. C. Yang, C. K. Siu, M. Der Su and C. W. So, *J. Am. Chem. Soc.*, 2019, **141**, 17629–17636.
- 20 S. Sinhababu, D. Singh, M. K. Sharma, R. K. Siwatch, P. Mahawar and S. Nagendran, *Dalton Trans.*, 2019, **48**, 4094–4100.
- 21 Stoe and Cie, *X-AREA: Diffractometer Control Program System*, Darmstadt, Germany, 2002.
- 22 G. M. Sheldrick, *Acta Crystallogr. Sect. A: Found. Crystallogr.*, 2008, **64**, 112–122.